5-2008

Time-Resolved PIV And Pressure Measurements Of Oscillating And Pulsating Flow In A Diffuser

Cameron V. King
Utah State University

TIME-RESOLVED PIV AND PRESSURE MEASUREMENTS OF OSCILLATING AND PULSATING FLOW IN A DIFFUSER

by

Cameron V. King

A thesis submitted in partial fulfillment
of the requirements for the degree

of

MASTER OF SCIENCE

in

Mechanical Engineering

Approved:

Dr. Barton Smith Major Professor	Dr. Byard Wood Committee Member
Dr. Heng Ban Committee Member	Dr. Byron R. Burnham Dean of Graduate Studies

UTAH STATE UNIVERSITY
Logan, Utah

2008

Abstract

Time-Resolved PIV and Pressure Measurements of Oscillating and Pulsating Flow in a Diffuser

by

Cameron V. King, Master of Science

Utah State University, 2008

Major Professor: Dr. Barton Smith
Department: Mechanical and Aerospace Engineering

Separating oscillating and pulsating flows in an internal adverse pressure gradient geometry are studied experimentally. Simultaneous velocity-pressure measurements demonstrate that the minor losses associated with oscillating flow in an adverse pressure gradient geometry can be smaller or larger than for steady flow. Separation is found to begin high in the diffuser and propagate downward. Flows are able to remain attached further into the diffuser with larger Reynolds numbers, larger stroke lengths, and smaller diffuser angles. The extent of separation grows with L_0/h. The minor losses grow with increasing displacement amplitude in the range $10 < L_0/h < 40$. Losses decrease with Re_δ in the range of 380 <Re< 740. It is found that the losses increase with increasing diffuser angle for $12° < \theta < 30°$. The losses for pulsating flow are found to be greater than for those of oscillating flow for small steady flow ratios and decrease to the oscillating flow value or below as the steady flow ratio approaches one. The nondimensional acoustic power dissipation increases with Reynolds number in the range of 380 <Re< 740 and decreases with stroke length in the range of $10 < L_0/h < 40$. The nondimensional resistance is independent of Reynolds number, decreases with increasing stroke length, and decreases with increasing

diffuser angle. The inertance decreases slightly with increasing stroke length and appears to be Reynolds number independent.

(123 pages)

To Tammy and Mason, the sources of the greatest joy in my life.

Contents

List of Figures

Chapter 1

Problem Statement

This thesis is a study of oscillating and pulsating flow through 2-D diffusers. When working with thermoacoustic or Stirling engines, blood flows, oceanic flows, or any case where there is oscillating or pulsating flow, one must understand how oscillating flows behave differently than steady flows through the same geometry. Failure to understand these differences leads to poor models and inefficient designs. Fundamental data, such as minor loss coefficients, can be readily obtained for steady flow through practically any geometry. However, only the simplest geometries have been studied for oscillating flow. These studies have mostly focused on flows through pipes, channels, and simple cardiovascular models. The addition of an oscillating velocity component makes fundamental investigations (ie. transition to turbulence, minor loss coefficients, and separation and reattachment) more complex.

To study these phenomena, time-resolved pressure and velocity measurements of oscillating flow through three 2-D diffusers ($12°, 20°$, and $30°$) were made in the USU oscillating flow facility. The USU Oscillating Flow facility generates oscillations using loudspeakers. A schematic of the test sections is shown in Figure 1.1.

Oscillations from 7 to 120 Hz with amplitudes of up to 50 m/s, as well as steady flow of up to 40 m/s can be produced, allowing data to be taken in the laminar, transitional, and turbulent regimes. These data were used to investigate separation and reattachment, calculate minor loss coefficients, and calculate quantities relevant to thermoacoustic engines, such as acoustic power dissipation and impedance.

One motivation for this study is the implementation of a diffuser geometry [1, 2] in thermoacoustic-sterling heat engines (see [3] for an introduction to the theory concerning these engines) to create more losses in one direction than in the other, providing an

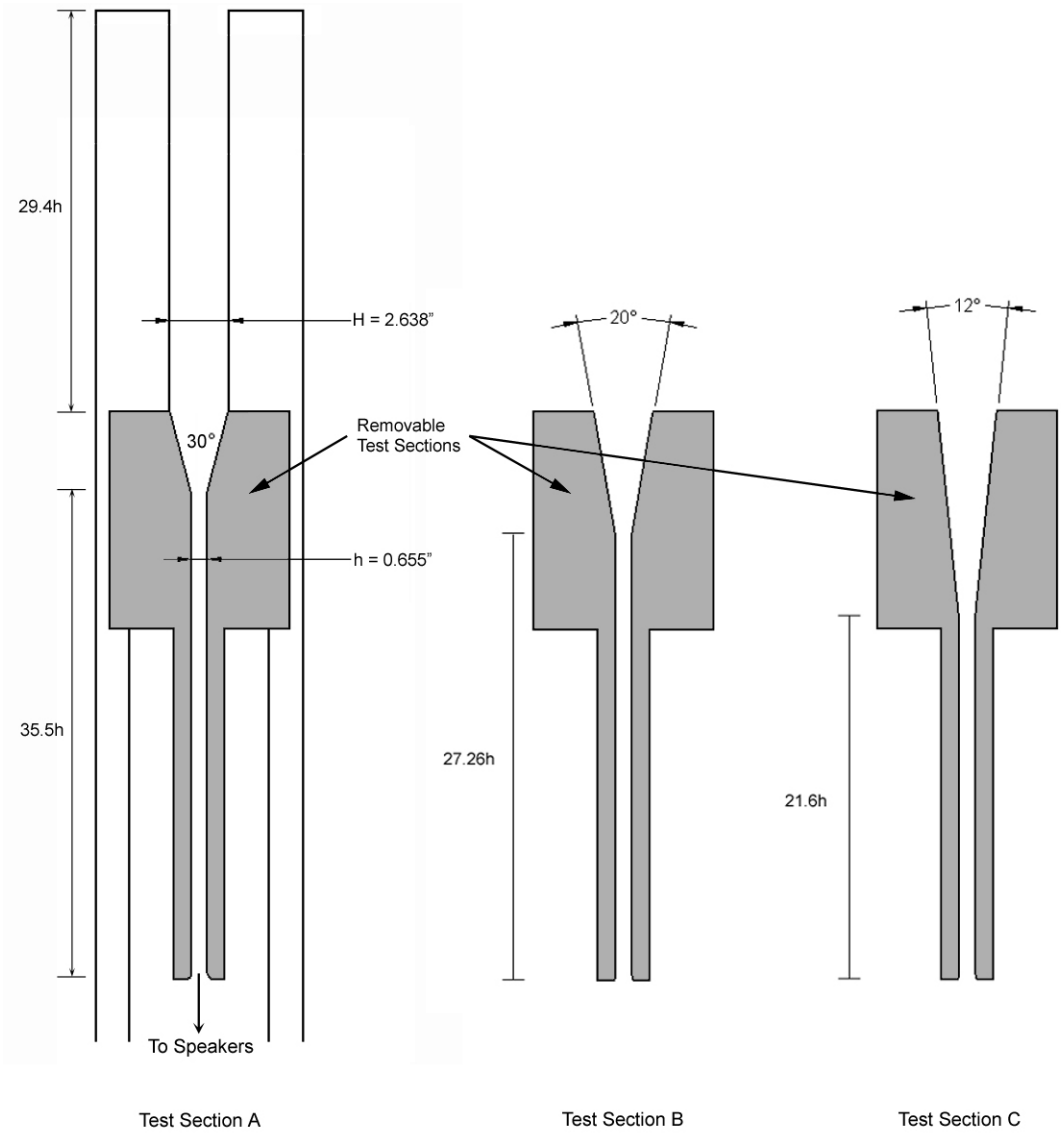

Fig. 1.1: Schematic of the removable test sections.

adjustable means of canceling unwanted steady flow.

Thermoacoustic engines are devices that convert heat energy into acoustic (sound) power as the heat moves from a high temperature region to a low temperature region. In these engines, when the temperature difference is sufficient, oscillating flow is created between the high temperature source and the low temperature sink. The source and sink are connected by a third heat exchanger, referred to as the stack, which facilitates heat transfer with the working fluid and is where the oscillations are created in a thermoacoustic engine. Researchers in this field have expressed the need for a detailed study of oscillating flow through a diffuser. Such a study would allow the engines to be made to run more efficiently.

In addition to thermoacoustic engines, arterial flows are another area where a better understanding of pulsating flows is needed. Minor losses, flow separation and stagnation, and shear stresses are of particular interest in bioengineering and cardiovascular research. Numerous studies have been conducted of pulsating flow in constricted arteries in an effort to understand the effect of plaque buildup and the implementation of arterial stents. The data collected for this thesis could be used to better understand the transition to turbulence (seen only in the largest vessels in the body), boundary layer profiles, and minor losses associated with pulsating flow through an expansion.

Those studying ocean flows also have an interest in oscillating flow, as ocean flows represent an oscillating flow (waves) superimposed on a steady flow (current). This research focuses on how the addition of oscillating flow affects the boundary layer profile, sediment movement, and wall shear stress.

Chapter 2

Literature Review

2.1 Exact Solutions

Despite the complexity of oscillating flow, analytic solutions to the Navier-Stokes equations (with many simplifying assumptions) can be found for various oscillating flow situations. The simplest of these is the solution to Stokes' second problem [4], which is flow with an oscillating boundary. Despite its simplicity, this solution is the basis for much of the existing oscillating flow theory. Assuming the pressure is constant everywhere in the fluid, that u does not vary in x, and that $v = 0$, the x-momentum equation can be reduced to

$$\frac{\partial u}{\partial t} = \nu \frac{\partial^2 u}{\partial y^2} \tag{2.1}$$

with boundary conditions

$$u(0,t) = U\cos(\omega t) \quad u(y,t) = \text{finite} \tag{2.2}$$

where U is the oscillation amplitude and ω is the angular oscillation frequency. These equations have the solution [4]

$$\frac{u(y,t)}{U} = \exp\left(-y\sqrt{\frac{\omega}{2\nu}}\right)\cos\left(\omega t - y\sqrt{\frac{\omega}{2\nu}}\right). \tag{2.3}$$

This solution is the product of a decaying exponential in y and a cosine function with a phase lag that is dependent on y. Experiments with oscillating channel flow [5–7] show the same spatial dependence for phase, with the boundary layer flow leading the bulk flow.

The governing equation for incompressible laminar channel flow with an imposed oscillating pressure gradient is very similar to the governing equation for Stokes' second problem.

Again, assuming $v = 0$ and that u does not vary in x, the x-momentum equation is reduced to

$$\frac{\partial u}{\partial t} = Pe^{i\omega t} + \nu \frac{\partial^2 u}{\partial y^2} \tag{2.4}$$

with boundary conditions

$$u(0,t) = u(h,t) = 0 \tag{2.5}$$

where P is the pressure amplitude and h is the channel width.

Landau and Lifshitz [8] give the solution to Equation 2.4 as

$$u(y,t) = \frac{P\delta_\nu^2}{i2\nu} e^{i\omega t} \left(1 - \frac{\cos(\kappa y - \kappa h)}{\cos(\kappa h)}\right) \tag{2.6}$$

where δ_ν is the Stokes-layer thickness (or viscous penetration depth) $\delta_\nu = \sqrt{2\nu/\omega}$ and $\kappa = \sqrt{-\frac{i\omega}{\nu}}$.

Poroseva et al. [9] used this solution to study the phase difference between pressure and velocity as a function of frequency and distance from the wall in oscillating flow. This relationship is dependent on the oscillation frequency. At very low frequencies ($\frac{\delta_\nu}{h} \gg 1$), the pressure and velocity are almost in phase, while at higher frequencies, ($\frac{\delta_\nu}{h} \ll 1$), the boundary layer velocity phase trails the pressure phase by about 45° and the bulk flow trails the pressure by 90°. This study was concerned with only the the higher frequency case.

2.2 Important Parameters

In describing oscillating flow with no steady component, two dimensionless parameters are necessary: the oscillation amplitude and frequency. The amplitude is given in terms of a Reynolds number, either based on the viscous penetration depth (Re_δ), the lower channel width h (Re_h), or the oscillation amplitude (Re_ω). These Reynolds numbers are defined as

$$\mathrm{Re}_\delta = \frac{u_{max}\delta}{\nu} \qquad \mathrm{Re}_\omega = \frac{a u_{max}}{\nu} = \frac{u_{max}^2}{\nu\omega} \qquad \mathrm{Re}_h = \frac{h u_{max}}{\nu} \tag{2.7}$$

where u_{max} is the maximum velocity through the cycle in the lower channel and $a = u_{max}/\omega$ is the oscillation amplitude. The Reynolds number based in Stokes-layer thickness was be used in this study. These Reynolds numbers are related by

$$\mathrm{Re}_\omega = \frac{\mathrm{Re}_\delta^2}{2} = \left(\frac{L_o}{h}\right)\frac{\mathrm{Re}_h}{2}. \tag{2.8}$$

The oscillation frequency is given either as the dimensionless stroke length L_o/h or as the ratio of the pipe radius to the Stokes-layer thickness, R/δ. Following the convention of [10,11] commonly used in studies of synthetic jets and thermoacoustic devices, the dimensionless stroke length L_o/h was used. The parameter $R/\delta = R\sqrt{\omega/2\nu}$ is a dimensionless frequency and the parameter $L_o/h = u_{max}/\pi f h$ is an inverse dimensionless frequency.

When steady flow is added, the ratio of the steady flow velocity to the maximum oscillation velocity, u_0/u_{max}, is needed in addition to Re_δ and L_o/h.

2.3 Transition to Turbulence

The transition to turbulence in oscillating flow has been studied extensively and found to be a function of Re_δ and R/δ. Four flow regimes have been identified (see Akhavan et al. [12]):

1. Laminar flow
2. Disturbed laminar flow: small perturbations appear in the accelerating portion of the cycle
3. Intermittently turbulent flow: turbulent bursts appear at the the beginning of the deceleration portion of the cycle while the acceleration portion of the cycle is laminar
4. Fully turbulent flow: flow is turbulent for the entire cycle.

Theoretical methods have had difficulty matching experimental results concerning the transition from disturbed laminar flow to intermittently turbulent flow. A quasi-steady approach has been used (see Obremski and Morkovin [13]), which examines a series of

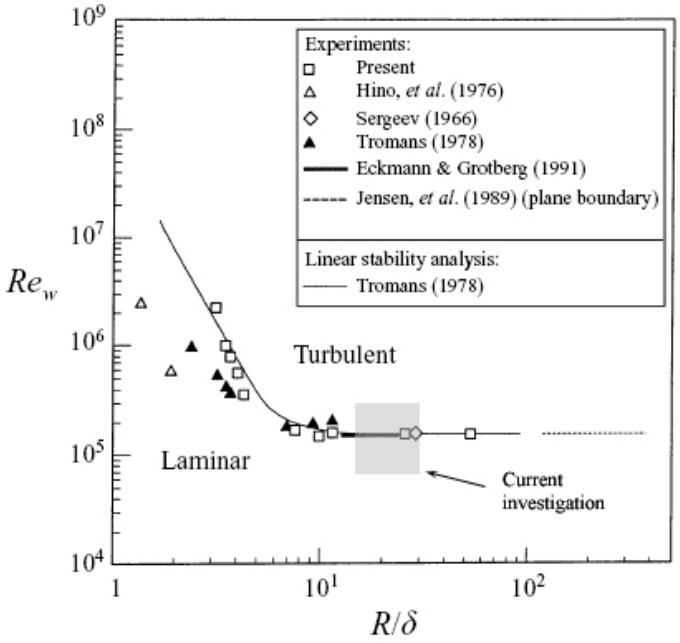

Fig. 2.1: Transition to turbulence in oscillating flow as a function of Re_δ and R/δ. From [19]

profiles individually at different phases for stability. This approach correctly predicted that some parts of the cycle generate more turbulence than others. However, it predicted that turbulent bursts would appear at the beginning of the acceleration (blowing) stroke, in contrast to experiment, where turbulent bursts appear at the beginning of the deceleration (suction) stroke. A linear stability analysis performed by Tromans [14] appears to most closely match the experimental data, as shown in Figure 2.1.

Experimental investigations by Eckmann and Grotberg [15], Sergeev [16], Hino et al. [17], Ohmi et al. [18], and Akhavan et al. [12] have shown that the transition between disturbed laminar flow and intermittently turbulent flow occurs in the range of $500 < \mathrm{Re}_\delta < 550$ for $R/\delta > 2$. Using a Reynolds number with the displacement amplitude $L_o = u_{max}/\pi f$ as the length scale, Lodahl et al. [19] plotted these results along with the stability analysis by Tromans [14]. Their result is shown in Figure 2.1. According to Tromans' stability analysis, the transition is independent of R/δ for $R/\delta > 10$. For $R/\delta < 10$, the critical Reynolds number becomes greater. The experimental findings support this conclusion. The parameter space we investigated is shown in the gray area.

There is less agreement on the appropriate boundary between fully laminar and disturbed laminar flow. Akhavan et al. [12] note that this value is particularly dependent on the experimental setup. Hino et al. [17] and Ohmi et al. [18] observed transition at about $\mathrm{Re}_\delta = 280$, while Poroseva and Girimaji [9] concluded that the flow was fully laminar for $\mathrm{Re}_\delta < 400$. The fully turbulent state has not been produced experimentally, although it has been observed that turbulence is generated through more of the cycle as Re_δ is increased, leading the aforementioned researchers to believe that at some high Reynolds number the flow will be turbulent through the entire cycle.

Many studies have also been done on the transition to turbulence in pulsating flows. When $u_0/u_{max} \ll 1$ (wave-dominated flow), experiments have shown [19] that the flow regime is dependent only on the oscillating flow parameters Re_δ and R/δ. The addition of oscillating flow has little effect on transition in current-dominated flow ($u_0/u_{max} > 1$).

The critical Reynolds numbers for transition to turbulence at various u_0/u_{max} ratios are shown in Figure 2.2. It can be seen that transition becomes independent of Re_ω for $u_0/u_{max} > 2.5$ and independent of Re_D for $u_0/u_{max} < 0.33$. As expected, when Re_ω goes to zero, the transition occurs at $\mathrm{Re}_D = 2300$. For $0.33 > u_0/u_{max} > 2.5$, it can be seen that the transition points move to the right on the plot. In this region, the transition to turbulence of a steady flow can be delayed by the addition of a laminar oscillating flow.

Studies by Costamagna and Blondeaux [20], and Vittori and Verzicco [21] have found that turbulence is generated in oscillating pipe flow in a process very similar to that of steady flow [22]. They found that toward the end of the accelerating portion of the cycle, low-speed streaks appear near the wall, which grow stronger at the beginning of the decelerating portion of the cycle. These streaks then oscillate, twist, and eventually break, forming small-scale vortices.

2.4 Shear Stress and Boundary-layer Profiles

The ratio of u_0 to u_{max} is also critically important to wall shear stress [19]. In wave-dominated flow, if the oscillating flow is laminar, the turbulence from the steady flow is not able to diffuse as much momentum to the wall, and the shear stress is less than the current-

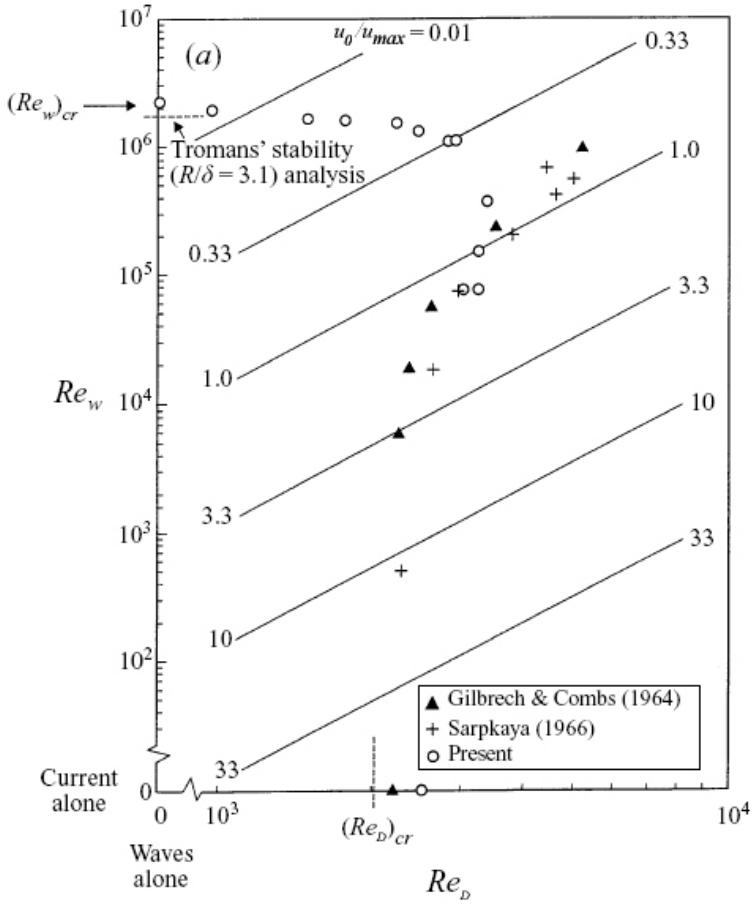

Fig. 2.2: Transition to turbulence for pulsating flow as a function of Re_ω and Re_D from Lodahl et al. [19]

alone case. If the oscillating flow is turbulent, more momentum is diffused to the wall and the shear stress is greater than the current alone case. As with the transition to turbulence, if $u_0/u_{max} > 1$, the oscillating component has little effect. The rate of momentum diffusion to the wall is important to the present study, even though the shear stress will not be measured directly. As more momentum is diffused to the wall, the flow is better able to withstand the adverse pressure gradient and remain attached for more of the cycle.

Boundary-layer profiles for oscillating flow in a rectangular duct can be found in Hino et al. [23]. As with steady flow, the authors were able to identify a viscous sublayer where $u^+ = y^+$ (to be expected, since this equation should hold for any pressure gradient), a logarithmic region, and a wake region (see Kays [24]). However, in the log layer, the

constants κ and A in the equation

$$u^+ = \frac{1}{\kappa} \ln y^+ + A \tag{2.9}$$

are found to vary with phase [23]. The constant κ is found to reach its steady-flow-only value of 0.41 only in the decelerating portion of the cycle, while the "constant" A is different for every phase. Additional investigations are necessary to fully collapse the data for oscillating flow as nicely as the steady flow data is collapsed using the Law of the Wall.

2.5 Flow Through Diffusers

Most studies concerning oscillating flow have been performed in pipes or rectangular channels. This study involved measuring flow oscillating through a diffuser. Diffusers are common devices which are used to decelerate a flow and recover flow work. As an incompressible fluid flows through an expanding cross-sectional area, mass conservation requires a decrease in the velocity. Along a streamline, the Bernoulli equation states that

$$\frac{P}{\rho} + \frac{u^2}{2} + gz = C \tag{2.10}$$

where C is a constant, P is the pressure, ρ is the density, u is the velocity, g is the acceleration due to gravity, and z is the height relative to a reference point. Thus a decrease in fluid velocity results in an increase in pressure. This pressure distribution of increasing pressure in the streamwise direction is referred to as an adverse pressure gradient. Adverse pressure gradients have the effect of slowing and eventually reversing the boundary layer flow. This causes separation and a loss of pressure recovery in the diffuser.

For 2-D diffusers, the ratio of the diffuser length to the inlet width determines the maximum diffuser angle that will keep the flow attached [25]. This ratio is 5.5 in our 30° diffuser, meaning the total diffuser angle would have to be less than 12° to prevent separation in steady flow. However, previous measurements taken in the USU oscillating flow facility [10] have shown that oscillating flow in a 20° diffuser can initially separate but reattach as the counterrotating vortices reach the diffuser walls. As shown in Figure 2.3, the flow

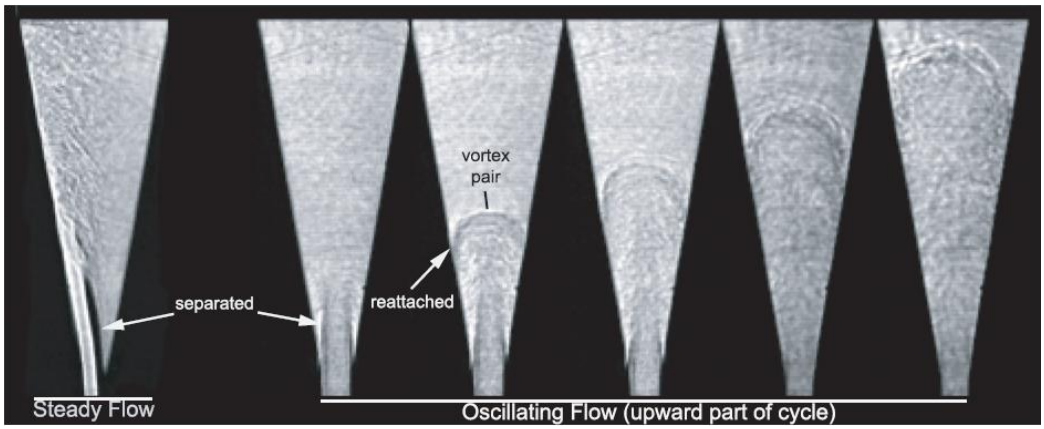

Fig. 2.3: Schlieren images of oscillating flow through a 20° diffuser compared to steady flow.

remains attached for the remainder of the blowing and suction cycles. These measurements were made using schlieren imaging. This study used high-speed PIV to acquire time-resolved velocity data, allowing a detailed study of separation and reattachment to be made.

2.6 Minor Losses

When a fluid flows through a sudden expansion or contraction, energy is often dissipated as flow separation leads to turbulence and vortex generation. These losses result in a pressure drop in addition to the pressure rise or drop predicted by the Bernoulli equation. The difference between the actual pressure and the "ideal" pressure predicted by the Bernoulli equation is referred to as a minor loss. The steady-flow pressure drop is normalized by the fluid density and velocity, giving a minor loss coefficient K, defined as [26]

$$K = \frac{\Delta p}{\frac{1}{2}\rho u^2}. \tag{2.11}$$

Minor loss coefficients are available for steady flow through practically any geometry (see Fried and Idelchik [27]). These coefficients can differ depending on whether the incoming flow is laminar or turbulent and whether or not it is fully developed [28].

In an oscillating flow, Eq. 2.11 could be used with the instantaneous pressure and velocity to give a value of K for each point in the cycle. A more practical approach, however, is to assume a minor loss coefficient for both the blowing and suction strokes that

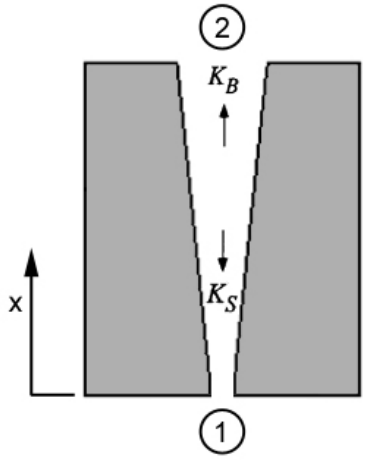

Fig. 2.4: Schematic of a diffuser section. K_B and K_S are the minor loss coefficients for the blowing and suction strokes.

is valid for the entire stroke. These will be referred to as K_B and K_S, as shown in Figure 2.4. The subscripts 1 and 2 refer to the bottom and top of the diffuser, respectively. The x direction is positive upward as shown.

An expression that relates the difference $(K_B - K_S)$ to the time-averaged pressure drop across the diffuser was suggested by Swift et al. [2]. This derivation begins with the unsteady Bernoulli equation with a general loss coefficient

$$p_1 + \frac{1}{2}\rho u_1^2 - \frac{1}{2}K\rho u_1^2 = p_2 + \frac{1}{2}\rho u_2^2 + \rho \int_{x_1}^{x_2} \frac{du}{dt} dx \tag{2.12}$$

or for the blowing portion of the cycle $0 < t/T < 0.5$

$$p_1 - p_2 = \frac{1}{2}\rho \left(u_2^2 + u_1^2(K_B - 1)\right) + \rho \int_{x_1}^{x_2} \frac{du}{dt} dx, \tag{2.13}$$

where p is the time-varying pressure, K_B is the minor loss coefficient for the blowing stroke, u is the lower channel velocity, and the subscripts 1 and 2 refer to the bottom and top of the diffuser. Introducing an area ratio $\eta = h/H$, where h is the lower channel width and H

is the upper channel width,

$$p_1 - p_2 = \Delta p = \frac{1}{2}\rho u_1^2 \left(K_B - 1 + \eta^2\right) + \rho \int_{x_1}^{x_2} \frac{du}{dt} dx. \tag{2.14}$$

Similarly, during the other half period $0.5 < t/T < 1$,

$$\Delta p = \frac{1}{2}\rho u_1^2 \left(\eta^2 - 1 - K_S\right) + \rho \int_{x_2}^{x_1} \frac{du}{dt} dx, \tag{2.15}$$

Averaging over a full period T, the integral terms go to zero for oscillating flow and are much smaller than the other terms for pulsating flow. This yields

$$\begin{aligned} \Delta P = \frac{1}{T} \int_0^{T/2} \frac{\rho}{2} \left[u_1^2 (K_B - 1 + \eta^2)\right] dt \\ + \frac{1}{T} \int_{T/2}^{T} \frac{\rho}{2} \left[u_1^2 (\eta^2 - 1 - K_S)\right] dt, \end{aligned} \tag{2.16}$$

or

$$\Delta P = \frac{\rho}{2} \left[(K_B - 1 + \eta^2)\alpha_B u_{1,max}^2 + (\eta^2 - 1 - K_S)\alpha_S u_{1,max}^2\right], \tag{2.17}$$

where

$$\begin{aligned} \alpha_B = \frac{1}{T u_{1,\max}^2} \int_0^{T/2} u_1^2 dt, \\ \alpha_S = \frac{1}{T u_{1,\max}^2} \int_{T/2}^{T} u_1^2 dt, \end{aligned} \tag{2.18}$$

ΔP is the time-averaged pressure difference, T is the period of a cycle, and $u_{1,\max} = \max[u_a(t)]$. If the flow is sinusoidal [29], then $\alpha_B = \alpha_S = 1/4$ and

$$\Delta P = \frac{\rho u_{1,\max}^2}{8} (K_B - K_S - 2 + 2\eta^2). \tag{2.19}$$

Thus, the difference in the minor loss coefficients can be calculated by measuring the time-averaged pressure drop across the diffuser. The minor loss coefficients in oscillating

flow vary greatly with the Reynolds number and stroke length. It has been shown [30] that oscillating flow through a diffuser can have a minor loss coefficient either less than or greater than that for steady flow through the same geometry.

Other oscillating flow studies [29,31] have been concerned with minor losses through a sudden expansion and contraction. This geometry is found in thermoacoustic heat engines as flow oscillates through the stack and exits into a larger space. Wakeland and Keolian [28] studied the effect of the velocity profile on losses, finding that uniform flow through an area change had less losses than fully-developed flow.

2.7 Thermoacoustic Engines

In most cases, minor losses are an unwanted dissipation of energy that designers work to minimize. In thermoacoustic engines, however, minor losses can be used to improve the efficiency of the engine by eliminating unwanted steady flow, known as streaming.

2.7.1 Streaming

In an ideal thermoacoustic engine, the flow would be purely oscillatory, with zero mean velocity (an exception is deliberate streaming introduced to eliminate the need for the heat exchangers–a subject beyond the scope of this thesis). In practice the temperature difference across the stack causes spacial density gradients and creates a nonzero mass flux over a cycle. This nonzero mass flux, known as Gedeon streaming, reduces the efficiency of the engine by convecting heat from the hot heat exchanger to the cold heat exchanger without producing work.

To eliminate Gedeon streaming and improve the efficiency of the engine, Swift and Backhaus [1,2] have implemented a passive device called a jet pump, shown in Figure 2.5 The jet pump is a diffuser geometry which creates DC flow by causing a larger pressure drop, or minor loss, when the flow exits the larger opening than when the flow exits the smaller end. The geometry of the jet pump is adjusted so that a DC flow cancels the Gedeon streaming. This is not done without a penalty, however, as the diffuser geometry also dissipates acoustic power. In introducing jet pumps, Swift and Backhaus mention the

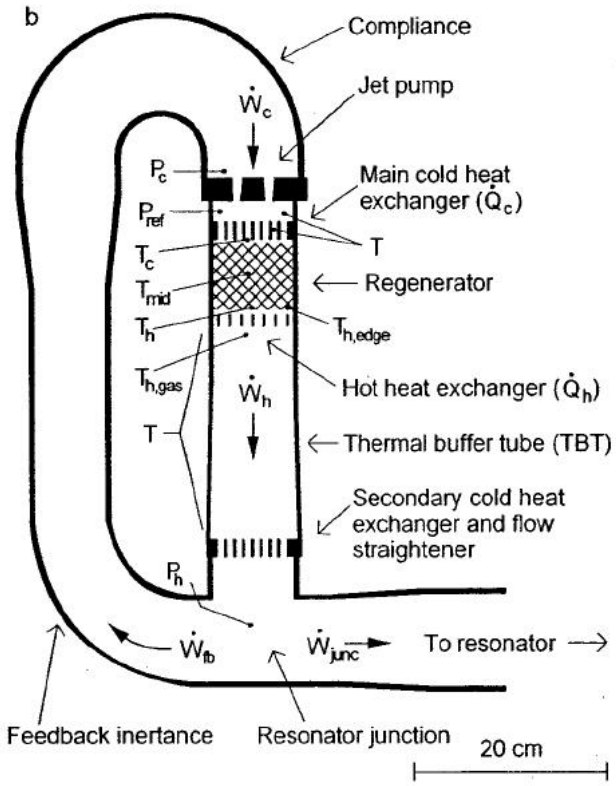

Fig. 2.5: Toroid section of a thermoacoustic-stirling heat engine showing the location of the jet pump. Figure from Swift and Backhaus [1].

need for a detailed study to be made of oscillating flow in a diffuser. This will allow future jet pump designs to dissipate as little power as possible while still canceling streaming.

Recent measurements by Biwa et al. [32] have shown that when 100 Watts were supplied to the hot heat exchanger in their thermoacoustic engine, the heat losses due to streaming were 30 W. After the jet pump was inserted, the losses dropped to 6.5 W, but it was found that 60% of the output power was consumed in the jet pump. A study of the losses as a function of the stroke length and Reynolds number would be beneficial in finding an operating range with fewer losses.

2.7.2 Acoustic Power

Using minor losses to cancel streaming has the unwanted effect of dissipating acoustic power. The acoustic power dissipation will be calculated as a function of Reynolds number,

stroke length, diffuser angle, and steady flow ratio. This will allow operating conditions to be chosen such that the power dissipation will be as small as possible while still canceling streaming.

The acoustic power over a cycle at a given location can be computed as

$$\dot{E} = \int_0^T PU dt \tag{2.20}$$

where P is the pressure, and U is the volume flow rate. This value will be calculated at each sensor location. The values from above and below the diffuser are extrapolated to the diffuser bottom ($x = 0$), and the difference is the acoustic power dissipated by the diffuser. This value can be multiplied by the driving frequency to calculate the acoustic power dissipation in Watts. This power can be thought of as a force multiplied by a velocity, or a measure of flow work, analogous to electric power.

Swift and Backhaus [1] performed measurements of acoustic power in thermoacoustic-sterling heat engines. They note that pressure scales with u^2, so acoustic power is assumed to scale by u^3.

The acoustic power dissipation for oscillating flow through a rounded exit was studied by Smith [33]. He concluded that the normalized power dissipation $\dot{E}/\rho A u^3$ increased with stroke length and decreased with Reynolds number, especially as the flow transitioned from laminar to turbulent. Increasing the exit radius had the effect of reducing the adverse pressure gradient and allowing the flow to expand more in the cross-stream direction, resulting in smaller losses.

To examine how the addition of steady flow affects the acoustic power calculation, let $U = |U| sin\,(\omega t) + U_0$ and $P = |P| sin\,(\omega t + \Phi) + P_0$, where $|U|$ is the magnitude of the flow rate (the product of u_{max} and the lower channel area), U_0 is the time-averaged flow rate, P_0 is the time-averaged pressure, ω is the angular frequency of the oscillations, and Φ is the phase difference between the pressure and velocity waveforms, typically around $\pi/2$

radians. Substituting these expressions into Eq. 2.20 yields

$$\dot{E} = \int_0^T \left[|P||U| sin\left(\omega t\right) sin\left(\omega t + \Phi\right) + |U| P_0 sin\left(\omega t\right) + |P| U_0 sin\left(\omega t + \Phi\right) + U_0 P_0 \right] dt \quad (2.21)$$

The second and third terms in the integral of Eq. 2.21 are purely sinusoidal, meaning they go to zero when integrated over a full period. The total acoustic power over a cycle at a given location is thus

$$\dot{E} = \int_0^T \left[|P||U| sin\left(\omega t\right) sin\left(\omega t + \Phi\right) + U_0 P_0 \right] dt \quad (2.22)$$

which is simply the sum of the oscillating-only acoustic power and the power contributed by the steady flow.

In an electric circuit, the addition of a DC component has no effect on the AC power. This is not likely the case, however, for pulsating fluid flow. This investigation concentrated, therefore, on how the acoustic power of the oscillating portion of the flow is affected by the presence of the steady flow. The steady power dissipation can be calculated easily from the time-averaged flow rate and pressure drop.

2.7.3 Acoustic Impedance

In addition to acoustic power, the acoustic impedance was calculated. Impedance is used to relate the flow rate to the pressure that drives the flow and is thus a useful parameter in describing sinusoidal flow through a specific geometry.

In modeling thermoacoustic engines, it is sometimes useful to use an electrical analog. In this analog, voltage is the equivalent of pressure, current is the equivalent of volume flow rate, and acoustic power is analogous to electric power. In a short channel with length Δx and area A, the lossless acoustic momentum equation is written [3]

$$\Delta p = -i\omega \frac{\rho_m \Delta x}{A} U \quad (2.23)$$

where $i = \sqrt{-1}$, ω is the driving frequency, ρ_m is the mean density, and U is the volume flow rate.

Using the electrical analog, impedance is the proportionality constant between pressure and velocity. Equation 2.23 is then written

$$\Delta P = -ZU \tag{2.24}$$

where Z is the acoustic impedance, equal to $i\omega L$, where L is the inertance (analogous to inductance). Assuming laminar flow, the inertance L is written

$$L = \frac{\rho_m \Delta x}{A} \tag{2.25}$$

As its name implies, the inertance is important where the gas inertia is important (e.g. long thin pipes). In areas where gas compressibility is important (e.g. at velocity nodes), the acoustic impedance is instead comprised of a compliance (analogous to capacitance) term. Both inertance and compliance are important in traveling-wave thermoacoustic engines. For this study, it was assumed that only the inertance was important due to the lack of compressibility in the flow.

To go beyond the assumption that the system is lossless, an additional resistance (analogous to electrical resistance) term is used to account for viscous dissipation at the channel walls. For laminar flow this can be approximated as

$$R_\nu = \frac{\mu \Delta S}{A^2 \delta_\nu} \tag{2.26}$$

where μ is the dynamic viscosity, ΔS is the surface area, A is the cross-sectional area, and δ_ν is the stokes-layer thickness.

The impedance is thus

$$Z = i\omega L + R_\nu \tag{2.27}$$

where L is the inertance and R_ν is the viscous resistance. Since L and R_ν are both real, the i implies that the contribution from the inertance leads the viscous resistance by 90°.

To relate Eq. 2.24 to measurable quantities, let $\Delta P = |\Delta P| exp\left[i(\omega t + \Phi_{\Delta P})\right]$ and $U = |U| exp\left[i(\omega t + \Phi_U)\right]$ where $|P|$ denotes the magnitude of ΔP, $|U|$ denotes the magnitude of U, $\Phi_{\Delta P}$ is the phase of ΔP, and Φ_U is the phase of U. The ΔP waveform is the difference between a pressure signal from above the diffuser and a pressure signal from below the diffuser. Substituting into Eq. 2.24 yields

$$Z = \frac{|\Delta P| exp\left[i(\omega t + \Phi_{\Delta P})\right]}{|U| exp\left[i(\omega t + \Phi_U)\right]} = \frac{|\Delta P|}{|U|} exp\left[i(\Phi_{\Delta P} - \Phi_U)\right]. \tag{2.28}$$

Taking the real and imaginary parts gives expressions for the resistance and the inertance:

$$\mathrm{Re}(Z) = R_\nu = \frac{|\Delta P|}{|U|} \cos\left(\Phi_{\Delta P} - \Phi_U\right) \tag{2.29}$$

$$\mathrm{Im}(Z) = \omega L = \frac{|\Delta P|}{|U|} \sin\left(\Phi_{\Delta P} - \Phi_U\right). \tag{2.30}$$

To evaluate these equations, an expression is needed for the magnitude and phase of ΔP. Letting point 1 represent the pressure signal below the diffuser and point 2 represent the pressure signal above the diffuser,

$$\Delta P = P_2 - P_1 = |\Delta P| exp\left[i(\omega t + \Phi_{\Delta P})\right] = |P_2| exp\left[i(\omega t + \Phi_{P_2})\right] - |P_1| exp\left[i(\omega t + \Phi_{P_1})\right] \tag{2.31}$$

Assuming the frequencies of each waveform are the same yields

$$|\Delta P| e^{\Phi_{\Delta P}} = |P_2| e^{\Phi_{P_2}} - |P_1| e^{\Phi_{P_1}}, \tag{2.32}$$

which, using Euler's formula and equating the real and imaginary parts yields

$$|\Delta P| \cos\left(\Phi_{\Delta P}\right) = |P_2| \cos\left(\Phi_{P_2}\right) - |P_1| \cos\left(\Phi_{P_1}\right) \tag{2.33}$$

$$|\Delta P| \sin\left(\Phi_{\Delta P}\right) = |P_2| \sin\left(\Phi_{P_2}\right) - |P_1| \sin\left(\Phi_{P_1}\right). \tag{2.34}$$

Dividing the second expression by the first,

$$\tan(\Phi_{\Delta P}) = \frac{|P_2|\sin(\Phi_{P_2}) - |P_1|\sin(\Phi_{P_1})}{|P_2|\cos(\Phi_{P_2}) - |P_1|\cos(\Phi_{P_1})} \doteq X. \tag{2.35}$$

or

$$\Phi_{\Delta P} = \arctan(X). \tag{2.36}$$

Solving Eq. 2.33 for $|\Delta P|$ yields

$$|\Delta P| = \frac{|P_2|\cos(\Phi_{P_2}) - |P_1|\cos(\Phi_{P_1})}{\cos(\arctan X)} = \left[|P_2|\cos(\Phi_{P_2}) - |P_1|\cos(\Phi_{P_1})\right]\sqrt{1+X^2} \tag{2.37}$$

The resistance and inertance are thus independent of time if calculated using Eqs. 2.36, 2.37, 2.29, and 2.30.

Studies have been performed to calculate the acoustic impedance of various geometries and flow conditions. A study was performed by Wilen and Petculescu [34] that measured the impedance of oscillating flow through a conical diffuser. They used a speaker to generate the oscillations, holding the frequency constant while varying the input power. They found that the resistance increases with Reynolds number and becomes linear at high amplitudes while the inertance decreases with Reynolds number for low Reynolds numbers (less than 2500) and becomes Reynolds number independent for high Reynolds numbers.

Chapter 3

Objectives

The objectives of the current research were as follows:

1. Acquire PIV and pressure data of oscillating and pulsating flow of various Reynolds numbers, stroke lengths, diffuser angles, and steady flow rates. PIV images were taken of the entire flow field, of the separation region only, and of the boundary layer only.

2. Compute the minor losses, acoustic power dissipation, and impedance as a function of the Reynolds number, stroke length, diffuser angle, and steady flow ratio. Software was written to perform the computations, as well as phase-average and time-average the data where appropriate.

3. Use the pressure and velocity data to examine transition to turbulence, separation, and reattachment.

Chapter 4

Procedure

4.1 Parameter Space and Facility

For oscillating flow alone, three Reynolds numbers were studied: $Re_\delta = 380, 580, 740$. The $Re_\delta = 380$ case probably falls into the disturbed laminar flow regime, while $Re_\delta = 580$ and $Re_\delta = 740$ probably are intermittently turbulent. Five stroke lengths were chosen for each Reynolds number such that the speaker frequency is between about 8 and 30 Hz. The required frequency to achieve a certain Reynolds number and stroke length is

$$f = \left(\frac{Re_\delta}{L_o/h}\right)^2 \frac{\nu}{\pi h^2}. \tag{4.1}$$

The maximum channel velocity needed in the cycle is calculated as

$$u_{max} = (L_o/h)\,\pi f h. \tag{4.2}$$

In the USU oscillating flow facility, oscillations were generated by eight JBL 600 Watt loudspeakers driven by two Crown CE4000 amplifiers (see Figure 4.1). The speaker waveform was generated using an HP 33120A arbitrary waveform generator. The input voltage could be set, but not the velocity amplitude in the test section. In previous research, Smith et al. [35] have found that the velocity amplitude scales linearly with the input voltage. PIV data was taken with a guess voltage, the data were processed, the voltage was adjusted accordingly, and the data will be retaken. A 3% error in the Reynolds number was considered acceptable. More detailed information on the facility can be found in Smith and Swift [36].

Steady flow was controlled by a Wilkerson mass flow controller and was added through a port at the bottom of the facility. Four steady flow values were taken for each Reynolds number and stroke length, holding the Stokes-layer Reynolds number constant. The total

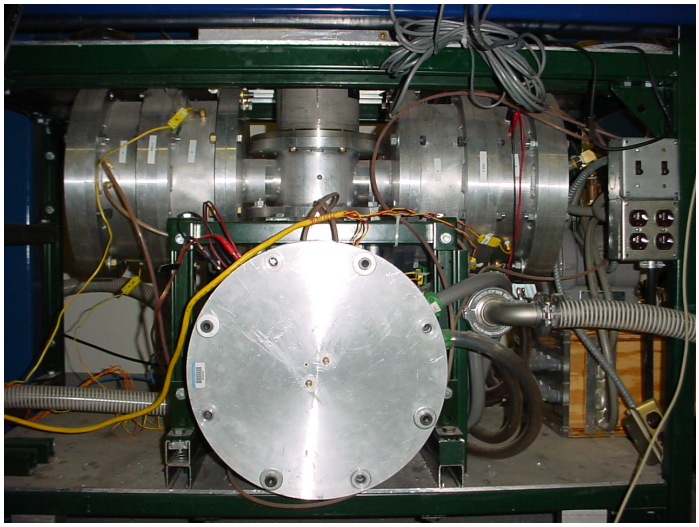

Fig. 4.1: Photograph of the oscillating flow facility. The aluminum cylinders contain the speakers used to generate the oscillations.

number of cases for the current study is 180 (three diffuser angles, three Reynolds numbers, five stroke lengths, and four steady flow values including zero). The parameter space is shown graphically in Figure 4.2. A complete list of cases taken is shown in Appendix B. Each case was taken using two fields of view (zoomed-in and zoomed-out) for a total of 360 sets of PIV and pressure data.

As shown in Figure 1.1, three diffuser angles were tested. To avoid entrance effects, the lower channel was made as long as possible and have rounded corners at the entrance. The upper channel is $29.4h$ units long (h = .655 in. is the lower channel width), but its volume is sufficient that entrance effects from the top of the facility were avoided.

4.2 Velocity Measurements

Velocity measurements were taken using a particle image velocimetry (PIV) system made by LaVision, Inc. This system includes a Photron Fastcam-APX RS high speed CCD camera capable of taking 3000 images per second at 1024 x 1024 pixel resolution. The camera was mounted on Velmex sliders, giving precise position control. The camera setup is shown in Figure 4.3. Tracer particles were created using a Laskin nozzle, which utilizes compressed air to fluidize olive oil droplets. These droplets were estimated to be about 1

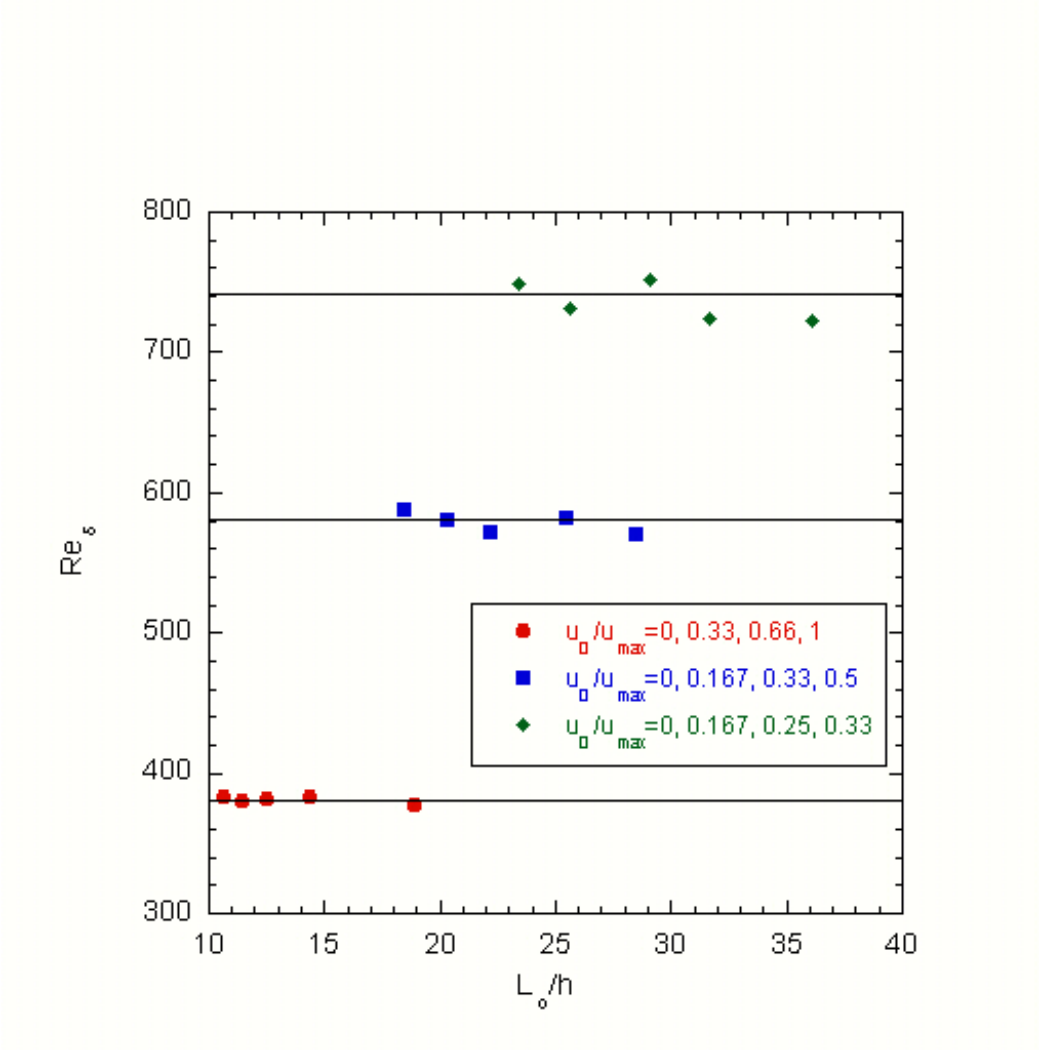

Fig. 4.2: Parameter space of this investigation. Each point shown here was taken in three diffuser angles and at two fields of view.

micron in diameter. They were assumed to have sufficient drag that they follow the flow field exactly. The flow field was illuminated by a 45 mJ Nd:YLF twin-pulsed laser made by Photonics with sheet optics.

A typical PIV setup is shown in Figure 4.4. PIV measures whole velocity fields by taking two images with a known small time interval (called "dt") between them. The images are divided into small sections, called interrogation regions, and the regions from each image are cross correlated. In the cross correlation, a peak is identified that corresponds to the location of the most probable displacement of the particles. The displacement is divided by

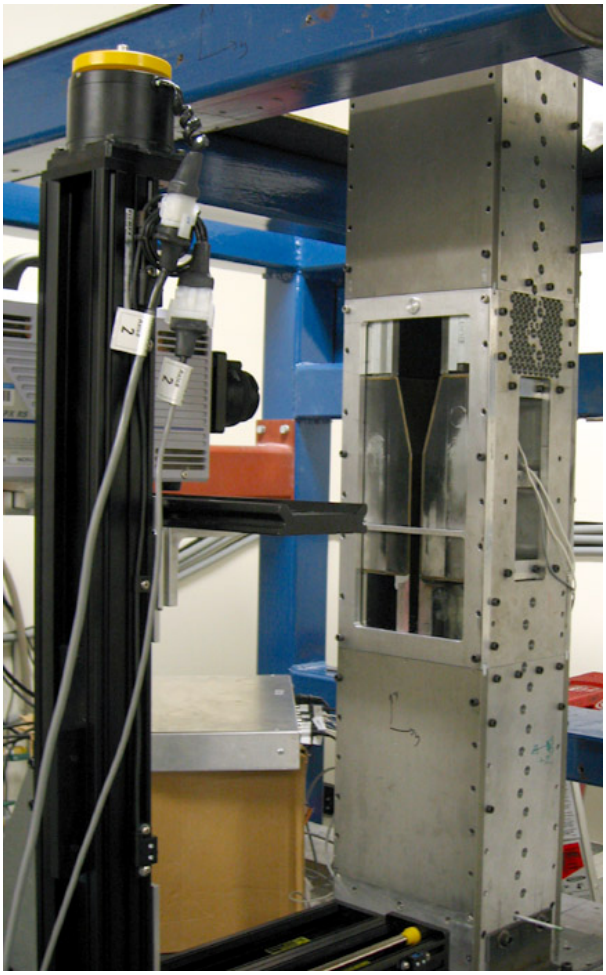

Fig. 4.3: Camera in front of test section. The laser was mounted above the facility and fired down through the test section.

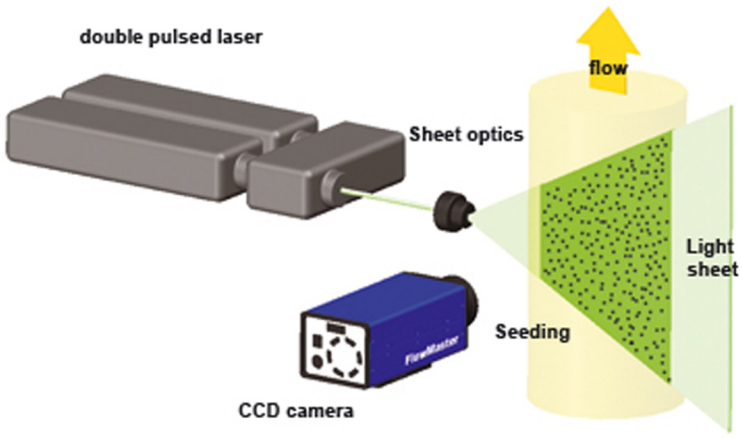

Fig. 4.4: Typical PIV setup (image from LaVision).

the time difference to find the velocity. These calculations were performed using software made by LaVision.

The camera RAM is able to hold 2048 images, so 20 cycles were sampled at 50 double-pulsed images per cycle (100 total images per cycle). The optimal pixel displacement between the pulses is about 5-10 pixels for the best accuracy [37].

Two different fields of view were taken for each case: a field of view that includes the entire diffuser section and part of the upper and lower channel (referred to as zoomed-out), and a zoomed-in field of view that includes only a small part of the lower channel and the diffuser at the beginning of the expansion. Additionally, data was taken for some cases in the lower channel section of the 30° diffuser in boundary layer region only. A schematic of the respective fields of view is shown in Figure 4.5.

The zoomed-out data was used to calculate the Reynolds number and stroke length of the case and to observe the separation, reattachment, and characteristics of the flow. A Fortran code (included in Appendix B) was written to perform the calculations. A typical PIV vector field of this view is shown in Figure 4.6. The vector resolution for these vector fields is 1 mm.

The zoomed-in data was used to make detailed calculations of the separation time at each location, to create boundary layer profiles, and to examine the relationship between

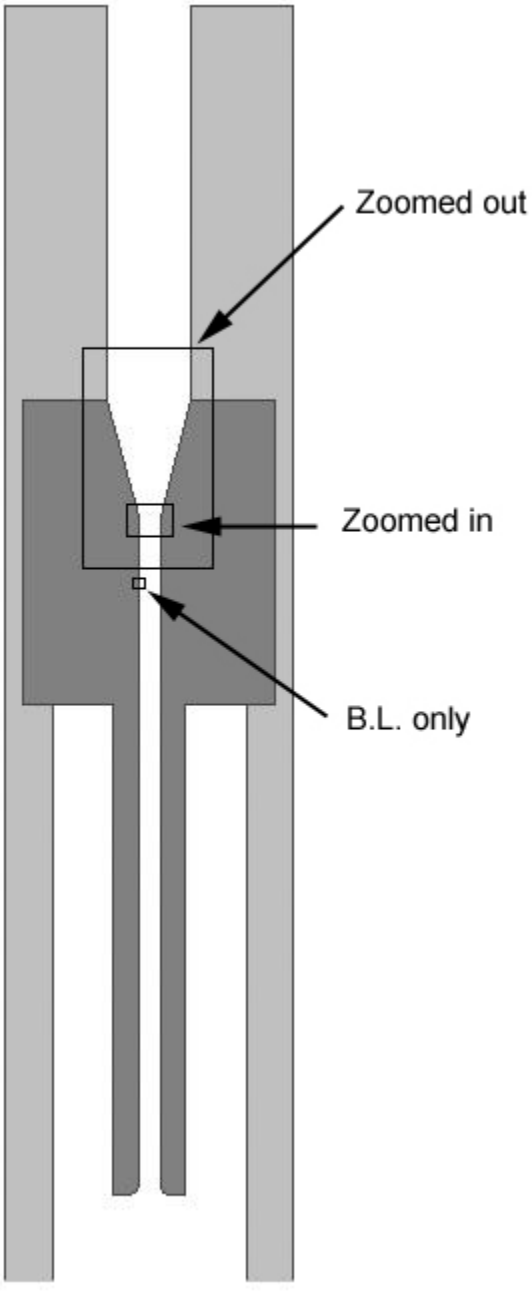

Fig. 4.5: Schematic of the fields of view of velocity data taken in the 30° test section.

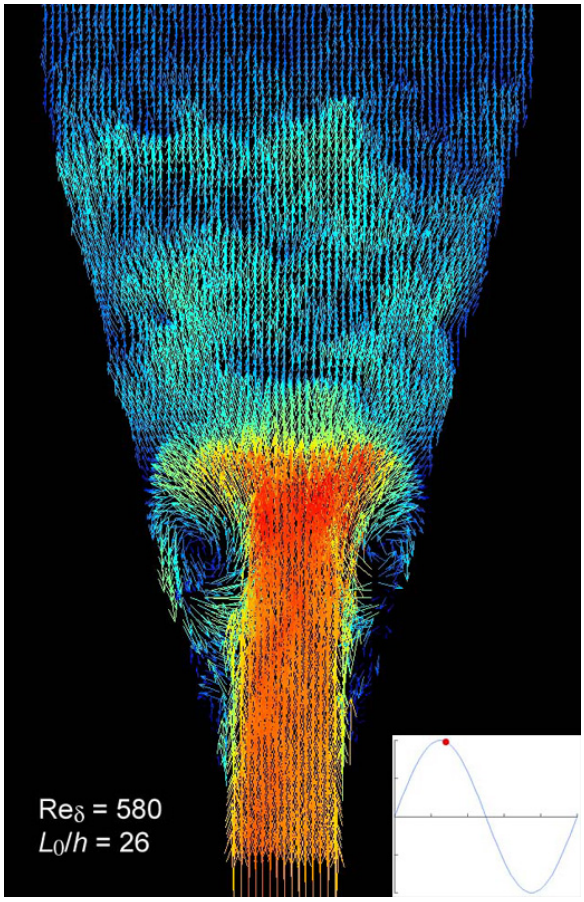

Fig. 4.6: Typical zoomed-out vector field.

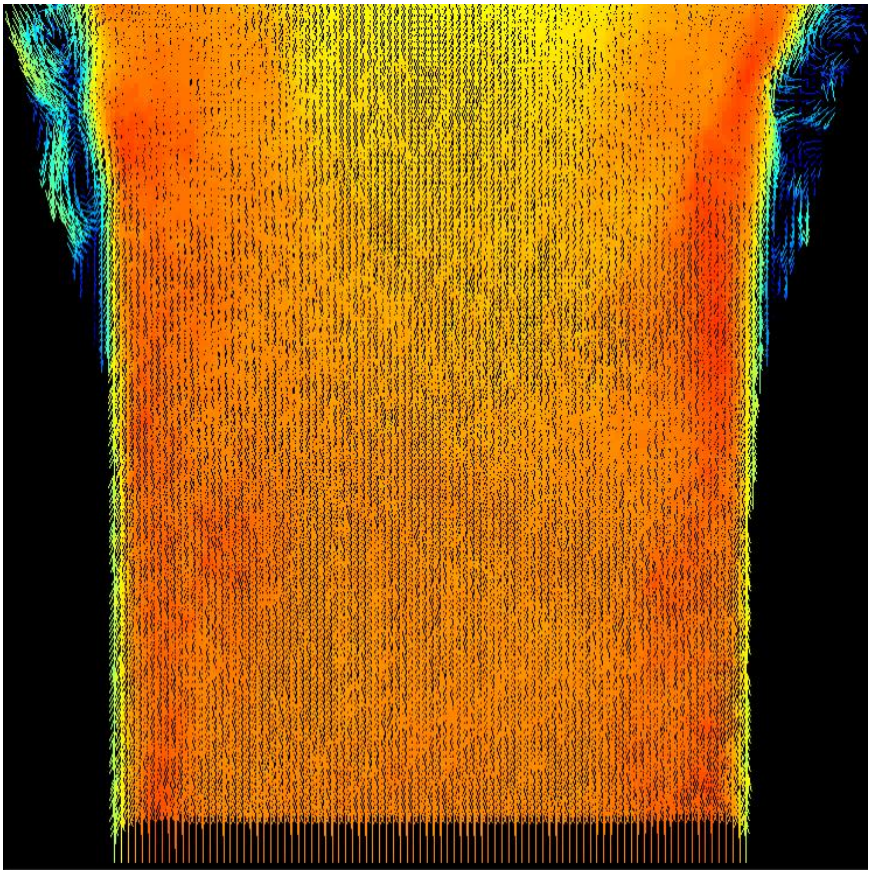

Fig. 4.7: Typical zoomed-in vector field.

the bulk flow and the boundary layer flow. A typical zoomed-in PIV vector field is shown in Figure 4.7. The vector resolution for these vector fields is 0.15 mm.

The boundary-layer data was used to examine the near-wall velocity profile and compare the results to existing theory, including the law of the wall. A vector field of this view is shown in Figure 4.8. This vector field has a 50 micron resolution.

4.3 Pressure Measurements

Simultaneous to the velocity measurements, pressure measurements were taken at 11 locations using Endevco 8510B-1 and 8510B-2 model pressure transducers. The sensor locations are shown shown in Figure 4.9. The facility was built such that the sensors mount flush with the test section wall. The sensors were powered by an external 10-V power supply, which also provided the connection to a National Instruments BNC-2090a connector block.

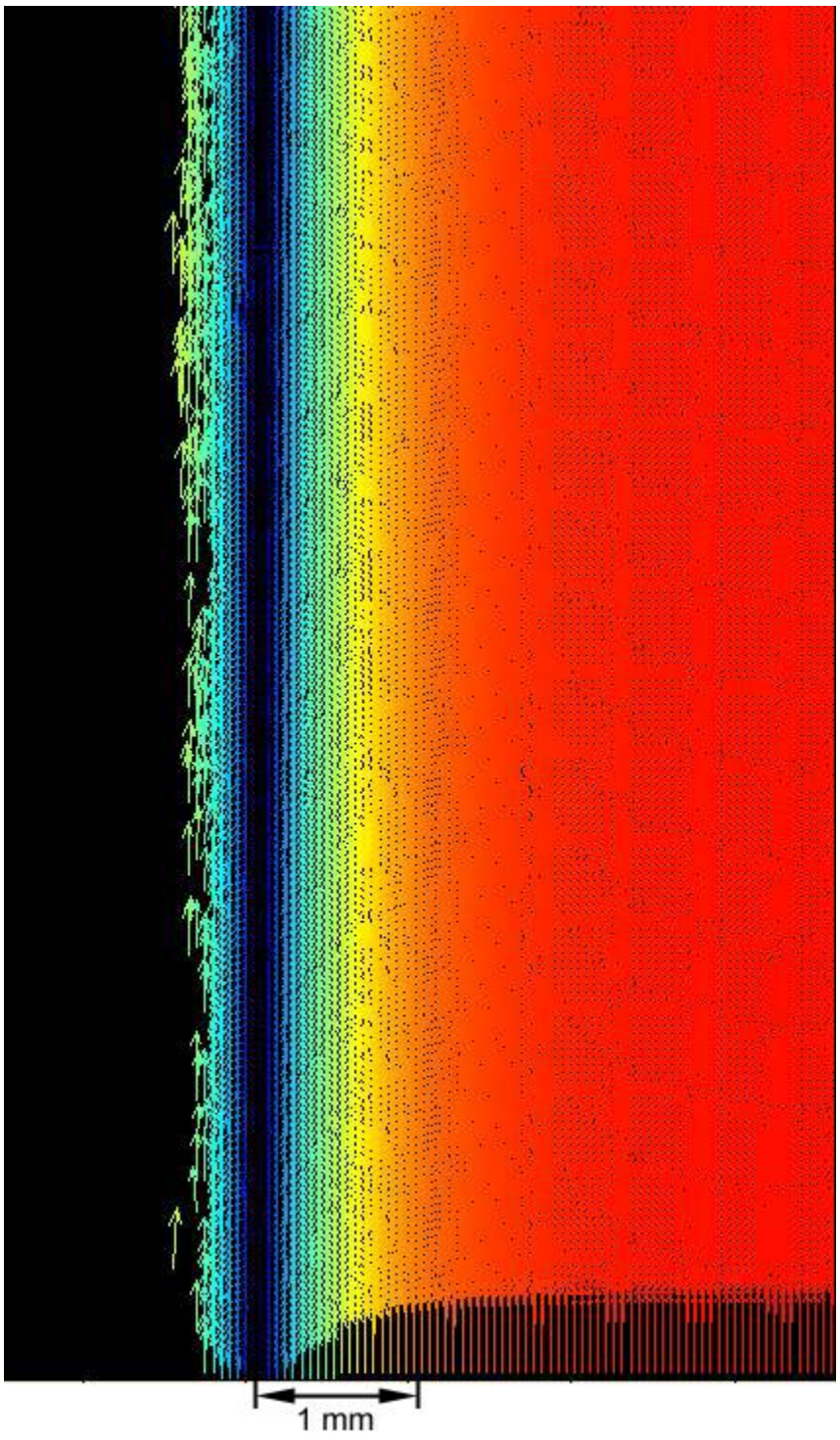

Fig. 4.8: Example of a boundary-layer only vector field.

This block was connected to the computer through a PCI-6052E card that can take up to 333 kilosamples per second. Labview software was used to control the data acquisition. A trigger signal from the PIV computer was connected to Labview to synchronize the pressure and velocity data.

The lowermost pressure sensor was left in place and connected to a multimeter. The AC voltage from the sensor was recorded for each case, allowing the case to be repeated. The sensors in the diffuser were placed on both sides to enable events (like separation) to be correlated to the velocity field.

The pressure sensor manufacturer gives a simple linear sensitivity for converting from voltage to pressure. According to the specifications, this introduces a 1% of full scale nonlinearity error. To eliminate this, each sensor was calibrated against a 100 torr MKS Baratron having an accuracy of 0.05% of reading (model 698A12TRA). The data were fit using a third order polynomial. A typical calibration curve is shown in Figure 4.10.

Every effort was made to minimize the noise present in the system, as the output from the pressure sensors will be on the order of 20-30 mV. The entire data acquisition system was powered on the same circuit. Pressure data is very inexpensive to acquire and store compared to the velocity data. In most cases, additional pressure measurements were made of 100 cycles for use in calculations that required phase-averaged or time-averaged data (the pressure measurements continued after the velocity measurements stopped).

Instantaneous pressure measurements made in the 30° diffuser over one cycle are shown in Figure 4.11. The sensors are numbered sequentially from number 2 below the diffuser to number 8 above the diffuser.

It can be seen in Figure 4.11 that the time-averaged pressure is negative compared to the ambient. This mean pressure is generated by the presence of minor losses, as shown in Eq. 2.19 and demonstrated by Smith and Swift [38]. The time-averaged pressure for the $Re_\delta = 740$ and $L_0/h = 25$ case is shown in Figure 4.12. The point $x/h = 0$ corresponds to the beginning of the expansion. It can be seen from Figure 4.12 that the pressure approaches the ambient at the upper channel exit. The pressure drop in the lower channel is constant,

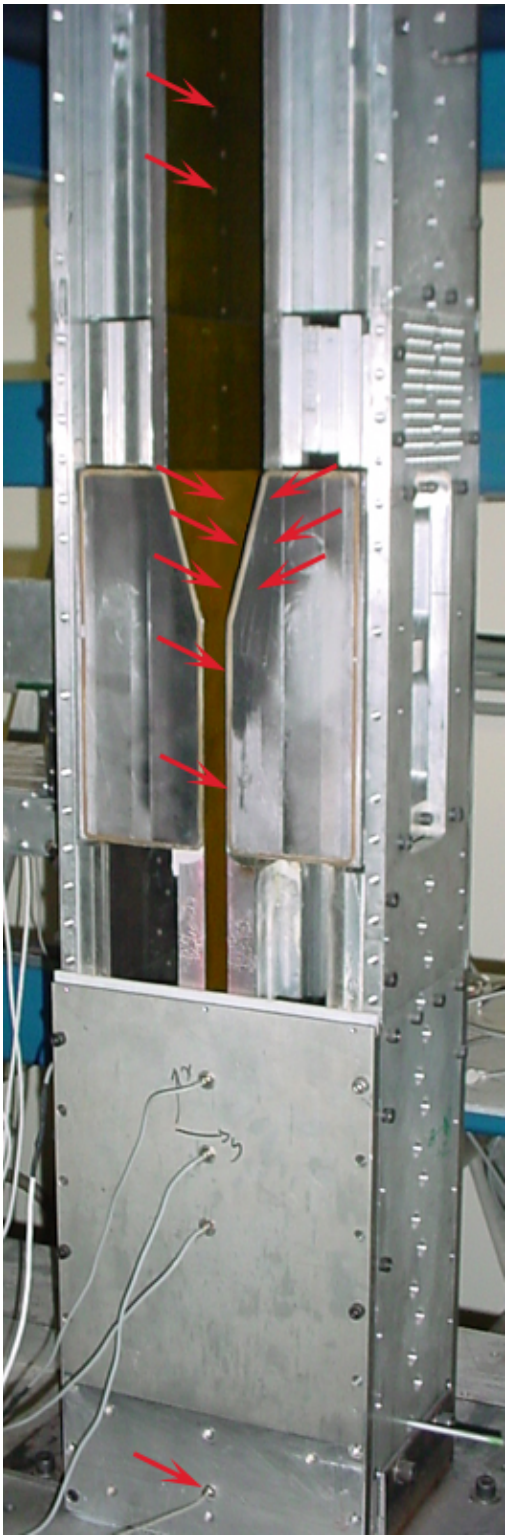

Fig. 4.9: Pressure sensor locations.

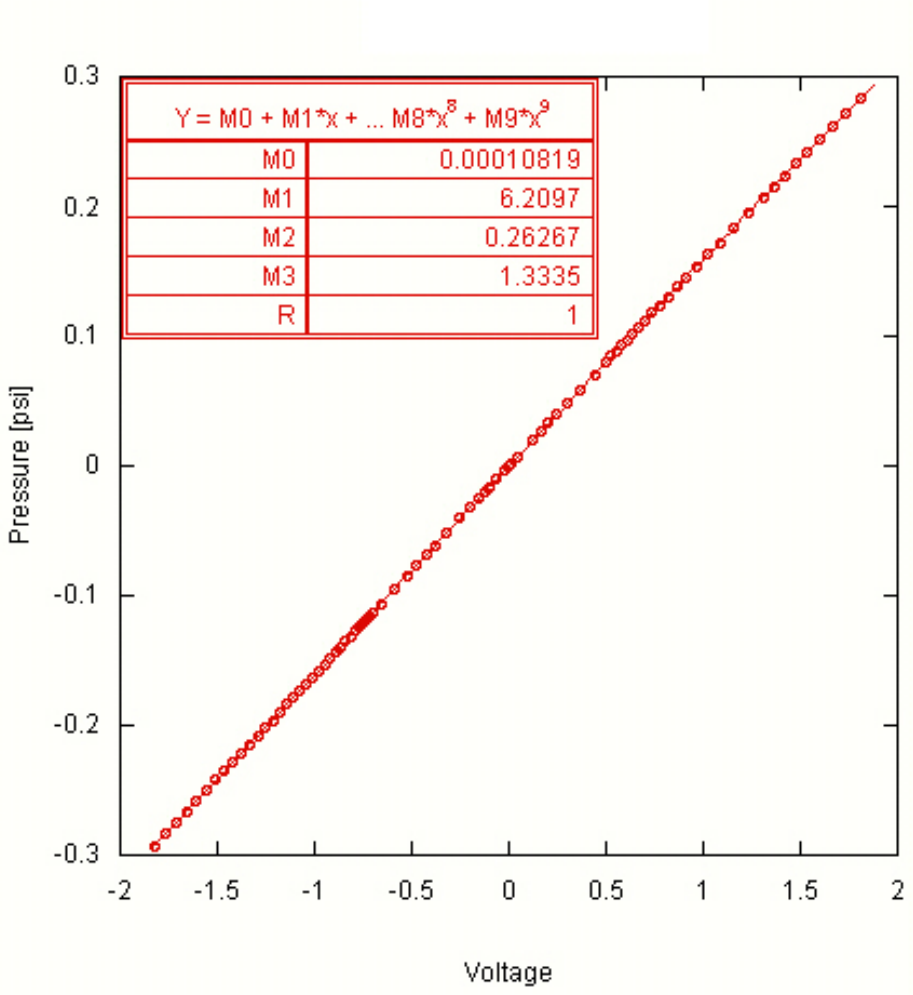

Fig. 4.10: Calibration curve for 8510B-1 pressure sensor.

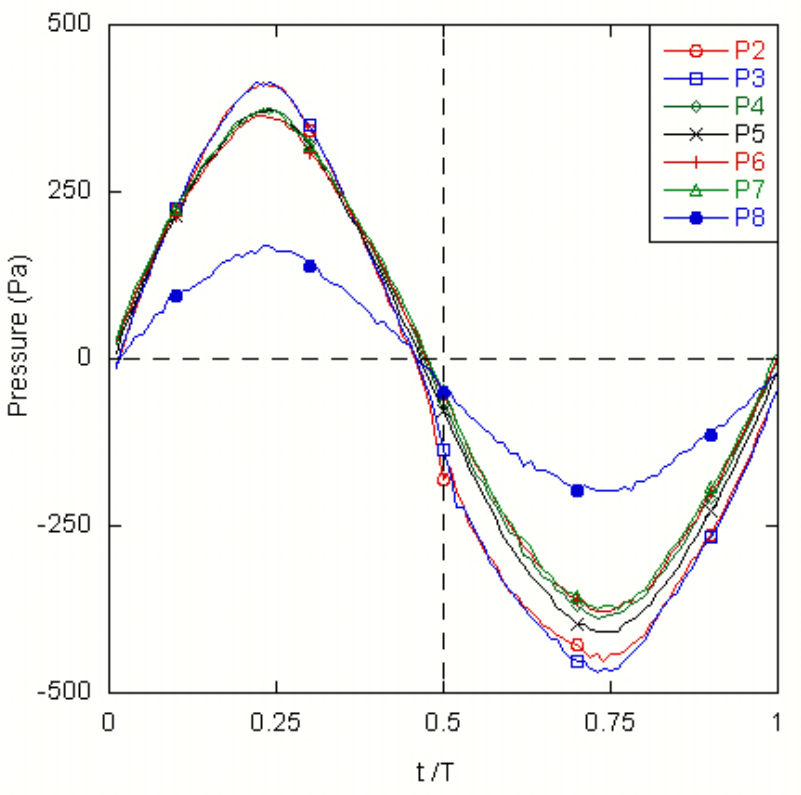

Fig. 4.11: Instantaneous pressure measurements over one cycle in the 30° diffuser for $Re_\delta = 380$ and $L_0/h = 11$.

as would be expected for a channel of constant width. A comparison of the diffuser angles shows that the mean pressure in the lower channel becomes more negative with increasing diffuser angle.

While the time-averaged pressure data is useful in calculating losses, phase-averaged pressure data can be used to correlate events (ie. separation) to the velocity fields, as well as reduce noise in calculations that involve the time-varying pressure signal. Figure 4.13 shows the phase-averaged pressure over one cycle in the 30° diffuser for $Re_\delta = 740$ and $L_0/h = 31$ and no steady flow. The thick black line represents the lower channel velocity. Note the sudden drop in pressure of sensors 4 and 5 (located at the same x on opposite sides of the diffuser) at $t/T = 0.3$, just as the flow begins to decelerate. This sudden loss of pressure recovery corresponds to the arrival of the separated flow at this location. In this case, the flow reattaches soon afterward.

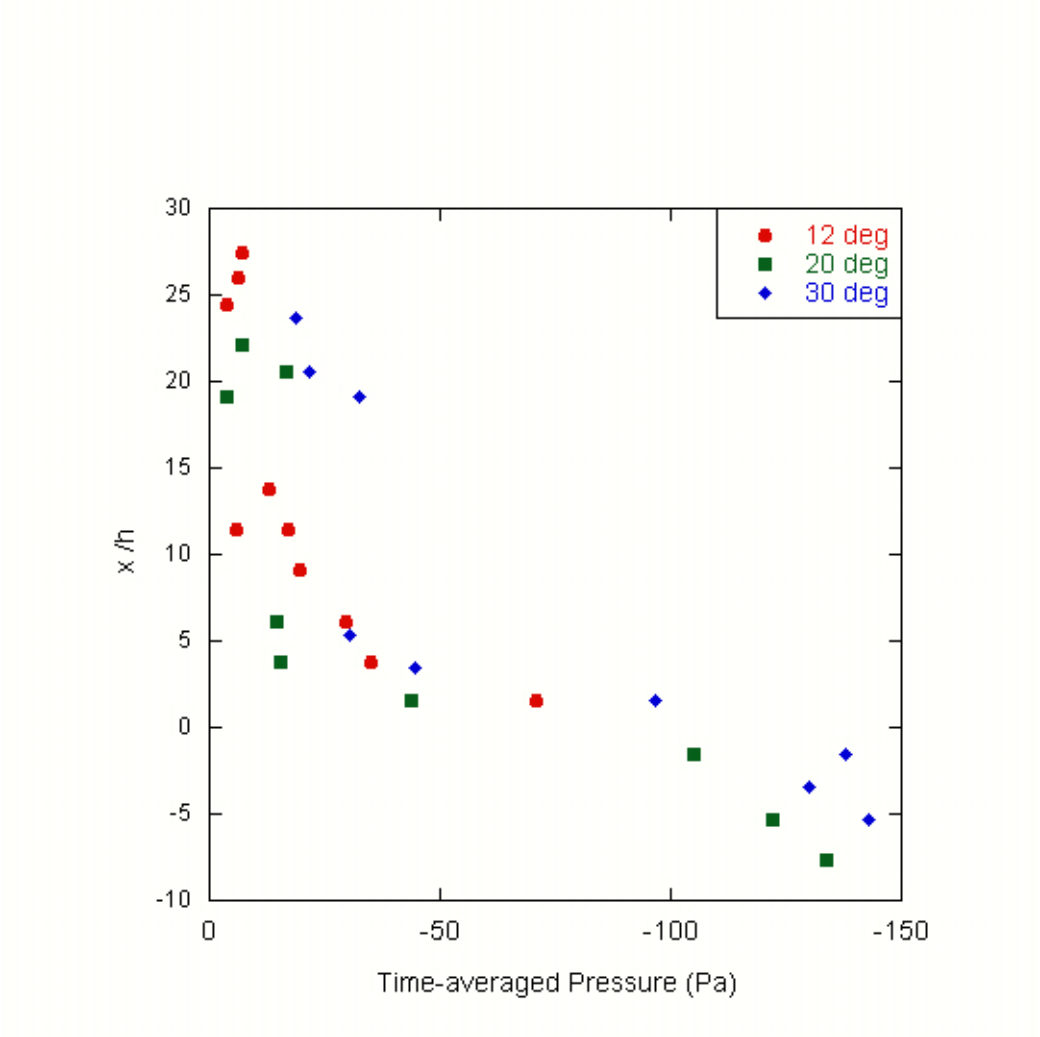

Fig. 4.12: Time-averaged pressure measurements from the three diffusers for $Re_\delta = 740$ and $L_0/h = 25$.

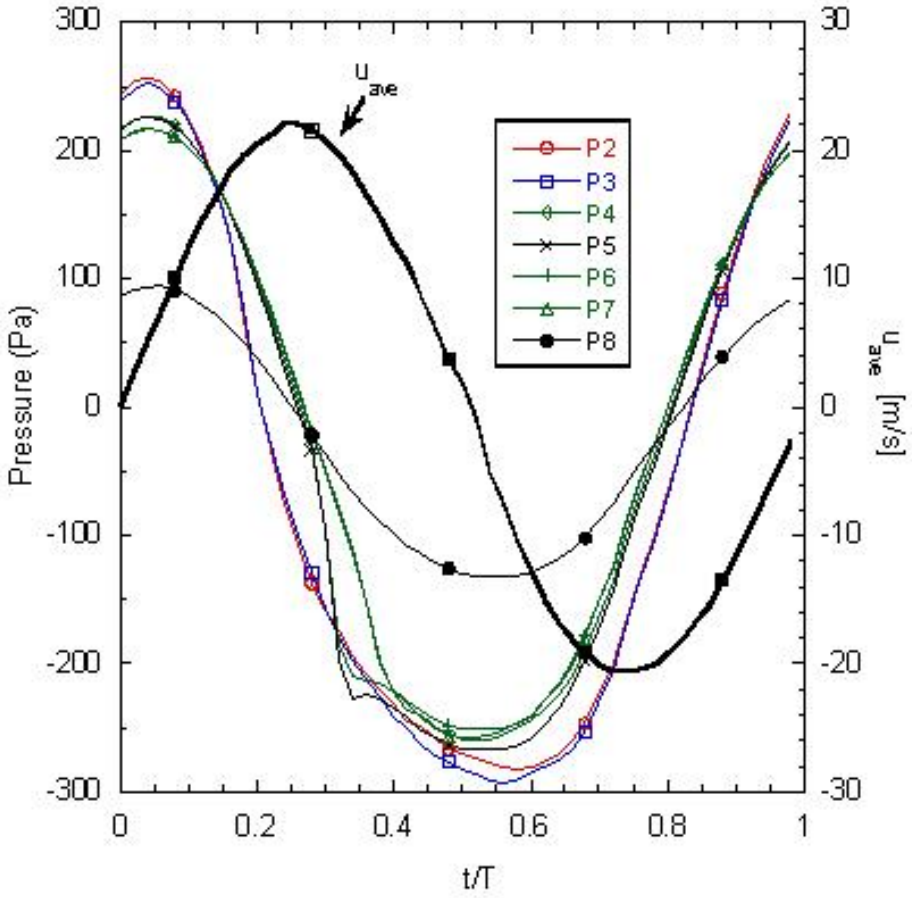

Fig. 4.13: Phase averaged pressure measurements from the 30° diffuser for $Re_\delta = 740$ and $L_0/h = 31$.

Chapter 5

Results

5.1 Minor Losses

The minor losses were calculated for each case, allowing the effect of the Reynolds number, displacement amplitude, diffuser angle, and steady flow ratio to be examined.

5.1.1 Oscillating Flow

Examination of the Time-resolved PIV data shows that for oscillating flow with zero mean velocity, the larger the displacement amplitude for a given Reynolds number, the earlier the flow separates, giving rise to greater irreversibilities and greater losses. For relatively small stroke lengths, the flow reattaches quickly, and the resulting minor losses can be smaller than for steady flow through the same geometry. For larger stroke lengths, the flow reattaches later in the cycle and more dissipation is present, meaning minor losses can be greater than for steady flow.

As the diffuser angle is increased, the flow separates earlier in the cycle and takes longer to reattach, leading to greater losses. This phenomenon is demonstrated in a side-by-side comparison of three velocity fields (Figures 5.1 and 5.2) at the same point in time of cases having the same Reynolds number and stroke length but different diffuser angles. Figure 5.1 shows the velocity fields at $t/T = 0.24$, or the point just before the peak velocity is reached. Figure 5.2 shows the velocity fields at $t/T = 0.32$, in the beginning of the deceleration portion of the cycle.

Figure 5.1 shows that the flow in the 30° diffuser has separated much earlier than in the other two geometries. The 30° diffuser expands quickly enough to allow counterrotating vortex pairs to form and propagate toward the diffuser walls, leading to reattachment. The flow remains attached for the remainder of the blowing cycle.

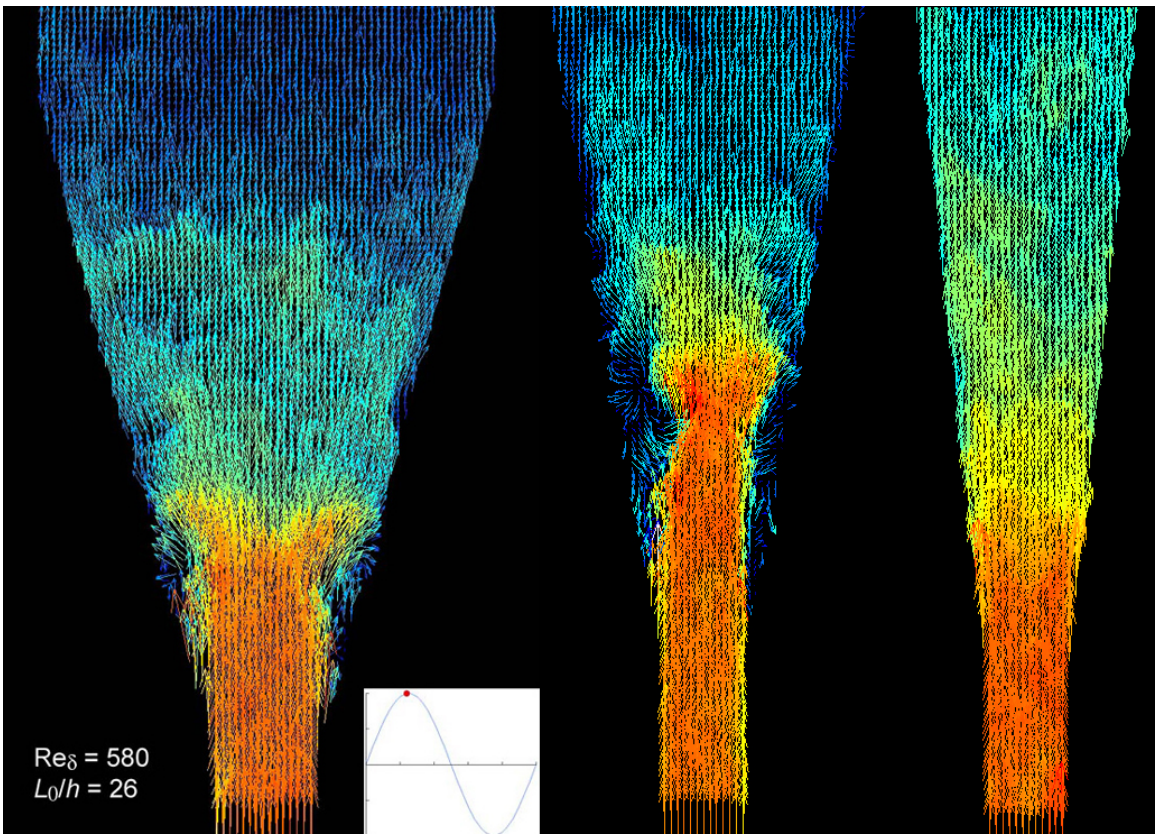

Fig. 5.1: Comparison at $t/T = 0.24$ of three cases where $Re_\delta = 580$ and $L_0/h = 26$ with $u_0 = 0$. The diffuser angles are 30°, 20°, and 12°. The vector colors indicate velocity magnitude and are scaled by the maximum velocity with red being the maximum and blue being zero.

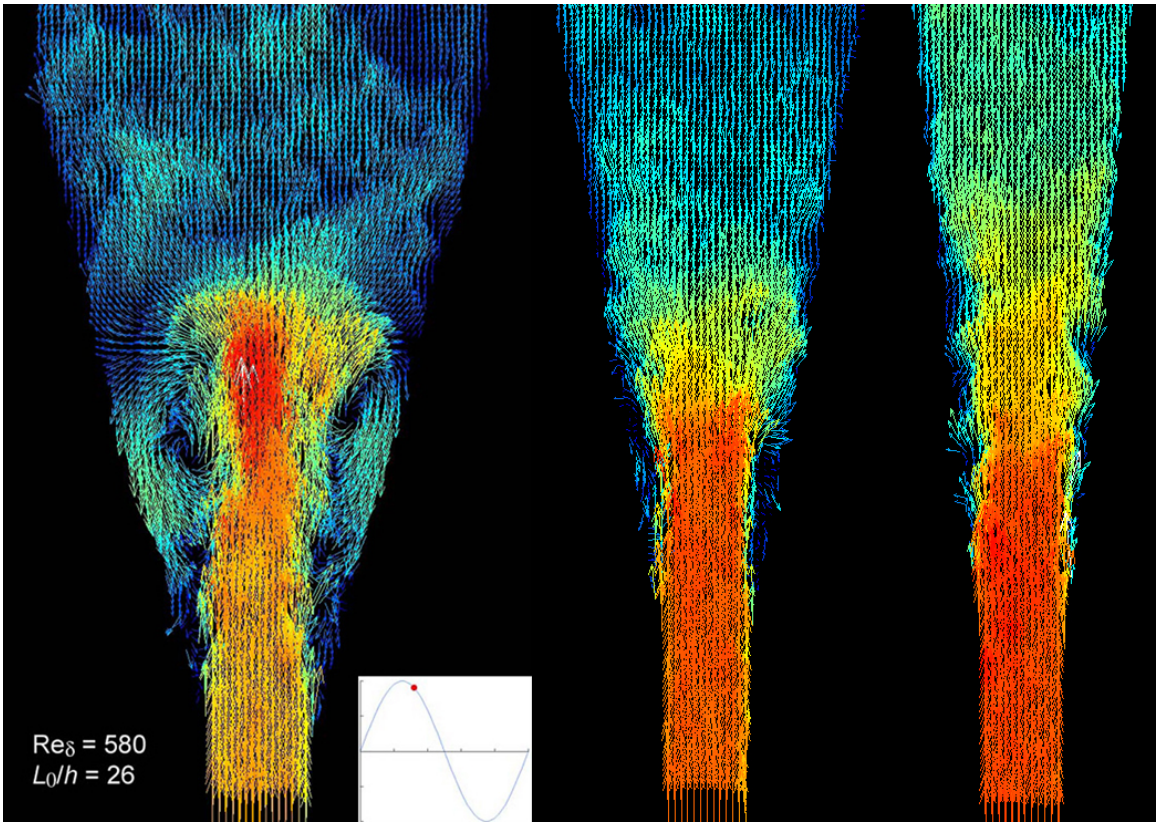

Fig. 5.2: Comparison at $t/T = 0.32$ of three cases where $Re_\delta = 580$ and $L_0/h = 26$ with $u_0 = 0$.

The flow in the 20° diffuser has also separated at $t/T = 0.24$, but the separation occurs after the separation in the 30° diffuser and the reattachment occurs sooner. As with all the geometries in this study, there is a sudden increase in turbulence when the flow begins to decelerate.

The flow in the 12° diffuser remains attached during the accelerating portion of the cycle in all cases. As the flow begins to decelerate (shown in Figure 5.2) there is a sudden onset of turbulence. The flow in this geometry, however, is attached for longer than the flow through the wider diffusers. These observations lead to the expectation that the losses decrease with decreasing diffuser angle (the same trend is seen in steady flow.) This observation is confirmed using the measured time-averaged pressure and Equation 2.19.

The zoomed-in PIV data can be used to plot the point in the cycle where the flow separates at a given location. Figure 5.3 shows the separation time for oscillating flow

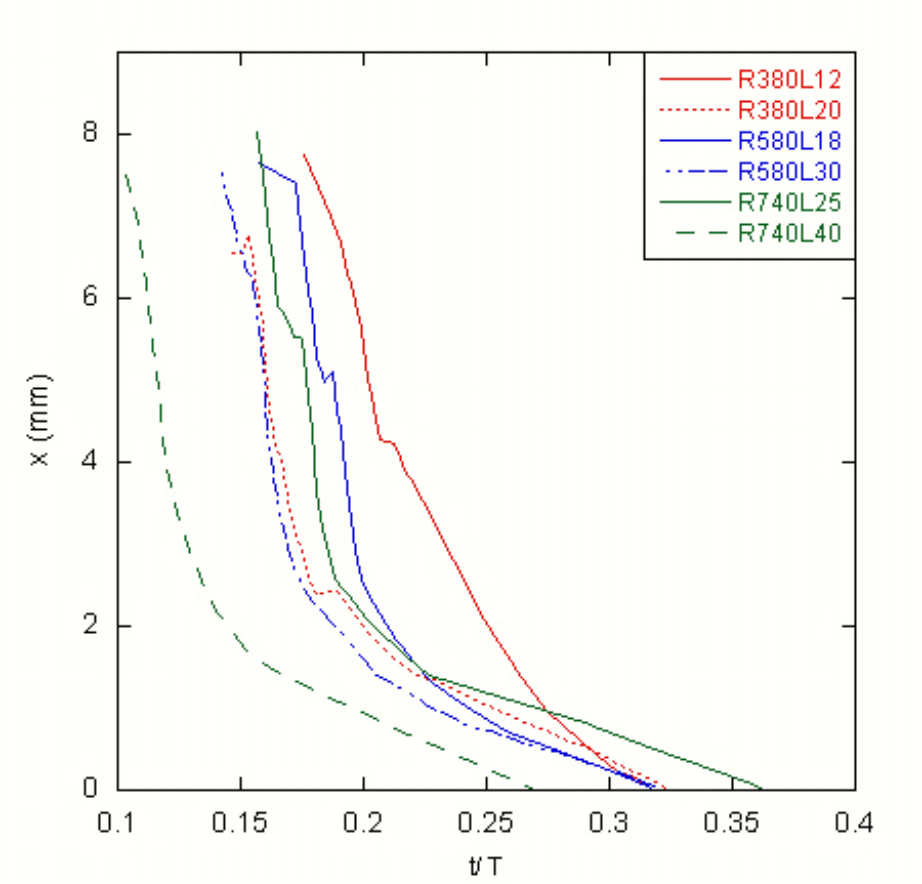

Fig. 5.3: Separation time for flow through the 30° diffuser.

through the 30° diffuser, where the separation time is defined as the first point in the blowing portion of the cycle where the velocity vector nearest to the wall has a negative x-component. Figure 5.4 shows the separation time in the 12° diffuser. Separation in the 20° diffuser closely resembles the flow through the 30° diffuser. In each plot, the beginning of the expansion is defined as $x = 0$.

In both geometries, the separation begins high in the diffuser and propagates downward. During the accelerating part of the blowing cycle, the flow stays attached further into the diffuser with increasing Reynolds number, increasing stroke length, and decreasing diffuser angle. During the decelerating portion of the blowing cycle, the flow remains attached longer with increasing Reynolds number and appears to be independent of the stroke length.

Watching movies of vector fields has already been mentioned as a way to visualize where

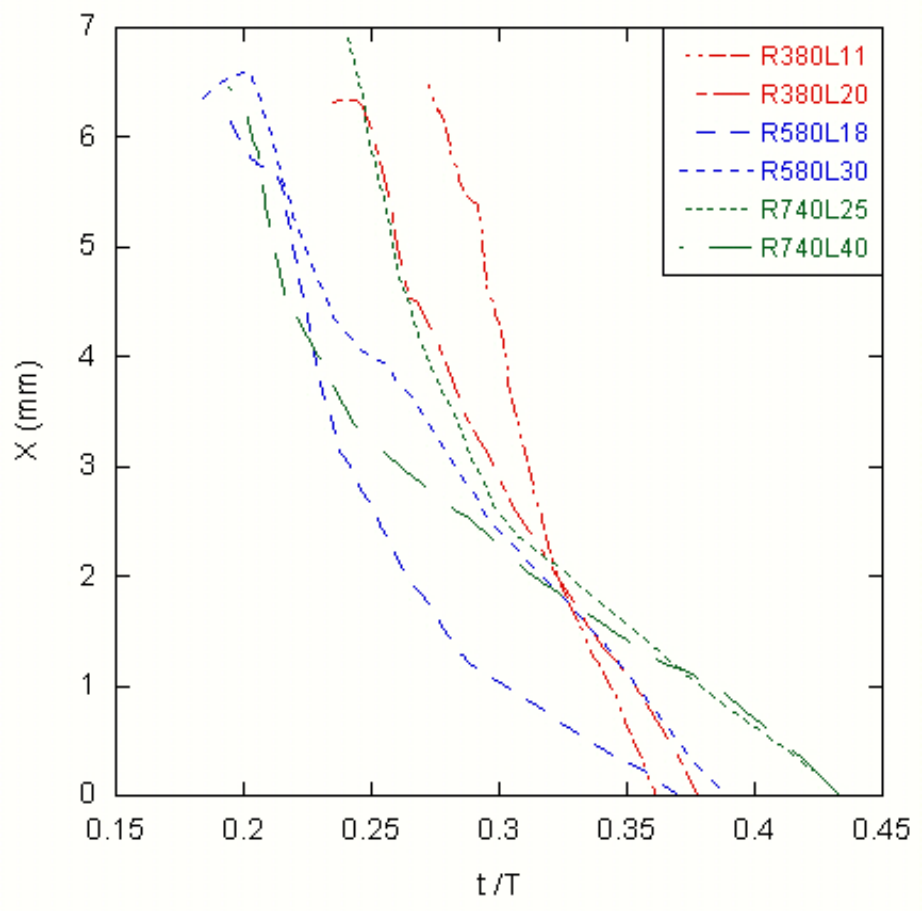

Fig. 5.4: Separation time for flow through the 12° diffuser.

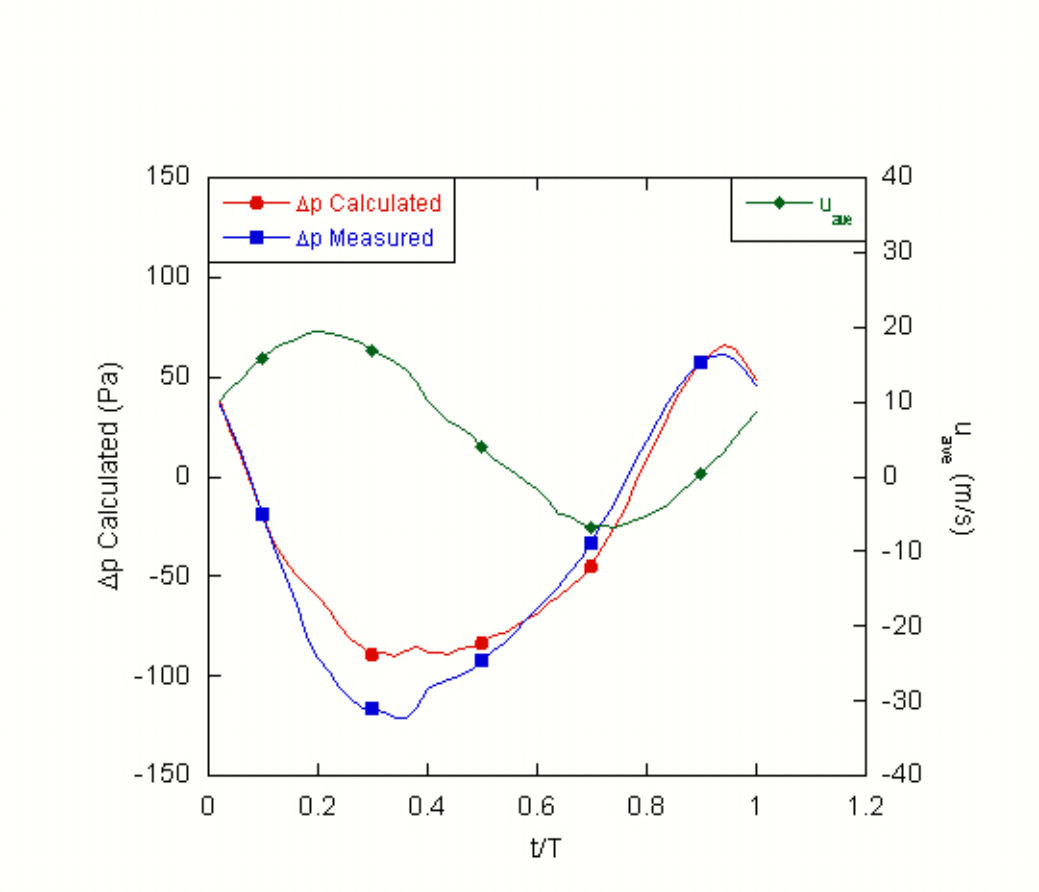

Fig. 5.5: Comparison of the measured pressure drop with the lossless pressure drop from the Bernoulli equation for $Re_\delta = 580$, $L_0/h = 30$, and $u_0/u_{max} = 0.5$.

in the cycle the losses are generated. Another way is to compare the pressure drop across the diffuser to that predicted by the Bernoulli equation. This is calculated using phase-averaged data for each point in the cycle and plotted. Figure 5.5 shows a case from the 30° diffuser with $Re_\delta = 580$, $L_0/h = 30$, and $u_0/u_{max} = 0.5$. The measured pressure drop closely matches the lossless pressure drop until the flow separates. The greatest difference occurs during the decelerating portion of the blowing cycle.

Studying the PIV images, separation plots, and instantaneous pressure drop helps explain the loss coefficients calculated using Eq. 2.19. The minor loss coefficients for oscillating flow through the 30° diffuser are shown in Figure 5.6 as a function of the nondimensional displacement amplitude. The time-averaged pressure used to compute these loss factors

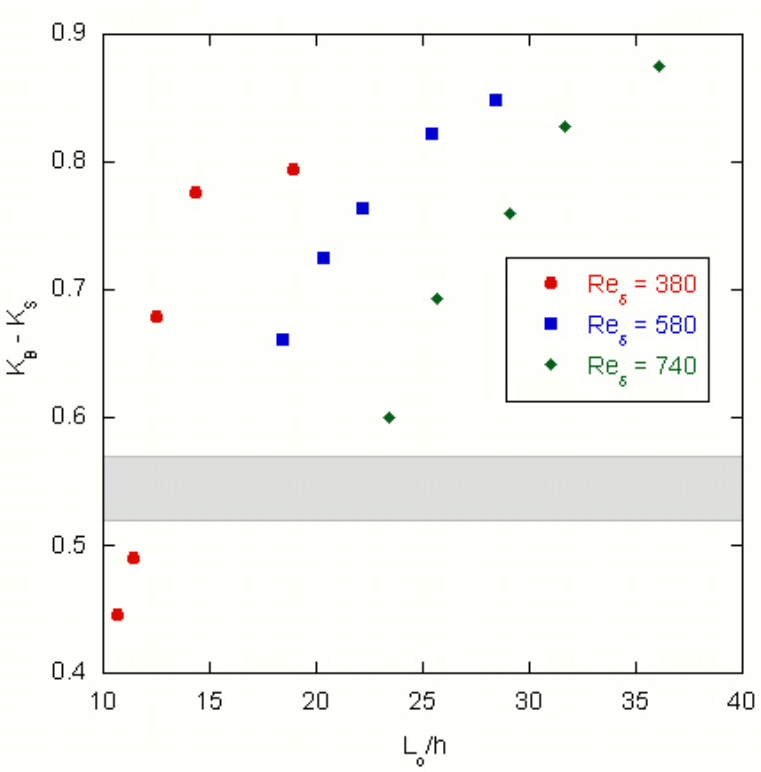

Fig. 5.6: The sum of the minor losses computed from the velocity waveform and the time-averaged pressure using Eq. 2.19 in the 30° diffuser. The gray region represents the range of minor loss coefficients for steady flow through the same geometry.

was taken from the sensors most central in the channel to avoid end effects. The gray region represents the range of minor loss coefficients for steady flow through an expansion in one plane (the value depends on the Reynolds number) from [39]. It can be seen that the losses increase with increasing stroke length and decrease with Reynolds number in the range shown in this plot.

For shorter stroke lengths, the losses associated with oscillating flow through this diffuser can be less than those of steady flow through the same geometry. While steady flow through a 30° diffuser would separate low in the diffuser and remain separated, oscillating flow through this geometry initially separates, then reattaches as the counterrotating vortices reach the walls. The flow remains attached for the remainder of the blowing cycle, leading to lower losses.

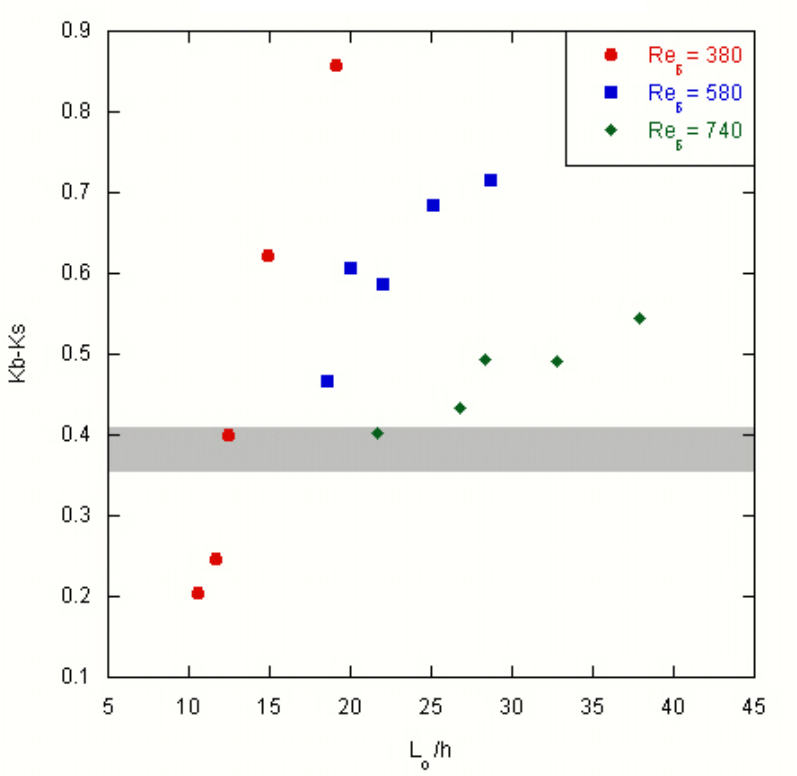

Fig. 5.7: The sum of the minor losses in the 20° diffuser computed from the velocity waveform and the time-averaged pressure using Eq. 2.19.

The minor loss coefficients for oscillating flow through the 20° diffuser are shown in Figure 5.7 and in the 12° diffuser are shown in Figure 5.8.

It can be seen that the trends in the losses are similar for all three diffusers. Three conclusions are drawn from the data:

1. The minor losses decrease with Reynolds number in the range of $380 < Re_\delta < 740$.

2. The losses increase with L_0/h in the range of $11 < L_0/h < 40$.

3. Depending on the stroke length, the loss can be greater than or less than the loss for steady flow through the same geometry.

To examine how the losses are affected with changes in diffuser angle, the losses are plotted by Reynolds number in Fig. 5.9 as a function of the stroke length. It can be seen that for a given stroke length, the losses decrease with decreasing diffuser angle. The

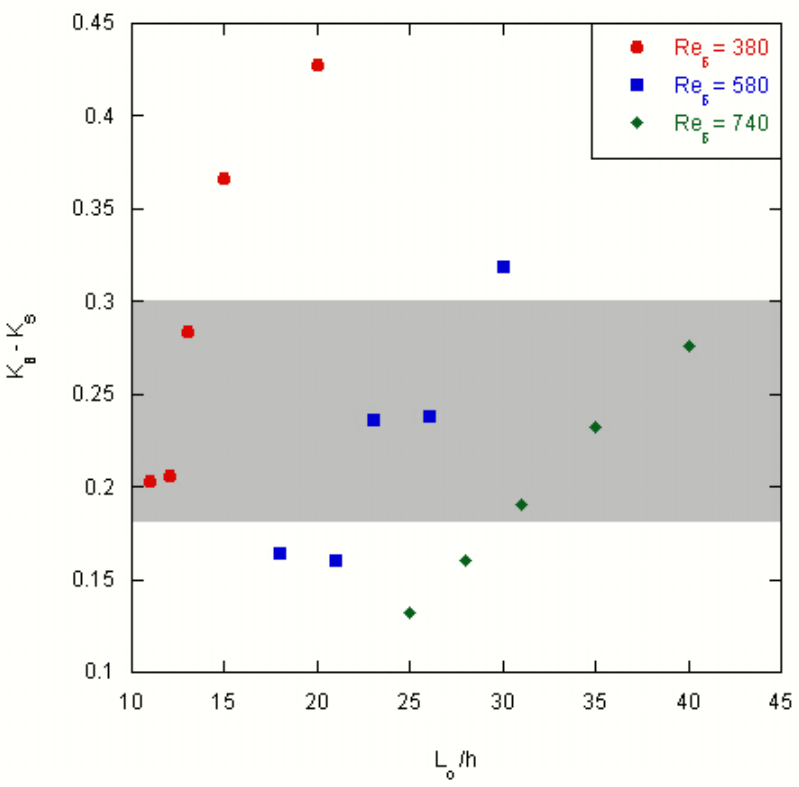

Fig. 5.8: The sum of the minor losses in the 12° diffuser computed from the velocity waveform and the time-averaged pressure using Eq. 2.19.

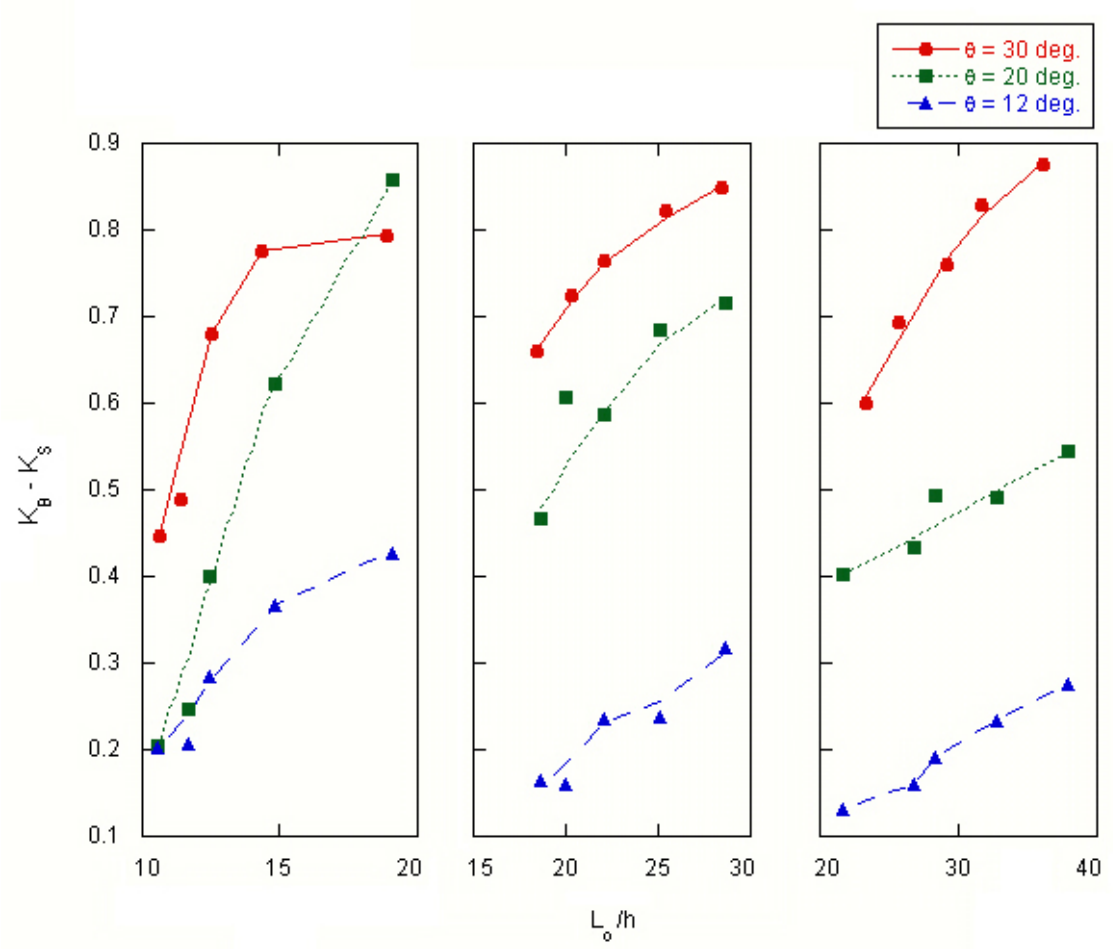

Fig. 5.9: The sum of the minor losses for $Re_\delta = 380$ (left plot), $Re_\delta = 580$ (center plot), and $Re_\delta = 740$ (right plot) as a function of the stroke length.

losses from the 20° diffuser appear in most cases to be closer to the 30° losses than to the 12° losses. This is likely because the flow in the 20° diffuser separates, forms vortex pairs (although the vortices reach the wall before they can form fully), and reattaches, much like the flow through the 30° diffuser. The flow in the 12° diffuser remains attached for the accelerating portion of the cycle, leading to less losses.

Due to the large amount of data collected, a correlation that predicts the loss coefficient for a given diffuser angle, Reynolds number, and stroke length is desirable. One possibility is

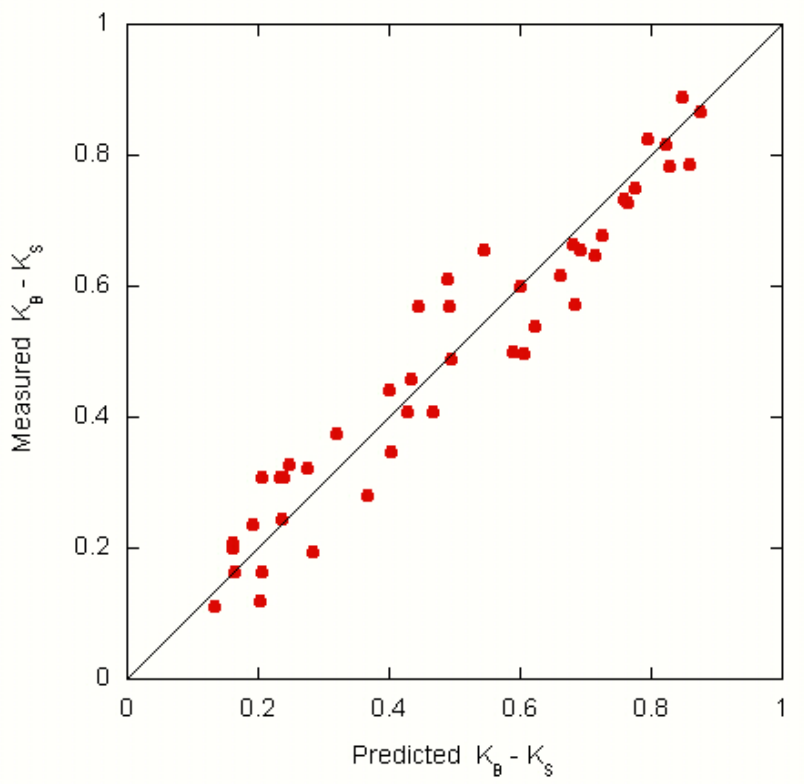

Fig. 5.10: Predicted loss coefficient versus measured loss coefficient for the oscillating only cases. A prediction with no error would lie on the 45° line.

$$K_B - K_S = 12.62(L_o/h)^{0.038} - 8.54(Re_\delta)^{1.36} - 0.96(l/h)^{0.31} - 11.65 \qquad (5.1)$$

where l is the diffuser length. Figure 5.10 shows the predicted loss coefficient versus the measured loss coefficient (an exactly correct prediction would lie on the 45° line).

5.1.2 Pulsating Flow

The minor losses for oscillating flow with a steady component vary with the Reynolds number, stroke length, diffuser angle, and with the ratio of the steady flow velocity to the peak oscillating velocity. Figure 5.11 shows flow in the 30° diffuser with $Re_\delta = 380$ and $L_0/h = 20$ at $t/T = 0.34$, or just as the flow begins to decelerate. The image on the left is flow with no steady component ($u_0/u_{max} = 0$) and the image on the right is flow with $u_0/u_{max} = 1$. While the purely oscillatory flow separates, forms counterrotating vortices,

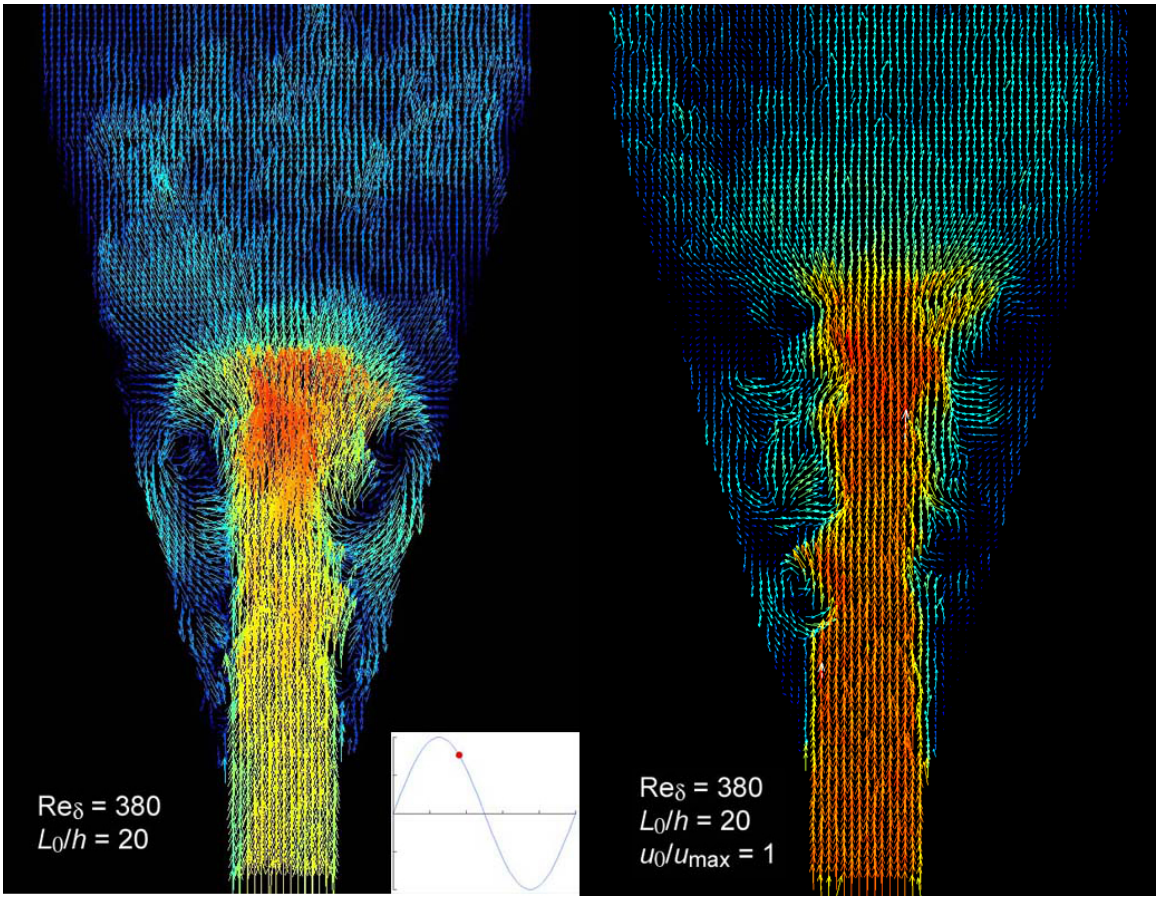

Fig. 5.11: PIV field comparison of $u_0/u_{max} = 0$ and $u_0/u_{max} = 1$ for $Re_\delta = 380$ and $L_0/h = 20$.

and reattaches, the steady component of the pulsating flow pushes the vortices through the diffuser before they can reach the walls to reattach. Thus the addition of steady flow can be thought of as increasing the "effective" blowing stroke length of the case. This would lead us to presume that losses increase with increasing steady flow ratio.

At the peak of the blowing cycle, however, the flow on the right of Figure 5.11 has an instantaneous channel-width-based Reynolds number twice that of the oscillating only case (which should reduce the losses). Thus, two competing effects are observed.

The loss coefficients were calculated using the time-averaged pressure data and phase-averaged velocity data using Eq. 2.19. The results for flow in the 30° diffuser for $Re_\delta = 380$ are shown in Figure 5.12, for $Re_\delta = 580$ in Figure 5.13, and for $Re_\delta = 740$ in Figure 5.14. For

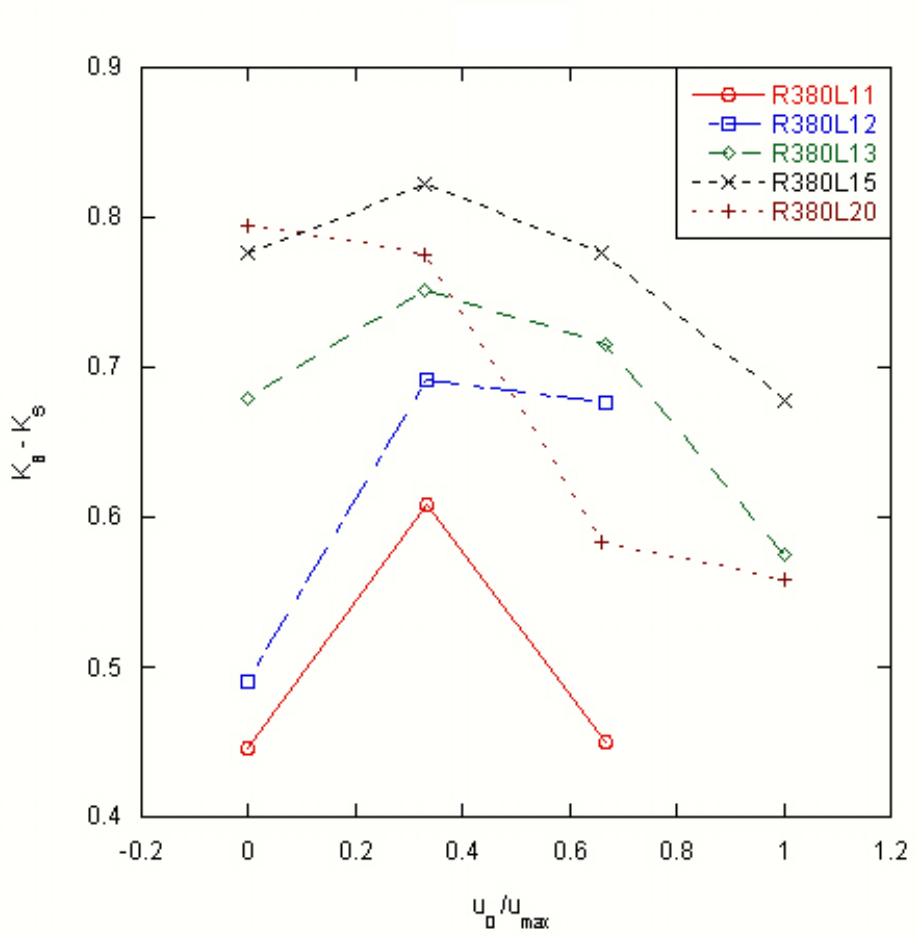

Fig. 5.12: Minor loss coefficients for varying u_0/u_{max} with $Re_\delta = 380$ in the 30° diffuser.

small u_0/u_{max}, the losses increase, suggesting that the "effective" stroke length dominates. As u_0/u_{max} approaches 1, the losses decrease, sometimes to below the oscillating only losses, suggesting that in this region the channel-width-based Reynolds number dominates.

The results were similar for flow in the 12° and 20° diffusers. The losses in the 20∘ diffuser for $Re_\delta = 380$ are shown in Figure 5.15, for $Re_\delta = 580$ in Figure 5.16, and for $Re_\delta = 740$ in Figure 5.17. The 12° results are shown in Figure 5.18, for $Re_\delta = 580$ in Figure 5.19, and for $Re_\delta = 740$ in Figure 5.20.

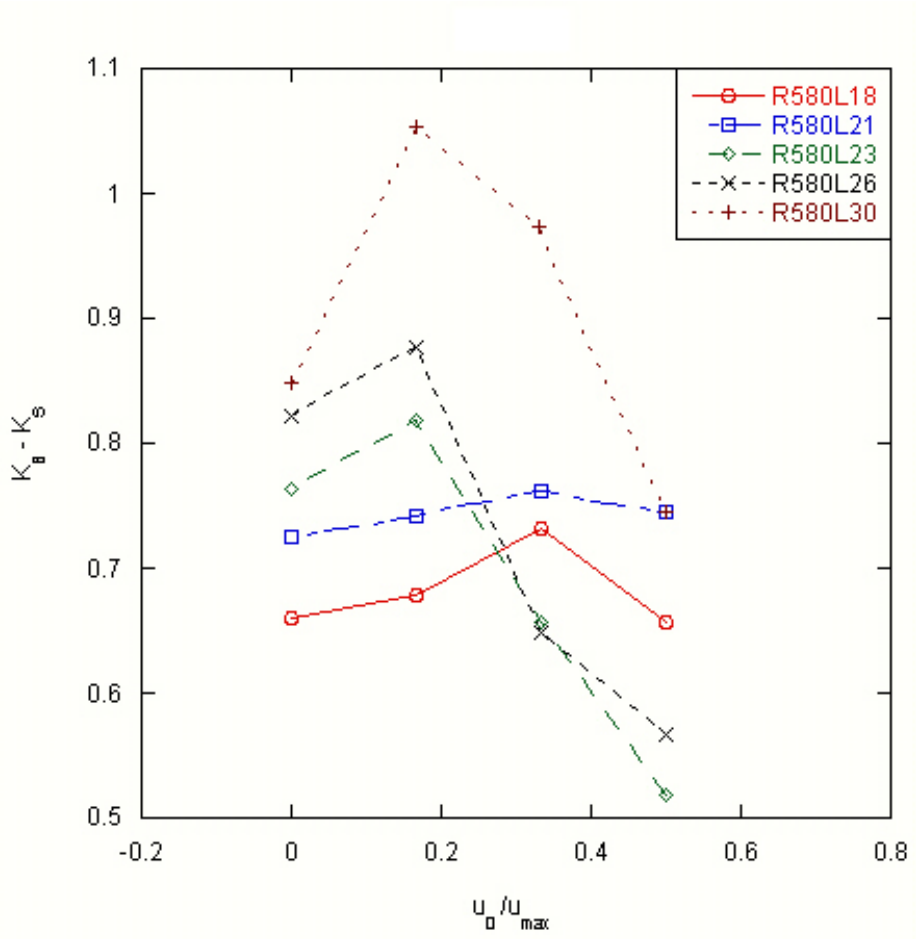

Fig. 5.13: Minor loss coefficients for varying u_0/u_{max} with $Re_\delta = 580$ in the 30° diffuser.

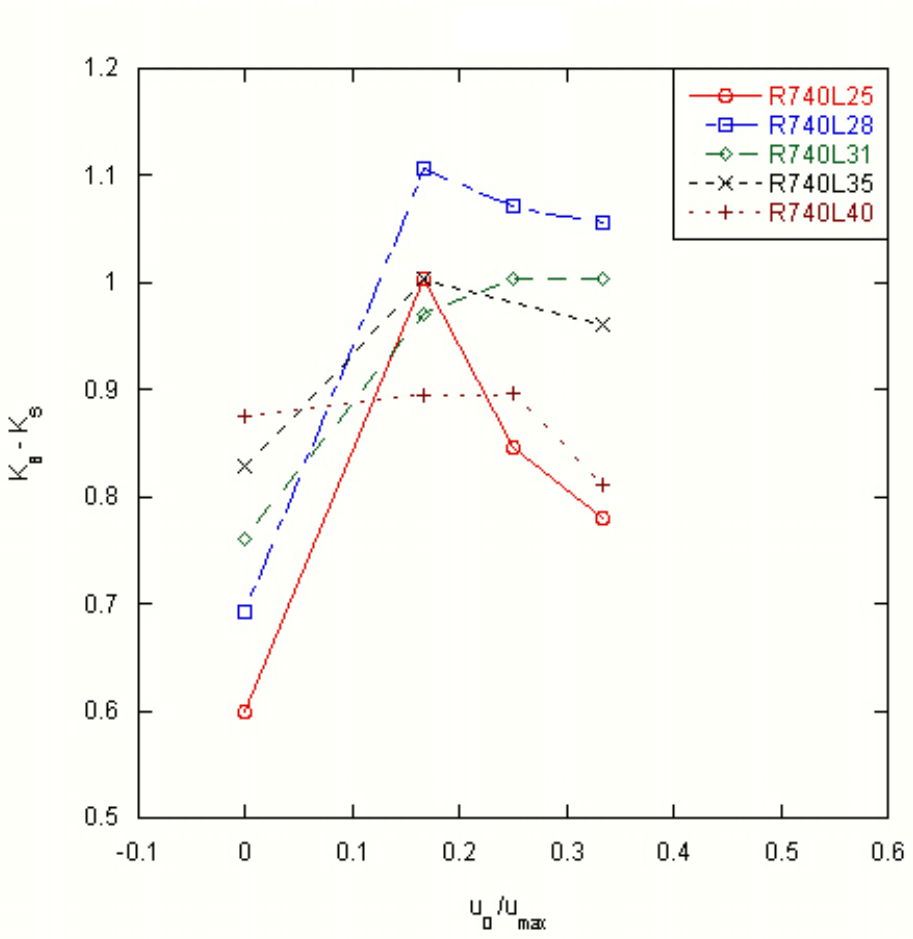

Fig. 5.14: Minor loss coefficients for varying u_0/u_{max} with $Re_\delta = 740$ in the 30° diffuser.

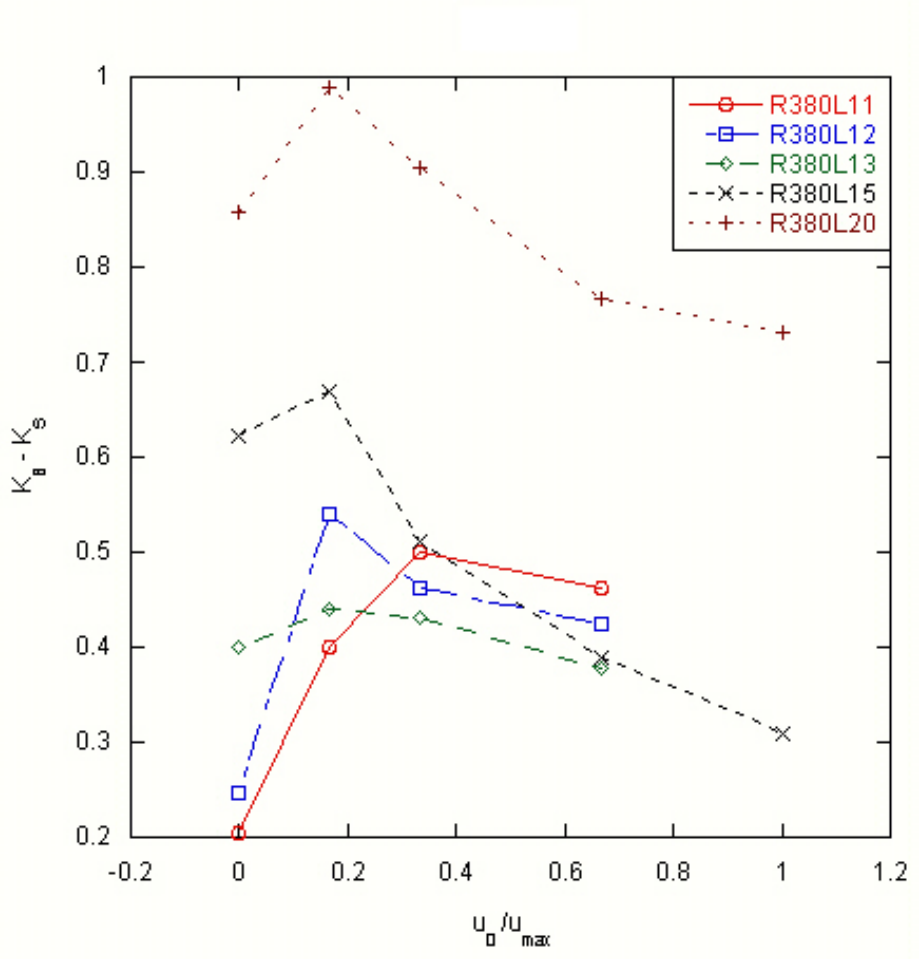

Fig. 5.15: Minor loss coefficients for varying u_0/u_{max} with $Re_\delta = 380$ in the 20° diffuser.

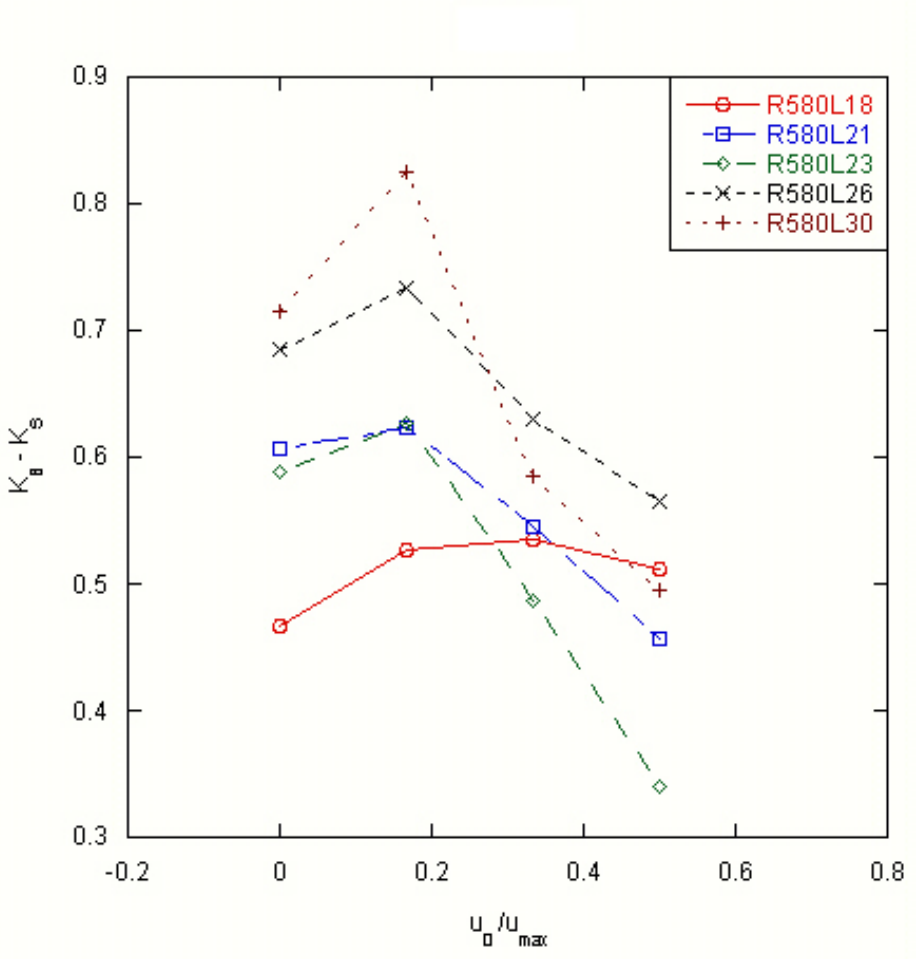

Fig. 5.16: Minor loss coefficients for varying u_0/u_{max} with $Re_\delta = 580$ in the 20° diffuser.

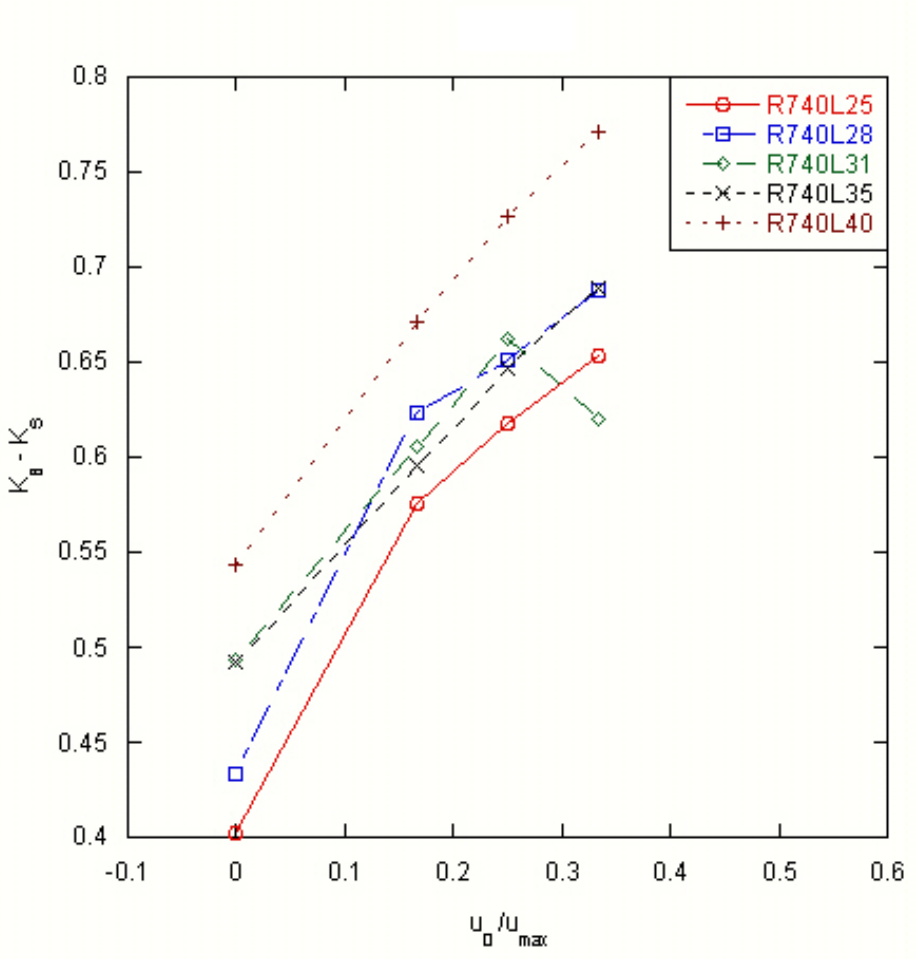

Fig. 5.17: Minor loss coefficients for varying u_0/u_{max} with $Re_\delta = 740$ in the 20° diffuser.

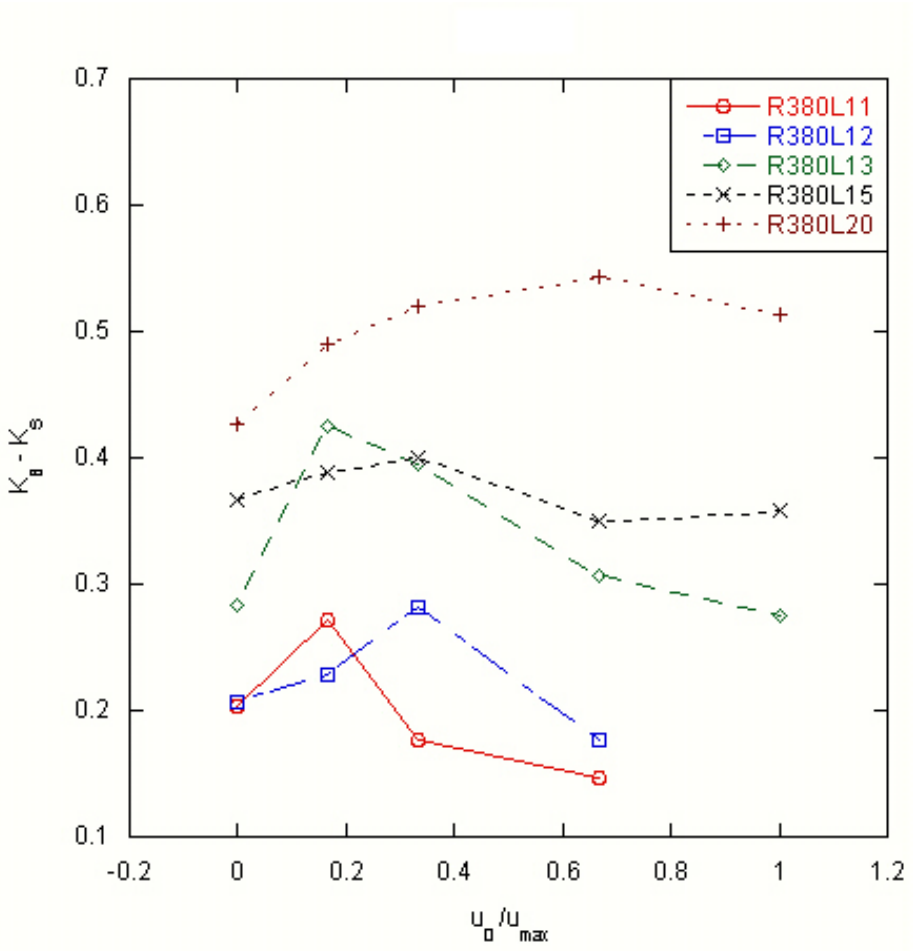

Fig. 5.18: Minor loss coefficients for varying u_0/u_{max} with $Re_\delta = 380$ in the 12° diffuser.

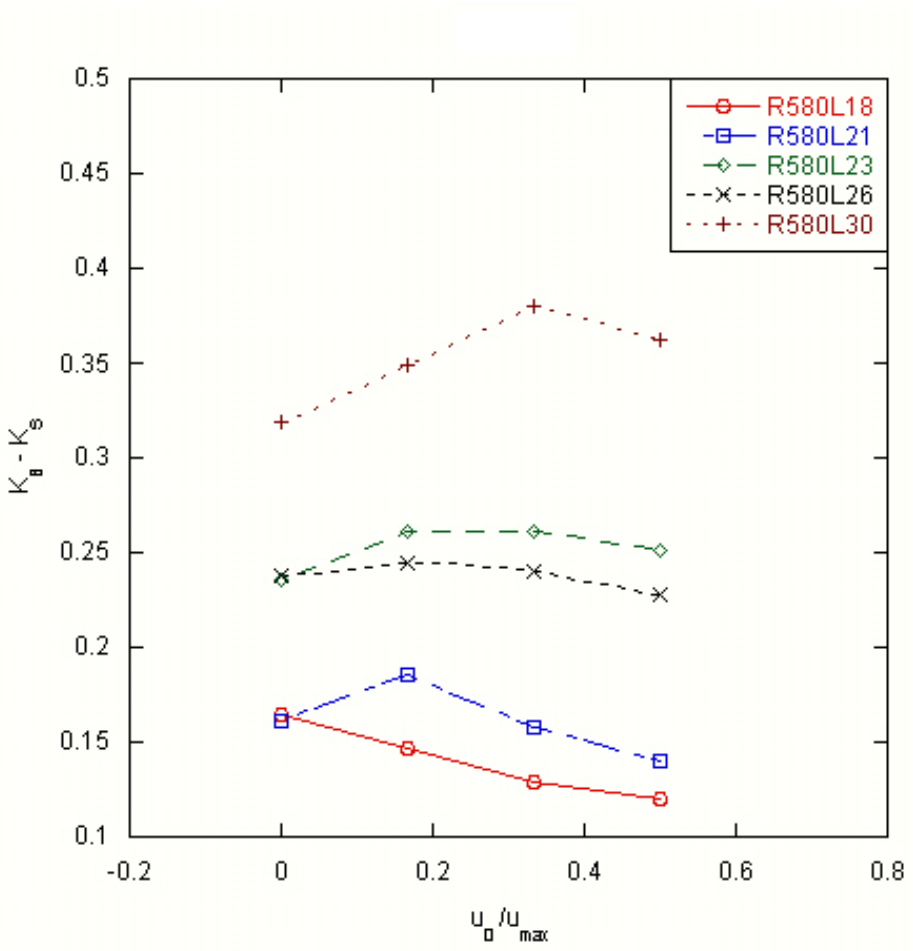

Fig. 5.19: Minor loss coefficients for varying u_0/u_{max} with $Re_\delta = 580$ in the 12° diffuser.

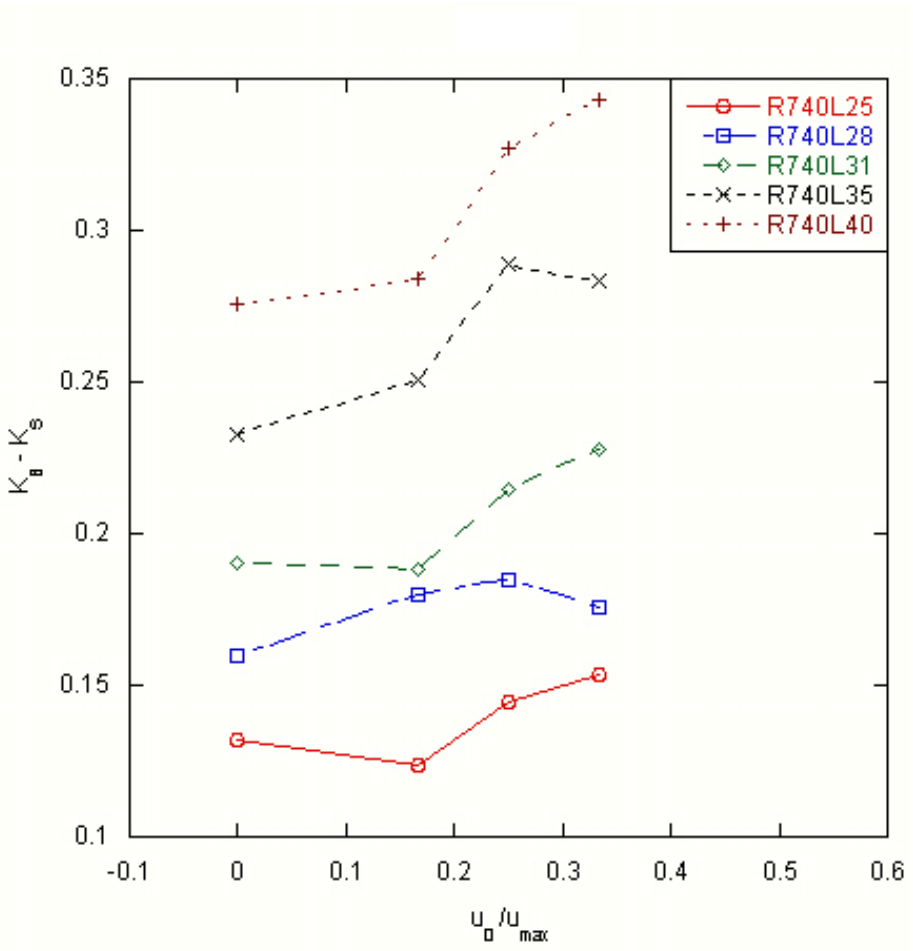

Fig. 5.20: Minor loss coefficients for varying u_0/u_{max} with $Re_\delta = 740$ in the 12° diffuser.

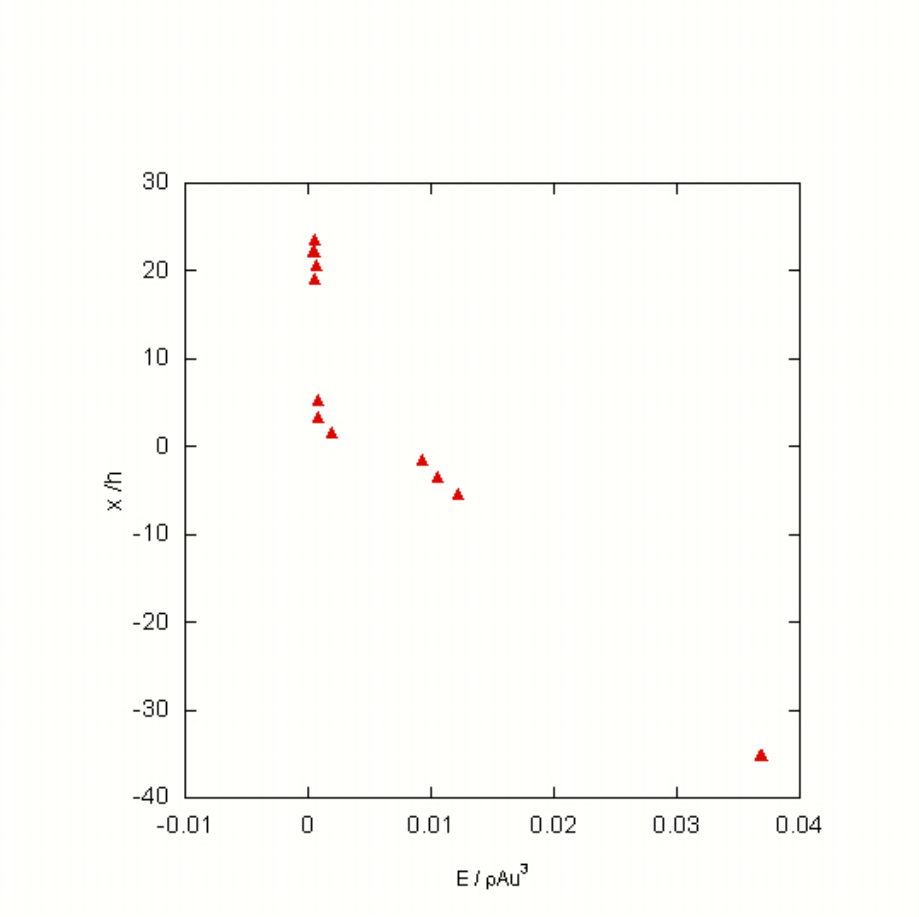

Fig. 5.21: Nondimensional acoustic power at each pressure sensor location in the 30° diffuser.

5.2 Acoustic Power Dissipation

5.2.1 Oscillating Flow

The average acoustic power over a cycle at each pressure sensor location was calculated using Eq. 2.20. Figure 5.21 shows how the average acoustic power over 100 cycles varies at each sensor location in the 30° diffuser for $Re_\delta = 580$ and $L_0/h = 30$. The data from the upper four sensors and from the three sensors below the diffuser is extrapolated to $x = 0$, and the difference is the acoustic power dissipation across the diffuser.

The nondimensional acoustic power dissipation in the 30° diffuser is shown in Figure 5.22. The 20° degree results are shown in Figure 5.23, and the 12° degree results are shown in Figure 5.24. The trends in the acoustic power dissipation follow those from the minor

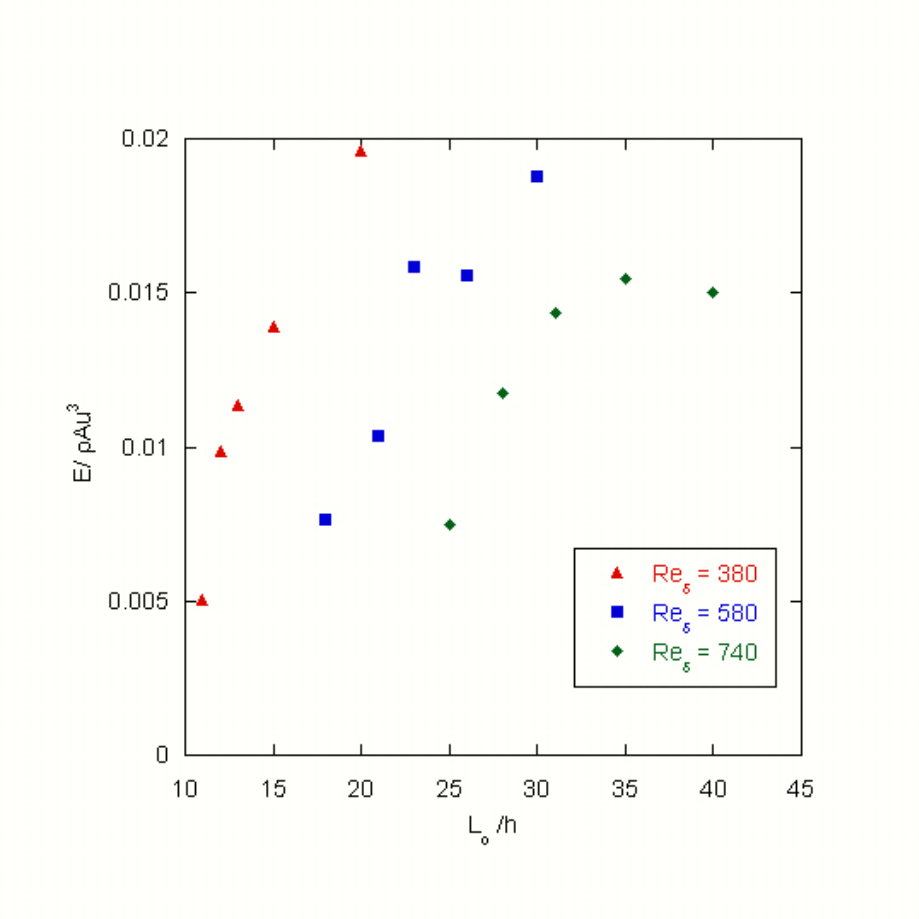

Fig. 5.22: Nondimensional acoustic power dissipation as a function of Reynolds number and stroke length in the 30° diffuser.

loss calculations, namely:

1. The nondimensional acoustic power dissipation increases with stroke length in the range of L_0/h in the range of $11 < L_0/h < 40$.

2. The acoustic power dissipation decreases with Reynolds number in the range of $380 < Re_\delta < 740$.

To examine how the acoustic power dissipation changes with the diffuser angle, the nondimensional power dissipation is plotted by Reynolds number in Figure 5.25. Just as with the losses, the power dissipation increases with increasing diffuser angle.

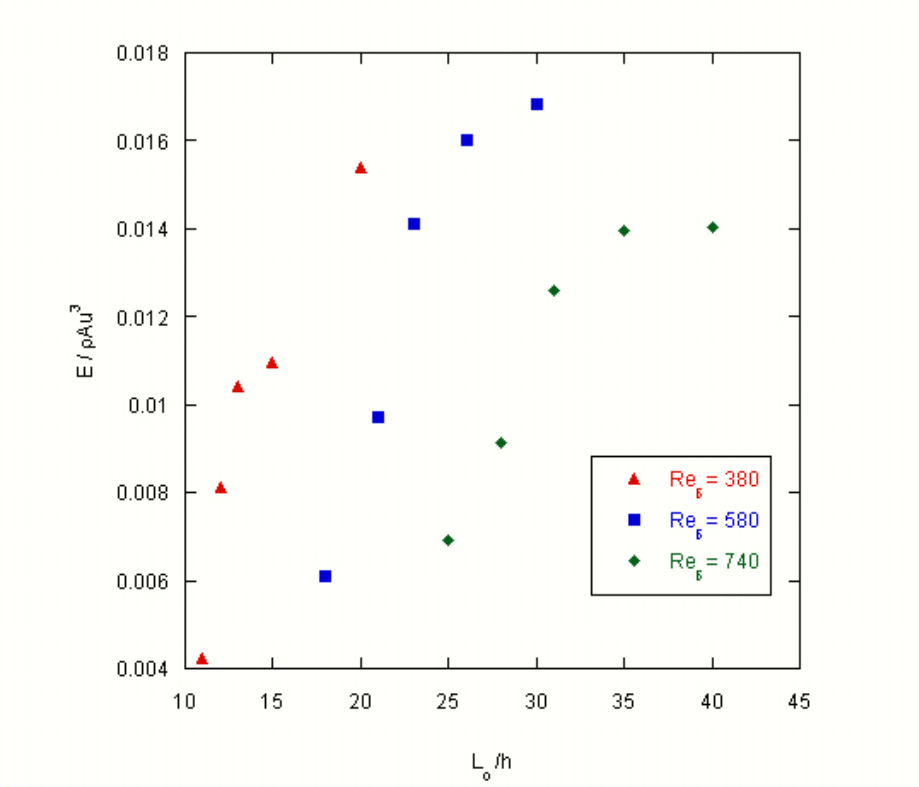

Fig. 5.23: Nondimensional acoustic power dissipation as a function of Reynolds number and stroke length in the 20° diffuser.

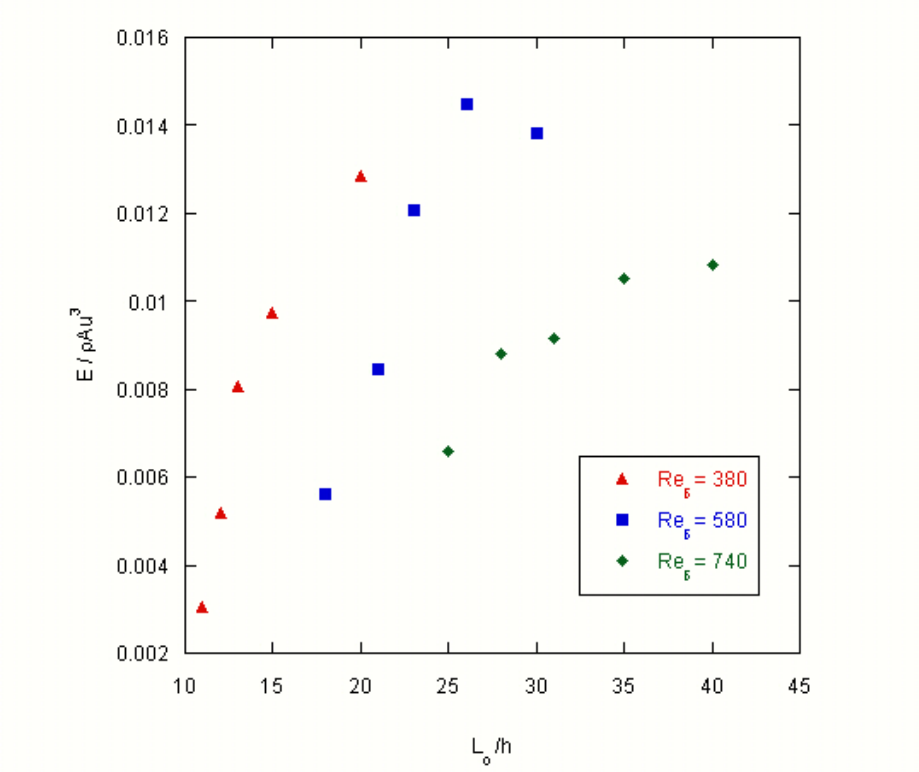

Fig. 5.24: Nondimensional acoustic power dissipation as a function of Reynolds number and stroke length in the 12° diffuser.

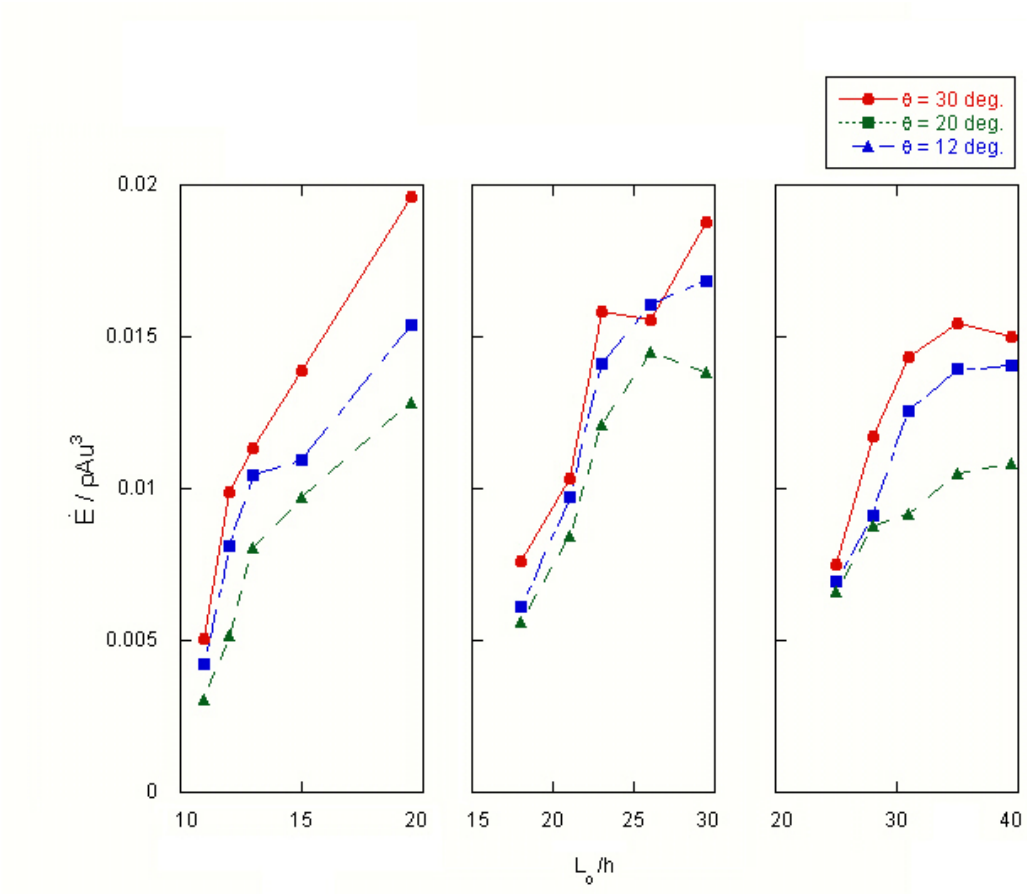

Fig. 5.25: Nondimensional acoustic power dissipation for $Re_\delta = 380$ (left plot), $Re_\delta = 580$ (center plot), and $Re_\delta = 740$ (right plot) as a function of the stroke length.

5.2.2 Pulsating Flow

As described in section 2.7.2, the acoustic power dissipated by the oscillating portion of the flow was calculated by finding the total acoustic power dissipation and subtracting the steady power dissipation. The data confirms that the addition of a steady component changes the oscillating portion of the acoustic power dissipation.

The oscillating component of the acoustic power dissipation in the 12° diffuser is shown in Figure 5.26 for the $Re_\delta = 380$ cases. In some cases, the power dissipation increases with u_0/u_{max} for small u_0/u_{max}, then decreases to the oscillating only level or below as u_0/u_{max} approaches one. However, it appears that the data is too inconsistent to establish a definite trend. It should be noted that this measurement is highly sensitive to the phase difference between the pressure and velocity waveforms (this topic is further discussed in section 5.3).

The oscillating component of the acoustic power dissipation in the 12° diffuser for the $Re_\delta = 580$ cases is shown in Figure 5.27 and for the $Re_\delta = 740$ cases in Figure 5.28. The 20° degree results are shown in Figure 5.29 for the $Re_\delta = 380$ cases, in Figure 5.30 for the $Re_\delta = 580$ cases, and in Figure 5.31 for the $Re_\delta = 740$. The 30° degree results are shown in Figure 5.32 for the $Re_\delta = 380$ cases, in Figure 5.33 for the $Re_\delta = 580$ cases, and in Figure 5.34 for the $Re_\delta = 740$.

5.3 Acoustic Impedance

The acoustic impedance for oscillating flow through each diffuser was calculated using Eqs. 2.29 and 2.30. The amplitudes and phases of the pressure and velocity signals were calculated using a discrete fourier transform. The nondimensional resistance results from each diffuser are shown in Figure 5.35. Also plotted are results from Wilen and Petculescu [34] from a 7° axisymmetric diffuser that is small in diameter compared to those used in the present study. The nondimensional resistance is independent of Reynolds number, decreases with increasing stroke length, and decreases with increasing diffuser angle.

The nondimensional inertance results from each diffuser are shown in Figure 5.36 along with those from [34]. While Wilen and Petculescu's data was taken over a wider range of

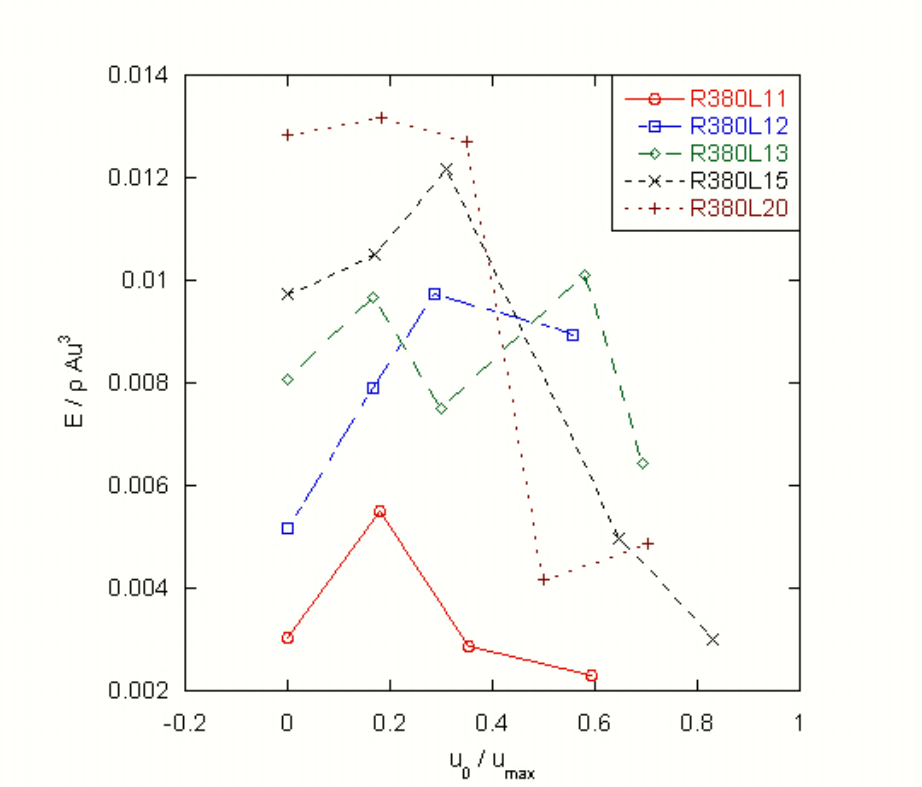

Fig. 5.26: Nondimensional acoustic power dissipation for the $Re_\delta = 380$ cases in the 12° degree diffuser.

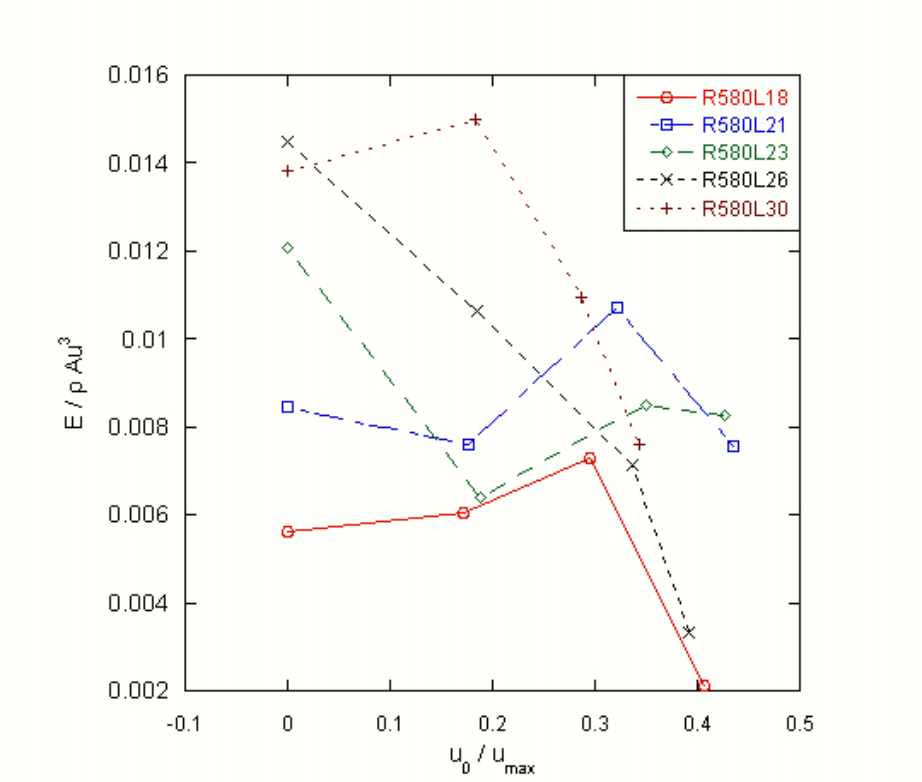

Fig. 5.27: Nondimensional acoustic power dissipation for the $Re_\delta = 580$ cases in the 12° degree diffuser.

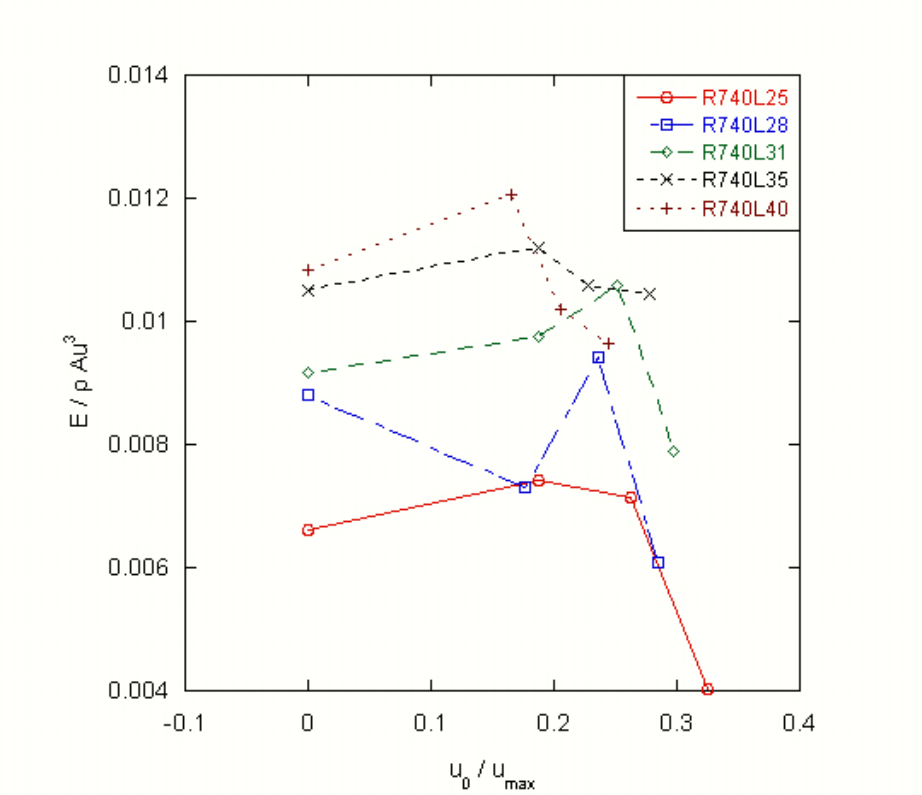

Fig. 5.28: Nondimensional acoustic power dissipation for the $Re_\delta = 740$ cases in the 12° degree diffuser.

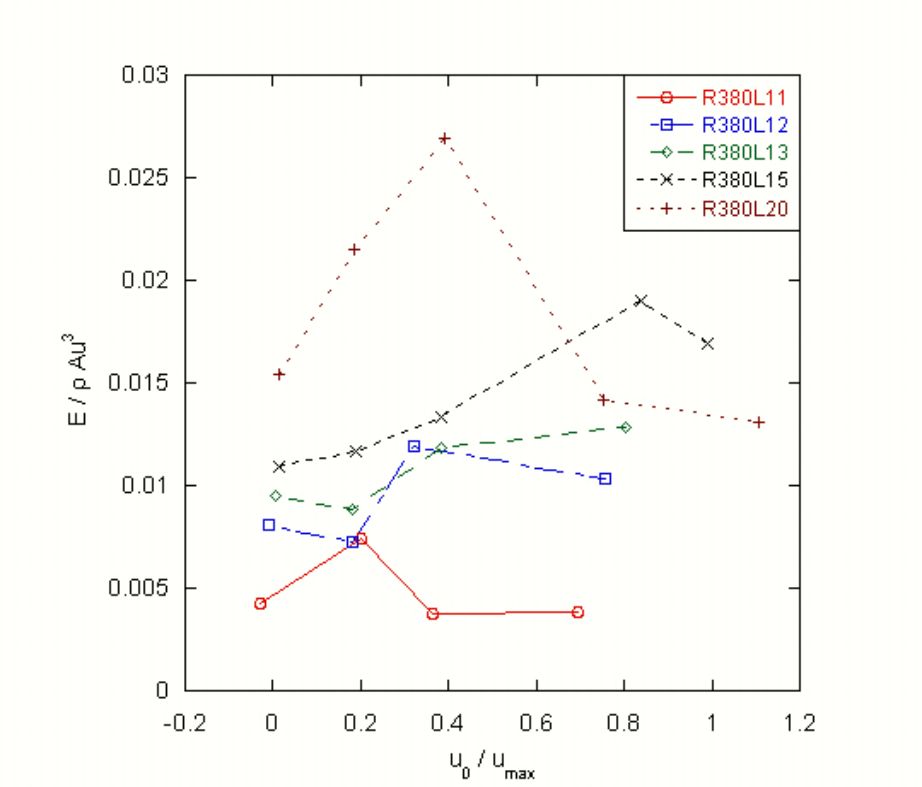

Fig. 5.29: Nondimensional acoustic power dissipation for the $Re_\delta = 380$ cases in the 20° degree diffuser.

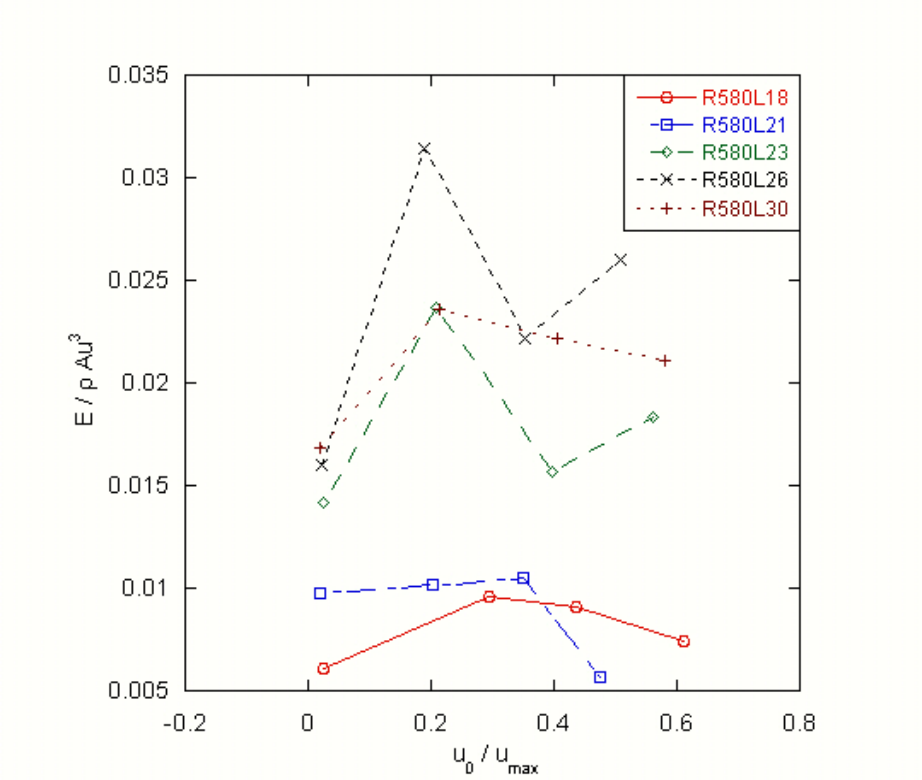

Fig. 5.30: Nondimensional acoustic power dissipation for the $Re_\delta = 580$ cases in the 20° degree diffuser.

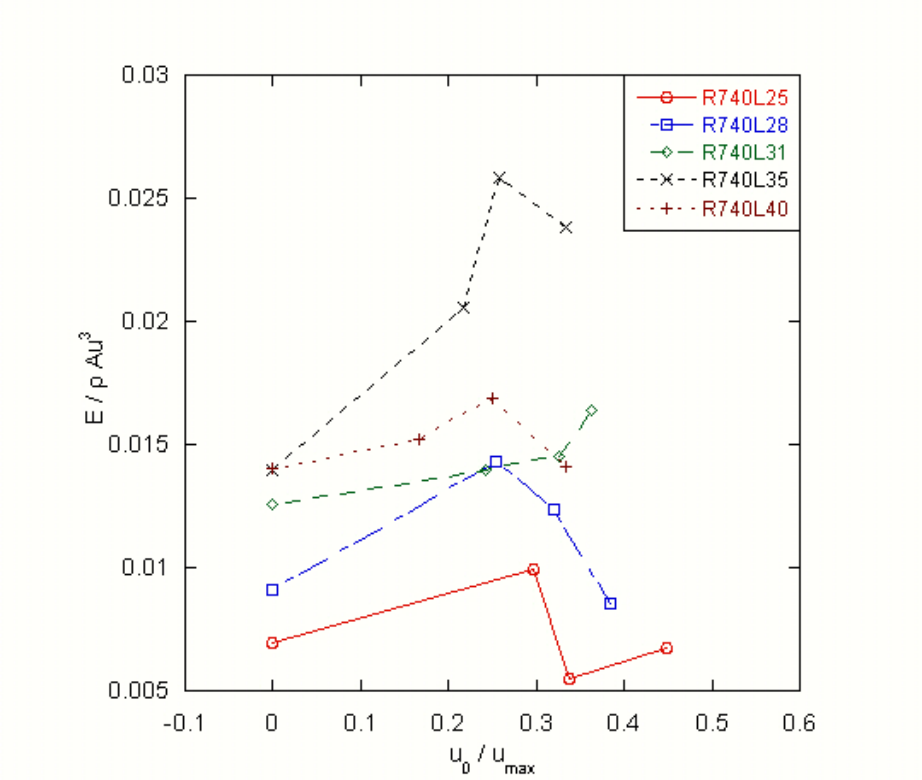

Fig. 5.31: Nondimensional acoustic power dissipation for the $Re_\delta = 740$ cases in the 20° degree diffuser.

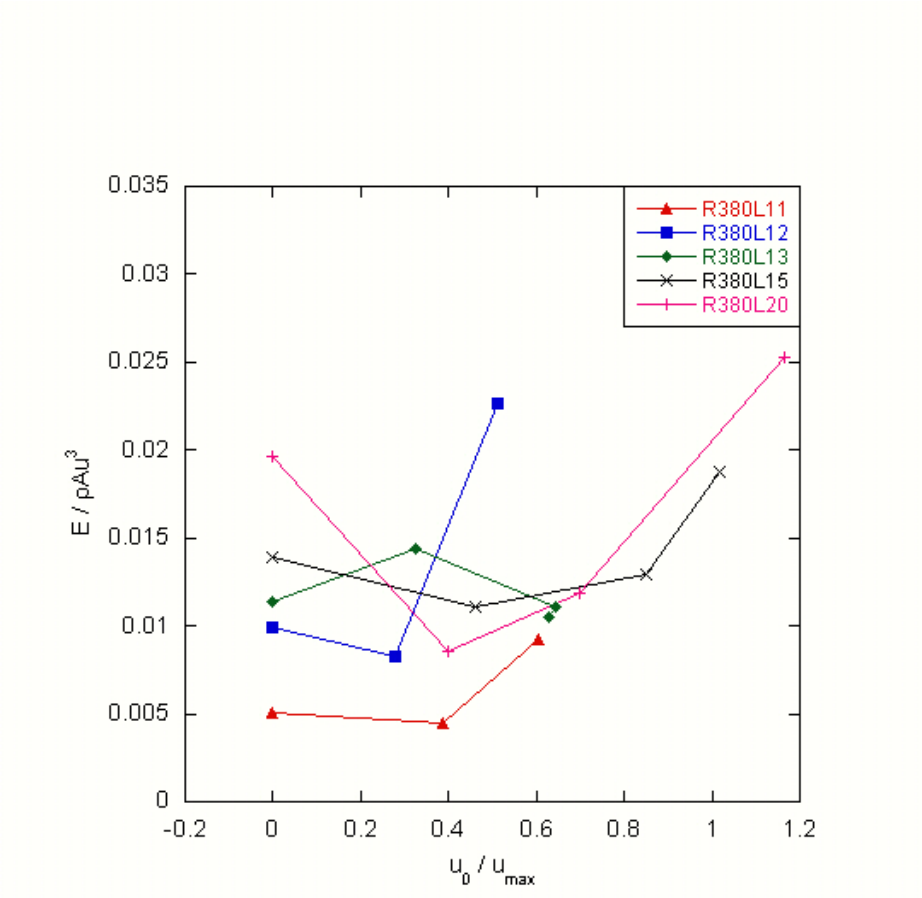

Fig. 5.32: Nondimensional acoustic power dissipation for the $Re_\delta = 380$ cases in the 30° degree diffuser.

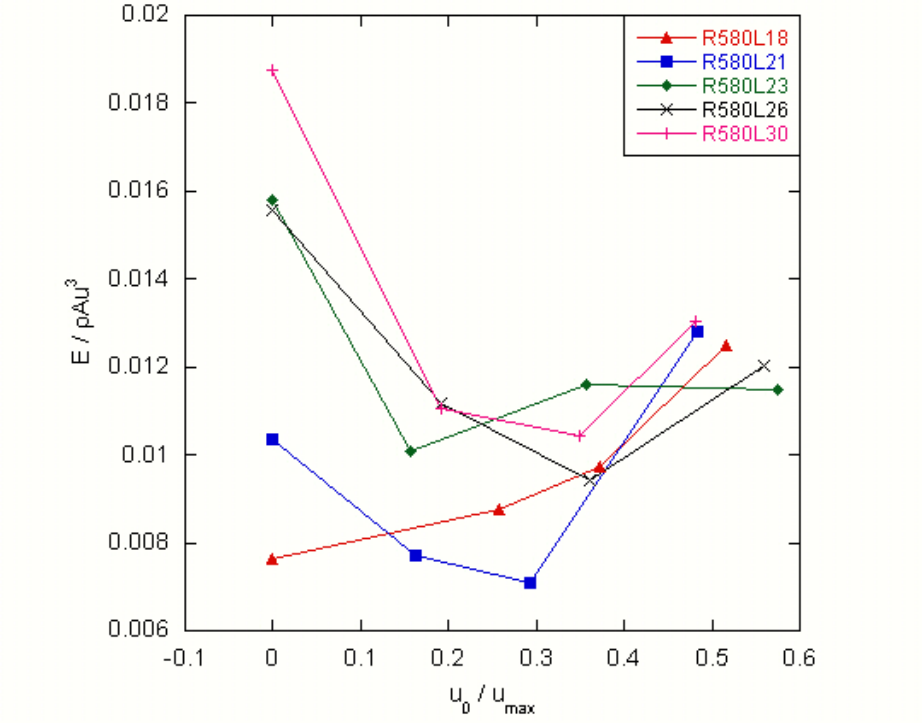

Fig. 5.33: Nondimensional acoustic power dissipation for the $Re_\delta = 580$ cases in the 30° degree diffuser.

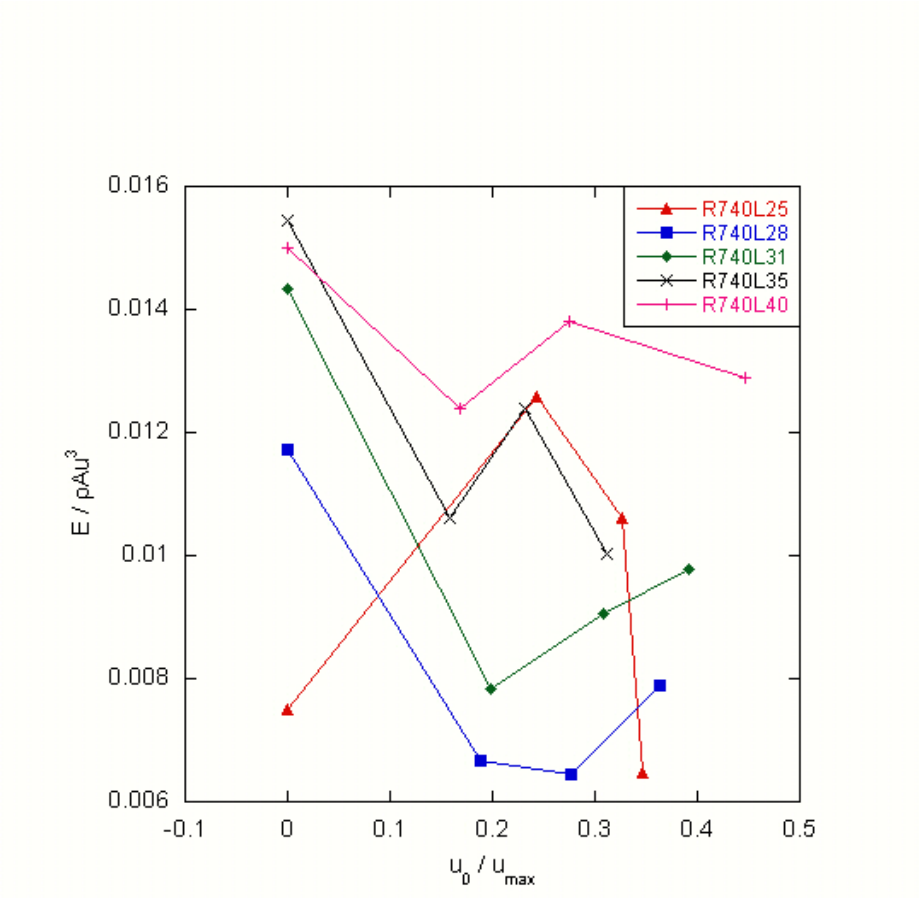

Fig. 5.34: Nondimensional acoustic power dissipation for the $Re_\delta = 740$ cases in the 30° degree diffuser.

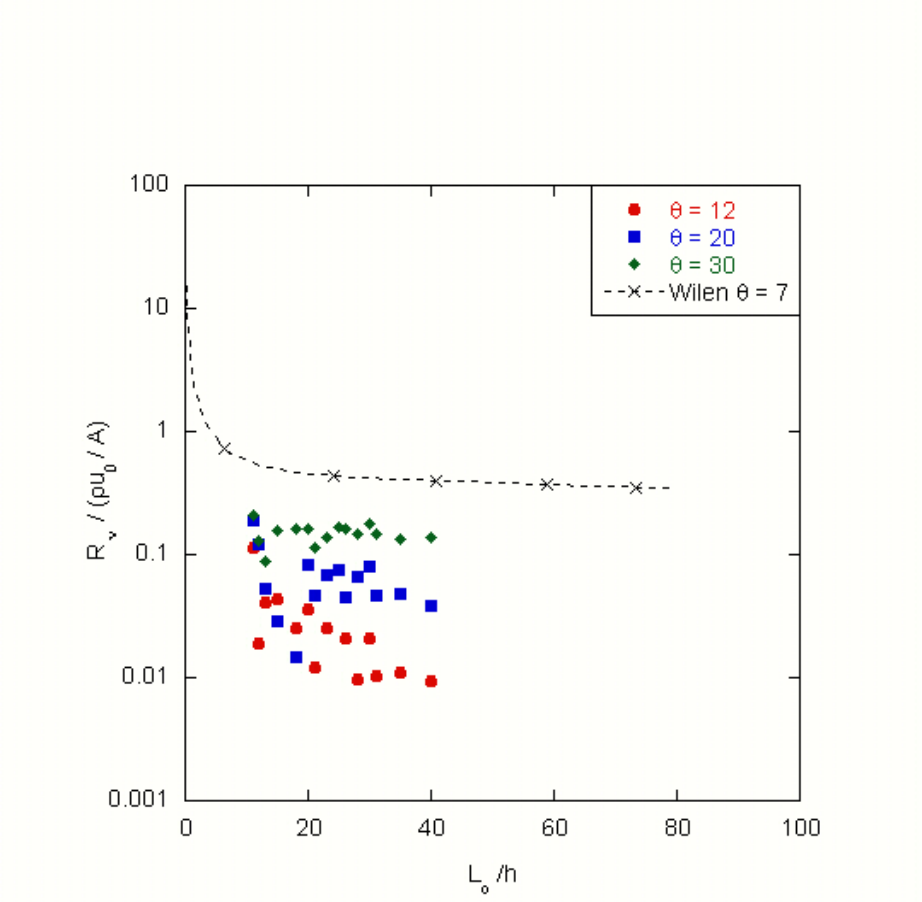

Fig. 5.35: Nondimensional resistance from each diffuser along with results from Wilen.

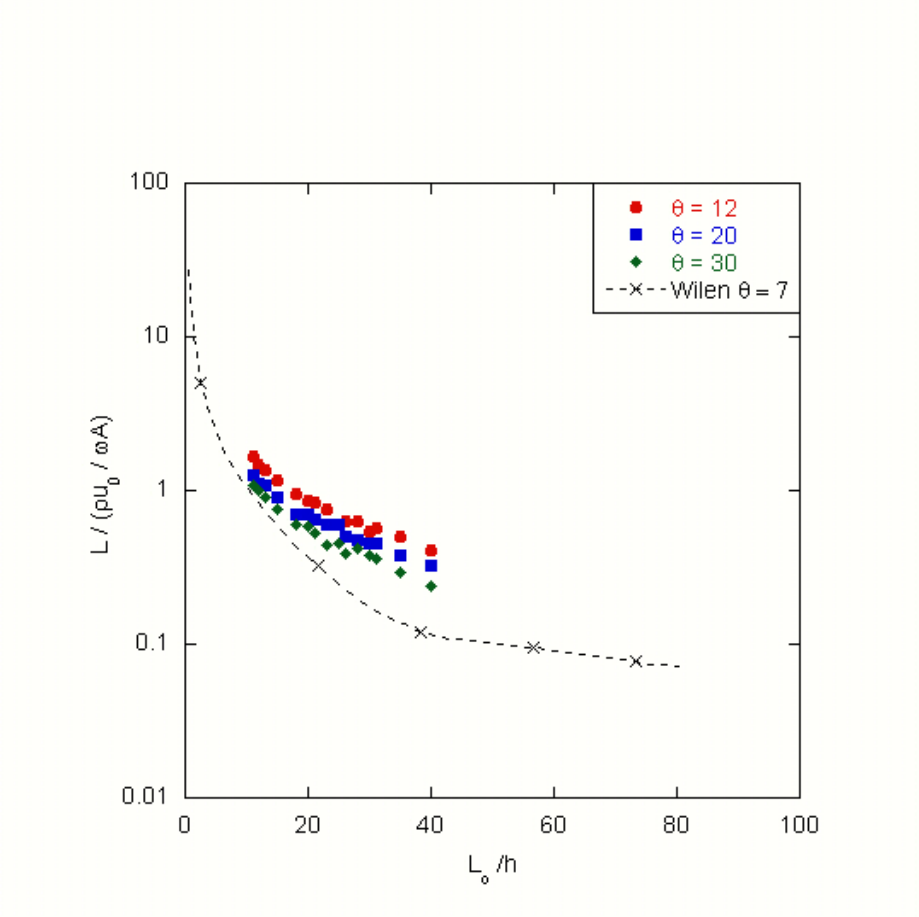

Fig. 5.36: Nondimensional inertance from each diffuser along with results from Wilen.

stroke lengths, the trends shown are the same, namely that the inertance decreases slightly with increasing stroke length and appears to be Reynolds number independent.

An examination of the uncertainty propagation in Eqs. 2.29 and 2.30 can explain why the resistance results (and also the acoustic power results) fluctuate. The uncertainty in the resistance measurement can be expressed as

$$(\sigma_{R_\nu})^2 = \left(\frac{\partial R_\nu}{\partial|\Delta P|}\right)^2 (\sigma_{|\Delta P|})^2 + \left(\frac{\partial R_\nu}{\partial|U|}\right)^2 (\sigma_{|U|})^2 + \left(\frac{\partial R_\nu}{\partial\Phi}\right)^2 (\sigma_\Phi)^2 \tag{5.2}$$

where σ is the uncertainty in the measurement of each quantity and Φ is the phase difference between the pressure and velocity waveforms. Substituting the necessary partial derivatives

yields

$$(\sigma_{R_\nu})^2 = \left(\frac{1}{|U|}\cos(\Phi)\right)^2 \left(\sigma_{|\Delta P|}\right)^2 + \left(|\Delta P|\cos(\Phi)\right)^2 \left(\sigma_{|U|}\right)^2 + \left(\frac{|\Delta P|}{|U|}\sin(\Phi)\right)^2 (\sigma_\Phi)^2 \quad (5.3)$$

Dividing Eq. 5.3 by $(R_\nu)^2$ gives the uncertainty in R_{nu} as a percent of reading:

$$\left(\frac{\sigma_{R_\nu}}{R_\nu}\right)^2 = \left(\frac{\sigma_{|\Delta P|}}{|\Delta P|}\right)^2 + \left(\frac{\sigma_{|U|}}{|U|}\right)^2 + \left(\sigma_\Phi \tan\Phi\right)^2. \quad (5.4)$$

The last term in Eq. 5.4 presents a problem, because the phase difference Φ between the pressure and velocity waveforms is typically around 90 degrees, meaning that any uncertainty in the phase measurement is greatly magnified. Since the acoustic power can be expressed as

$$\dot{E} = \int_0^T PUdt \approx |P||U|\cos\phi = R_\nu |U|^2, \quad (5.5)$$

the acoustic power measurement also requires the phase to measured precisely to avoid large uncertainty.

To calculate the phase of the pressure and velocity waveforms, a discrete fourier transform was used. The calculations were performed over 20 cycles for the velocity waveform and 100 cycles for the pressure waveform in an effort to minimize the precision uncertainty in the phase measurement. However, as seen in the resistance results and the acoustic power results for pulsating flow, there still appears to be fluctuation in the data. In these cases, the use of other measurement techniques (such as the lumped-element method) would likely produce more consistent results.

References

[1] Backhaus, S. and Swift, G. W., "A thermoacoustic-Stirling heat engine: Detailed study," *Journal of the Acoustical Society of America*, Vol. 107, 2000, pp. 3148–3166.

[2] Swift, G. W., Gardner, D. L., and Backhaus, S., "Acoustic recovery of lost power in pulse tube refrigerators," *Journal of the Acoustical Society of America*, Vol. 105, 1999, pp. 711–724.

[3] Swift, G. W., *Thermoacoustics: A Unifying Perspective for some Engines and Refrigerators*, Acoustical Society of America, 2002.

[4] Currie, I. G., *Fundamental Mechanics of Fluids*, Vol. III, McGraw Hill, 1993.

[5] Mittal, R., Simmons, S. P., and Najjar, F., "Numerical study of pulsatile flow in a constricted channel," *Journal of Fluid Mechanics*, Vol. 485, 2003, pp. 337–378.

[6] Gaver, D. P. and Grotberg, J. B., "An experimental investigation of oscillating flow in a tapered channel," *Journal of Fluid Mechanics*, Vol. 172, 1986, pp. 47–61.

[7] Tardu, S. F., Binder, G., and Blackwelder, R. F., "Turbulent channel flow with large-amplitude velocity oscillations," *Journal of Fluid Mechanics*, Vol. 267, 1994, pp. 109–151.

[8] Landau, L. D. and Lifshitz, E. M., *Fluid Mechanics*, Pergamon, 1982.

[9] Poroseva, S. V. and Girimaji, S. S., "Analytical study of the oscillating channel flow solution with application to the turbulent case," *Proceedings of FEDSM2003 ASME Fluids Engineering Summer Conference*, July 2003, Paper number 2003-45616.

[10] Smith, B. L., Mortensen, K. V., and Wendel, S., "Oscillating flow in adverse pressure gradients," *Proceedings of FEDSM2005 ASME Fluids Engineering Summer Conference*, June 2005, Paper number 2005-77458.

[11] Smith, B. L. and Swift, G. W., "Synthetic jets at large Reynolds number and comparison to continuous jets," 31st AIAA Fluid Dynamics Conference, 2001, Paper 2001-3030.

[12] Akhavan, R., Kamm, R. D., and Shapiro, A. H., "An investigation of transition to turbulence in bounded oscillatory Stokes flows. Part 1. Experiments," *Journal of Fluid Mechanics*, Vol. 225, 1991, pp. 395, Part 2. Numerical simulations. p. 423.

[13] Obremski, H. and Morkovin, M., "Application of a quasi-steady stability model to periodic boundary-layer flows," *AIAA Journal*, Vol. 7, No. 7, 1969, pp. 1298–1301.

[14] Tromans, P. S., *Stability and transition of periodic pipe flows*, Ph.D. thesis, Cambridge University, 1978.

[15] Eckmann, D. M. and Grotberg, J. B., "Experiments on transition to turbulence in oscillatory pipe flow," *Journal of Fluid Mechanics*, Vol. 222, 1991, pp. 329–350.

[16] Sergeev, S. I., "Fluid oscillations in pipes at moderate Reynolds numbers," *Mekhaniki Zhidkostei i Gazov*, Vol. 1, No. 1, 1966, pp. 21.

[17] Hino, S. M., Sawamoto, M., and Takasu, S., "Experiments on transition to turbulence in an oscillatory pipe flow," *Journal of Fluid Mechanics*, Vol. 75, 1976, pp. 193–207.

[18] Ohmi, M., Iguchi, M., Kakehashi, K., and Tetsuya, M., "Transition to turbulence and velocity distribution in an oscillating pipe flow," *Bulletin of the JSME*, Vol. 25, 1982, pp. 365–371.

[19] Lodahl, C. R., Sumer, B. M., and Fredsoe, J., "Turbulent combined oscillatory flow and current in a pipe," *Journal of Fluid Mechanics*, Vol. 373, 1998, pp. 313–348.

[20] Costamagna, P., Vittori, G., and Blondeaux, P., "Coherent structures in oscillatory boundary layers," *Journal of Fluid Mechanics*, Vol. 474, Jan. 2003, pp. 1–33.

[21] Vittori, G. and Verzicco, R., "Direct simulation of transition in an oscillatory boundary layer," *Journal of Fluid Mechanics*, Vol. 371, 1998, pp. 207–232.

[22] Hof, B., Casimir, W. H., and Westerweel, J., "Experimental Observation of Nonlinear Traveling Waves in Turbulent Pipe Flow," *Science*, Vol. 305, No. 5690, 2004, pp. 1594–1598.

[23] Hino, M., Kashiwayanagi, M., Nakayama, A., and Hara, T., "Experiments on the turbulence statistics and the structure of reciprocating oscillatory flow," *Journal of Fluid Mechanics*, Vol. 131, 1983, pp. 363–400.

[24] Kays, W. M. and Crawford, M. E., *Convective Heat and Mass Transfer*, McGraw-Hill, 1993.

[25] Smith, C. R. and Kline, S. J., "An experimenal investigation of the transitory stall regime in two-dimensional diffusers," *ASME Journal of Fluids Engineering*, Vol. 96, No. 1, 1974, pp. 11–15.

[26] Cengel, Y. A. and Cimbala, J. M., *Fundamental Mechanics of Fluids*, Vol. I, 2006.

[27] Fried, E. and Idelchik, I. E., *Flow Resistance: A Design Guide for Engineers*, Hemisphere, 1989.

[28] Wakeland, R. S. and Keolian, R. M., "Influence of velocity profile nonuniformity on minor losses for flow exiting thermoacoustic heat exchangers," *Journal of the Acoustical Society of America*, Vol. 112, 2002, pp. 1249–1252.

[29] Smith, B. L. and Swift, G. W., "Power dissipation and time-averaged pressure in oscillating flow through a sudden area change," *Journal of the Acoustical Society of America*, Vol. 113, No. 5, 2003, pp. 2455–2463.

[30] Smith, B. L. and King, C. V., "Time-Resolved PIV and pressure measurements of oscillating and pulsating flow in a rapid expansion," Bulletin of the American Physical Society, DFD, 2006.

[31] Morris, P. J., Boluriaan, S., and Shieh, C. M., "Computational thermoacoustic simulation of minor losses through a sudden contraction and expansion," 7th AIAA/CEAS Aeroacoustics Conference, 2001, Paper 2001-2272 .

[32] Biwa, T., Tashiro, Y., Ishigaki, M., Ueda, Y., and Yazaki, T., "Measurements of acoustic streaming in a looped-tube thermoacoustic engine with a jet pump," *Journal of Applied Physics*, Vol. 101, 2007, pp. 4914.

[33] Smith, B. L., "Pressure recovery in a radiused sudden expansion," *Experiments in Fluids*, Vol. 36, 2004, pp. 901–907.

[34] Petculescu, A. and Wilen, L., "Oscillatory flow in jet pumps: Nonlinear effects and minor losses," *Journal of the Acoustical Society of America*, Vol. 113, No. 3, 2003, pp. 1282–1292.

[35] Smith, B. L., Jackson, D., and Mortensen, K., "Oscillating flow in adverse pressure gradients," Bulletin of the American Physical Society, DFD, 2004, p. 37, Presentation is available at `http://www.mae.usu.edu/faculty/bsmith/EFDL/EFDL.htm`.

[36] Smith, B. L. and Swift, G. W., "Measuring second-order time-averaged pressure," *Journal of the Acoustical Society of America*, Vol. 110, No. 2, 2001, pp. 717–723.

[37] Stanislas, M., Okamoto, K., Kähler, C. J., and Westerweel, J., "Main results of the second international PIV challenge," *Experiments in Fluids*, Vol. 39, Aug. 2005, pp. 170–191.

[38] Smith, B. L. and Swift, G. W., "A comparison between Synthetic Jets and continuous jets," *Experiments in Fluids*, Vol. 34, 2003, pp. 467–472.

[39] Idelchik, I. E., *Handbook of Hydraulic Resistance*, Begell House, 3rd ed., 1994.

Appendices

Appendix A

List of Cases Taken

Each case listed here was taken with two different fields of view.

Case Name	Angle	Re_delta	L_o/h	u_0/u_{max}	Frequency	u_{max} (m/s)	u_0 (m/s)
R380L11V000	12	380	11	0	27.80	15.98409	0
R380L11V058	12	380	11	0.167	27.80	15.98409	2.669342
R380L11V115	12	380	11	0.333	27.80	15.98409	5.322701
R380L11V230	12	380	11	0.666	27.80	15.98409	10.6454
R380L12V000	12	380	12	0	23.36	14.65208	0
R380L12V053	12	380	12	0.167	23.36	14.65208	2.446897
R380L12V105	12	380	12	0.333	23.36	14.65208	4.879142
R380L12V211	12	380	12	0.666	23.36	14.65208	9.758285
R380L13V000	12	380	13	0	19.91	13.525	0
R380L13V048	12	380	13	0.167	19.91	13.525	2.258674
R380L13V097	12	380	13	0.333	19.91	13.525	4.503824
R380L13V195	12	380	13	0.666	19.91	13.525	9.007648
R380L13V292	12	380	13	1	19.91	13.525	13.525
R380L15V000	12	380	15	0	14.95	11.72166	0
R380L15V042	12	380	15	0.167	14.95	11.72166	1.957518
R380L15V084	12	380	15	0.333	14.95	11.72166	3.903314
R380L15V169	12	380	15	0.666	14.95	11.72166	7.806628
R380L15V253	12	380	15	1	14.95	11.72166	11.72166
R380L20V000	12	380	20	0	8.41	8.791248	0
R380L20V032	12	380	20	0.167	8.41	8.791248	1.468138
R380L20V063	12	380	20	0.333	8.41	8.791248	2.927485
R380L20V127	12	380	20	0.666	8.41	8.791248	5.854971
R380L20V190	12	380	20	1	8.41	8.791248	8.791248
R580L18V000	12	580	18	0	24.19	22.75605	0
R580L18V076	12	580	18	0.167	24.19	22.75605	3.80026
R580L18V152	12	580	18	0.333	24.19	22.75605	7.577763
R580L18V228	12	580	18	0.5	24.19	22.75605	11.37802
R580L21V000	12	580	21	0	17.77	19.50518	0
R580L21V068	12	580	21	0.167	17.77	19.50518	3.257365
R580L21V136	12	580	21	0.333	17.77	19.50518	6.495226
R580L21V204	12	580	21	0.5	17.77	19.50518	9.752591

R580L23V000	12	580	23	0	14.81	17.80908	0
R580L23V062	12	580	23	0.167	14.81	17.80908	2.974116
R580L23V123	12	580	23	0.333	14.81	17.80908	5.930423
R580L23V184	12	580	23	0.5	14.81	17.80908	8.90454
R580L26V000	12	580	26	0	11.59	15.75419	0
R580L26V054	12	580	26	0.167	11.59	15.75419	2.630949
R580L26V109	12	580	26	0.333	11.59	15.75419	5.246144
R580L26V163	12	580	26	0.5	11.59	15.75419	7.877093
R580L30V000	12	580	30	0	8.71	13.65363	0
R580L30V048	12	580	30	0.167	8.71	13.65363	2.280156
R580L30V095	12	580	30	0.333	8.71	13.65363	4.546658
R580L30V143	12	580	30	0.5	8.71	13.65363	6.826814
R740L25V000	12	740	25	0	20.41	26.67084	0
R740L25V102	12	740	25	0.167	20.41	26.67084	4.454031
R740L25V153	12	740	25	0.25	20.41	26.67084	6.667711
R740L25V203	12	740	25	0.333	20.41	26.67084	8.881391
R740L28V000	12	740	28	0	16.27	23.81325	0
R740L28V091	12	740	28	0.167	16.27	23.81325	3.976813
R740L28V136	12	740	28	0.25	16.27	23.81325	5.953313
R740L28V182	12	740	28	0.333	16.27	23.81325	7.929813
R740L31V000	12	740	31	0	13.27	21.50874	0
R740L31V082	12	740	31	0.167	13.27	21.50874	3.59196
R740L31V123	12	740	31	0.25	13.27	21.50874	5.377186
R740L31V164	12	740	31	0.333	13.27	21.50874	7.162412
R740L35V000	12	740	35	0	10.41	19.0506	0
R740L35V073	12	740	35	0.167	10.41	19.0506	3.181451
R740L35V109	12	740	35	0.25	10.41	19.0506	4.762651
R740L35V145	12	740	35	0.333	10.41	19.0506	6.343851
R740L40V000	12	740	40	0	7.97	16.66928	0
R740L40V064	12	740	40	0.167	7.97	16.66928	2.783769
R740L40V095	12	740	40	0.25	7.97	16.66928	4.167319
R740L40V127	12	740	40	0.333	7.97	16.66928	5.550869
R380L11V000	20	380	11	0	27.80	15.98409	0
R380L11V065	20	380	11	0.167	27.80	15.98409	2.669342
R380L11V130	20	380	11	0.333	27.80	15.98409	5.322701
R380L11V400	20	380	11	0.666	27.80	15.98409	10.6454

R380L12V000	20	380	12	0	23.36	14.65208	0
R380L12V053	20	380	12	0.167	23.36	14.65208	2.446897
R380L12V105	20	380	12	0.333	23.36	14.65208	4.879142
R380L12V325	20	380	12	0.666	23.36	14.65208	9.758285
R380L13V000	20	380	13	0	19.91	13.525	0
R380L13V055	20	380	13	0.167	19.91	13.525	2.258674
R380L13V110	20	380	13	0.333	19.91	13.525	4.503824
R380L13V410	20	380	13	0.666	19.91	13.525	9.007648
R380L15V000	20	380	15	0	14.95	11.72166	0
R380L15V047	20	380	15	0.167	14.95	11.72166	1.957518
R380L15V095	20	380	15	0.333	14.95	11.72166	3.903314
R380L15V190	20	380	15	0.666	14.95	11.72166	7.806628
R380L15V390	20	380	20	1	8.41	8.791248	8.791248
R380L20V000	20	380	20	0	8.41	8.791248	0
R380L20V032	20	380	20	0.167	8.41	8.791248	1.468138
R380L20V063	20	380	20	0.333	8.41	8.791248	2.927485
R380L20V127	20	380	20	0.666	8.41	8.791248	5.854971
R380L20V190	20	380	18	1	10.38	9.768053	9.768053
R580L18V000	20	580	18	0	24.19	22.75605	0
R580L18V115	20	580	18	0.167	24.19	22.75605	3.80026
R580L18V175	20	580	18	0.333	24.19	22.75605	7.577763
R580L18V400	20	580	18	0.5	24.19	22.75605	11.37802
R580L21V000	20	580	21	0	17.77	19.50518	0
R580L21V075	20	580	21	0.167	17.77	19.50518	3.257365
R580L21V145	20	580	21	0.333	17.77	19.50518	6.495226
R580L21V325	20	580	21	0.5	17.77	19.50518	9.752591
R580L23V000	20	580	23	0	14.81	17.80908	0
R580L23V070	20	580	23	0.167	14.81	17.80908	2.974116
R580L23V140	20	580	23	0.333	14.81	17.80908	5.930423
R580L23V220	20	580	23	0.5	14.81	17.80908	8.90454
R580L26V000	20	580	26	0	11.59	15.75419	0
R580L26V063	20	580	26	0.167	11.59	15.75419	2.630949
R580L26V125	20	580	26	0.333	11.59	15.75419	5.246144
R580L26V188	20	580	26	0.5	11.59	15.75419	7.877093
R580L30V000	20	580	30	0	8.71	13.65363	0
R580L30V053	20	580	30	0.167	8.71	13.65363	2.280156
R580L30V108	20	580	30	0.333	8.71	13.65363	4.546658
R580L30V160	20	580	30	0.5	8.71	13.65363	6.826814

R740L25V000	20	740	25	0	20.41	26.67084	0
R740L25V123	20	740	25	0.167	20.41	26.67084	4.454031
R740L25V170	20	740	25	0.25	20.41	26.67084	6.667711
R740L25V275	20	740	25	0.333	20.41	26.67084	8.881391
R740L28V000	20	740	28	0	16.27	23.81325	0
R740L28V098	20	740	28	0.167	16.27	23.81325	3.976813
R740L28V148	20	740	28	0.25	16.27	23.81325	5.953313
R740L28V198	20	740	28	0.333	16.27	23.81325	7.929813
R740L31V000	20	740	31	0	13.27	21.50874	0
R740L31V090	20	740	31	0.167	13.27	21.50874	3.59196
R740L31V145	20	740	31	0.25	13.27	21.50874	5.377186
R740L31V183	20	740	31	0.333	13.27	21.50874	7.162412
R740L35V000	20	740	35	0	10.41	19.0506	0
R740L35V078	20	740	35	0.167	10.41	19.0506	3.181451
R740L35V110	20	740	35	0.25	10.41	19.0506	4.762651
R740L35V150	20	740	35	0.333	10.41	19.0506	6.343851
R740L40V000	20	740	40	0	7.97	16.66928	0
R740L40V063	20	740	40	0.167	7.97	16.66928	2.783769
R740L40V103	20	740	40	0.25	7.97	16.66928	4.167319
R740L40V175	20	740	40	0.333	7.97	16.66928	5.550869
R380L11V000	30	380	11	0	27.80	15.98409	0
R380L11V065	30	380	11	0.167	27.80	15.98409	2.669342
R380L11V130	30	380	11	0.333	27.80	15.98409	5.322701
R380L11V400	30	380	11	0.666	27.80	15.98409	10.6454
R380L12V000	30	380	12	0	23.36	14.65208	0
R380L12V053	30	380	12	0.167	23.36	14.65208	2.446897
R380L12V105	30	380	12	0.333	23.36	14.65208	4.879142
R380L12V325	30	380	12	0.666	23.36	14.65208	9.758285
R380L13V000	30	380	13	0	19.91	13.525	0
R380L13V055	30	380	13	0.167	19.91	13.525	2.258674
R380L13V110	30	380	13	0.333	19.91	13.525	4.503824
R380L13V410	30	380	13	0.666	19.91	13.525	9.007648
R380L15V000	30	380	15	0	14.95	11.72166	0
R380L15V047	30	380	15	0.167	14.95	11.72166	1.957518
R380L15V095	30	380	15	0.333	14.95	11.72166	3.903314
R380L15V190	30	380	15	0.666	14.95	11.72166	7.806628
R380L15V390	30	380	15	1	14.95	11.72166	11.72166

R380L20V000	30	380	20	0	8.41	8.791248	0
R380L20V032	30	580	20	0.167	19.59	20.48044	3.420234
R380L20V063	30	580	20	0.333	19.59	20.48044	6.819987
R380L20V127	30	580	20	0.666	19.59	20.48044	13.63997
R380L20V190	30	580	20	1	19.59	20.48044	20.48044
R580L18V000	30	580	18	0	24.19	22.75605	0
R580L18V115	30	580	18	0.167	24.19	22.75605	3.80026
R580L18V175	30	580	18	0.333	24.19	22.75605	7.577763
R580L18V400	30	580	18	0.5	24.19	22.75605	11.37802
R580L21V000	30	580	21	0	17.77	19.50518	0
R580L21V075	30	580	21	0.167	17.77	19.50518	3.257365
R580L21V145	30	580	21	0.333	17.77	19.50518	6.495226
R580L21V325	30	580	21	0.5	17.77	19.50518	9.752591
R580L23V000	30	580	23	0	14.81	17.80908	0
R580L23V070	30	580	23	0.167	14.81	17.80908	2.974116
R580L23V140	30	580	23	0.333	14.81	17.80908	5.930423
R580L23V220	30	580	23	0.5	14.81	17.80908	8.90454
R580L26V000	30	580	26	0	11.59	15.75419	0
R580L26V063	30	580	26	0.167	11.59	15.75419	2.630949
R580L26V125	30	580	26	0.333	11.59	15.75419	5.246144
R580L26V188	30	580	26	0.5	11.59	15.75419	7.877093
R580L30V000	30	740	30	0	14.17	22.2257	0
R580L30V053	30	740	30	0.167	14.17	22.2257	3.711692
R580L30V108	30	740	30	0.333	14.17	22.2257	7.401159
R580L30V160	30	740	30	0.5	14.17	22.2257	11.11285
R740L25V000	30	740	25	0	20.41	26.67084	0
R740L25V123	30	740	25	0.167	20.41	26.67084	4.454031
R740L25V170	30	740	25	0.25	20.41	26.67084	6.667711
R740L25V275	30	740	25	0.333	20.41	26.67084	8.881391
R740L28V000	30	740	28	0	16.27	23.81325	0
R740L28V098	30	740	28	0.167	16.27	23.81325	3.976813
R740L28V148	30	740	28	0.25	16.27	23.81325	5.953313
R740L28V198	30	740	28	0.333	16.27	23.81325	7.929813
R740L31V000	30	740	31	0	13.27	21.50874	0
R740L31V090	30	740	31	0.167	13.27	21.50874	3.59196
R740L31V145	30	740	31	0.25	13.27	21.50874	5.377186
R740L31V183	30	740	31	0.333	13.27	21.50874	7.162412
R740L35V000	30	740	35	0	10.41	19.0506	0

R740L35V078	30	740	35	0.167	10.41	19.0506	3.181451
R740L35V110	30	740	35	0.25	10.41	19.0506	4.762651
R740L35V150	30	740	35	0.333	10.41	19.0506	6.343851
R740L40V000	30	740	40	0	7.97	16.66928	0
R740L40V063	30	740	40	0.167	7.97	16.66928	2.783769
R740L40V103	30	740	40	0.25	7.97	16.66928	4.167319
R740L40V175	30	740	40	0.333	7.97	16.66928	5.550869

Appendix B

Fortran Code for Processing PIV and Pressure Data

```
program Oscflow implicit none

real::asdf,vamp,vphase,X,phideltap,deltap,omega,l,rnu,alphas,alphab
real::eta=.248,area=.0025355,correction,topaverage,bottomaverage
real::left, right, top, bottom,total=0.,average=0.,freq,nu,rho
real::velocityrecordrate,sums,strokeb=0.,strokes=0.,corr=0.,vavg
real::topedot,xdifference, tr,trshot,vzeroshotup, vzeroshotdown
real::phinew,T,dx,integral,topvamp,topvphase,upleft,upright,uptop
real::upbottom,bottomarea,toparea,averagearea,dist,theta,length,H
real,allocatable,dimension(:,:)::velocity,pcosines,psines,pressure
real,allocatable,dimension(:,:)::acycle,bcycle,cycleamp,acceleration
real,allocatable,dimension(:,:)::topaveragev,cyclephase,averagev,pap
real,allocatable,dimension(:,:)::paphalf,input,velsums,fluctuation
real,allocatable,dimension(:,:)::vcosines,vsines,xvaverage,xv,dudt
real,allocatable,dimension(:)::a,b,pamp,pphase,avcycle,bvcycle
real,allocatable,dimension(:)::vcycleamp,vcyclephase,tap,pav,edot,abspav
REAL,ALLOCATABLE,DIMENSION(:)::VAMPS,VPHASES,AVEL,BVEL
real,dimension(50)::intdudt
integer::iodefault,fileflag,nshots,iovel,nx,ny,nrows
integer::i,j,k,count=0,nsensors,npshots,samppercycle,vshotspercycle
integer::nfiles,filenumber,ncycles,nvcycles,stat,row,phase
integer::MINlocation,Q,NHARMONICS=10,fileio,m,bottomrow,toprow
integer::uppersensor, lowersensor
```

```
character(len=300)::diffdefault,velfile,pfile,directoryout,velfileout
character(len=300)::veldirectory,junk,casename,sensorline,inputfile
character(len=300)::outputfile,flufile
character(len=300),allocatable,dimension(:)::infiles

!========================================== !Parameters I didn't
want to have to add every time !box for channel velocity   (most
cases) left=3. right=13. top=10. bottom=2.

left=3.    !(zoomed in 12 degree stuff) right=13. top=2. bottom=-2.

!box for upper channel velocity upleft=-16. upright=32. uptop=117.
upbottom=110.

!for du/dt calculation, vector row (integer from 1 at the !top of
the vector field to 128 !at the bottom) of the bottom of the
diffuser and top bottomrow=128 toprow=1

!========================================== !Stuff to loop a bunch
of files

!inputfile="Y:\20deg_zout_steady_ascii_disk2\na& !&mes.txt"
!20steadyzout !outputfile="Y:\20deg_zout_steady_ascii_disk2\20&
!&_STEADY_outs_withcorr.txt"  !20steadyzout

!inputfile="C:\data\20degree_zout_redo\names.txt"  !20nosteadyzout
!outputfile="C:\data\20degree_zout_redo\outs.txt"  !20nosteadyzout
```

```
!inputfile="C:\data\12_degree_REDO_zoomedout\& !&12-20\names.txt"
!12nosteadyzout !outputfile="C:\data\12_degree_REDO_zoomedout\&
!&12-20\outs.txt"  !12nosteadyzout

!inputfile="C:\data\30degree_nosteady\names.txt"  !30nosteadyzout
!outputfile="C:\data\30degree_nosteady\outs.txt"  !30nosteadyzout

inputfile="Y:\12degzinexport\names.txt"    !12 zin all  (change box)
outputfile="y:\12degzinexport\outs.txt"    !12 zin all  (change box)

!inputfile="W:\Cameron\fullascii30degzout\names.txt"
!outputfile="W:\Cameron\fullascii30degzout\outs.txt"



H=.655/.248*.016637 theta=30.*3.14159/180. dist=H*(1.-eta)/2.
length=dist/tan(theta/2.)

open(unit=99,file=inputfile) open(unit=98,file=outputfile) !count
the number of cases in names.txt nfiles=0 do
  read(99,*,iostat=fileio)junk
  if(fileio == 0)then
    nfiles=nfiles+1
  else
    exit
  end if
end do rewind(99)

allocate(infiles(nfiles))
```

```
do i=1,nfiles
  read(99,*)infiles(i)
end do

!write(*,*)"Enter the case name" !read(*,*)casename

!Big do loop do filenumber=1,nfiles
   casename=trim(infiles(filenumber))
   write(*,*)"Working on file:",trim(casename)



!veldirectory="Y:\20deg_zout_steady_ascii_disk2\"/&
!&/TRIM(CASENAME)//"_PIV_Vec_MP(16x16_50ov)_PostProc=unknown\"
!Pfile="C:\data\20degree_zoomedout\"//trim(casename& !&)//".pdt"
!20steadyzout

!veldirectory="F:\20deg_exported_nosteady_zout\"//&
!&TRIM(CASENAME)//"_PIV_Vec_MP(16x16_50ov)_PostProc&
!&_postproc=unknown\"                              !20nosteadyzout
!Pfile="C:\data\20degree_zout_redo\"//trim(casename)//".pdt"

!veldirectory="Y:\12deg_zout_nosteady_ascii_disk2\"//TRIM(CAS&
!&ENAME)//"_PIV_Vec_MP(16x16_50_ov)_PostProc\" !12nosteadyzout
!Pfile="C:\data\12_degree_REDO_zoomedout\12-20\"//trim(casenam&
!&e)//".pdt"  !12nosteadyzout

!veldirectory="C:\Oscflow\data\30deg\ascii\"//TRIM(CASENAME)&
```

```
!&//"\" !30nosteadyzout
!Pfile="C:\data\30degree_nosteady\"//trim(casename)//".pdt"

veldirectory="Y:\12degzinexport\"//Trim(casename)//"_PIV_Vec&
&_MP(16x16_50ov)_PostProc=unknown\"   !12 all zin
pfile="C:\data\12_degree_zin\"//trim(casename)//".pdt" !12 all zin

!pfile="c:\data\30 degree steady 707\"//trim(casename)//".pdt"
!veldirectory="W:\Cameron\fullASCII30DEGZOUT\"//trim(casename)&
!&//"_PIV_Vec_MP(16x16_50_ov)_diff_masking_PostProc\"

110 write(*,*)"================================================"
write(*,*)"Velocity data input type?" write(*,*)"(1)B00___.txt ascii
files, (2) R___L__averageV.txt" !read(*,*)fileflag fileflag=1

if(fileflag==1) then
  write(*,*)"How many ascii files to read in (must be at&
  & least one cycle)?"
  !read(*,*)nshots
  NSHOTS=1000

  call name(1,velfile,veldirectory)
  open(unit=10,file=velfile,iostat=iovel)
  if(iovel/=0) then
     write(*,*)"file input problem, iostat =",iovel
  end if
  read(10,*)junk,junk,junk,junk,nx,ny
  close(10)
```

```
nrows=nx*ny
allocate(velocity(nrows,4))
allocate(averagev(nshots,2))
allocate(topaveragev(nshots,2))

open(unit=12,file="c:\data\averagev\12\"//trim(casename)//".txt")
          allocate(xv(nshots,nx),xvaverage(50,nx),dudt(50,nx))
          intdudt=0.

!At this point the program just creates the averageV file
write(*,*)"Creating averageV file..."
write(*,*)"The box is defined as x (mm) = ",left," to ",right
write(*,*)"and y (mm) = ",BOTTOM," to ",TOP
do k=1,nshots
  call name(k,velfile,veldirectory)
  open(unit=10,file=velfile)
  read(10,*)junk
      do i=1,nrows
          read(10,*)(velocity(i,j),j=1,4)
      end do
  do j=1,nrows
      if (velocity(j,1)>left .and. velocity(j,1)<right&
      & .and. velocity(j,2)<top .and.velocity(j,2)>bottom) then
          total=total+velocity(j,4)
          count=count+1
      end if
  end do
```

```
    write(12,*)k,", ",total/real(count)
    averagev(k,2)=total/real(count)
    averagev(k,1)=real(k)
    total=0.
    count=0

    do j=1,nrows
        if (velocity(j,1)>upleft .and. velocity(j,1)<upright&
        & .and. velocity(j,2)<uptop .and.velocity(j,2)>upbottom) then
            total=total+velocity(j,4)
            count=count+1
        end if
    end do

    topaveragev(k,2)=total/real(count)
    topaveragev(k,1)=real(k)
    total=0.
    count=0

!I need to evaluate int(du/dt,x=x1..x2) for the steady flow stuff
!Find the velocity of each row and average     xv(shot,row)
            do i=1,nx
              do j=nx*(i-1)+1,nx*(i-1)+nx
                total=total+velocity(j,4)
                if(velocity(j,4)/=0.)count=count+1
              end do
              xv(k,i)=total/real(count)
                total=0.
```

```
                count=0
            end do
            end do
  write(*,*)"Done"
  write(*,*)"=================================================="

!Phase average the xv matrix to form         xvaverage(shot,row)
            do m=1,nx
              do i=1,50
                do j=i,nshots,50
                  total=total+xv(j,m)
                  count=count+1
                end do
              xvaverage(i,m)=total/real(count)
              total=0.
              count=0
              end do
            end do

!Calculate the derivative du/dt for each x location and each shot
dudt(shot,row)
            open(unit=14,file=pfile,iostat=iovel)
            if(iovel/=0) then
              write(*,*)"file error, iostat =",iovel
            end if

            read(14,*)junk
            read(14,*)freq,junk,samppercycle,junk,nu,rho
```

```
            close(14)
            velocityrecordrate=freq*50.

            dudt(1,:)=(xvaverage(1,:)-xvaverage(50,:))*freq
            do i=2,50
              dudt(i,:)=(xvaverage(i,:)-xvaverage(i-1,:))*freq
            end do

!Correct the sign if the velocity is negative (I've assumed !row 123
is somewhere in the lower channel)
!int(int(du/dt,x=x1..x2),t=0..tc)+int(int(du/dt,x=x2..x1),t=
!tc..T)=int(int(du/dt if u>0 or -du/dt if u<0)),t=0..T) !Integrate
du/dt over x from bottomrow to toprow (first find !x resolution and
convert to mm)
            intdudt=0.
            dx=abs(velocity(1,1)-velocity(2,1))/1000.
            do j=1,50
              do i=toprow, bottomrow
                intdudt(j)=intdudt(j)+dudt(j,i)
              end do
              intdudt(j)=intdudt(j)*dx
              if(xv(j,123)<0.)intdudt(j)=intdudt(j)-1.
            end do


            integral=sum(intdudt(1:50))*rho/velocityrecordrate
            write(*,*)integral
! Option 2 else if(fileflag==2) then
```

```
  write(*,*)"Enter the averageV file name"
  read(*,*)velfile
  open(unit=13,file=velfile,iostat=iovel)
    if(iovel/=0) then
      write(*,*)"file input problem, iostat=", iovel
    end if
  count=0
  do
    read(13,*,iostat=iovel)junk
    if(iovel/=0) then
      exit
    else
    count=count+1
    end if
  end do
  write(*,*)count," values were read."
  nshots=count
  allocate(averagev(nshots,2))
  rewind(13)
  do i=1,nshots
    read(13,*)(averagev(i,j),j=1,2)
  end do
  write(*,*)"===================================================="
else
  goto 110
end if


!ppppppppppppppppppppppppppppppppppppppppppppppppppppppppppp
```

```
!Pressure file stuff

!write(*,*)"Enter the pressure data file name" !read(*,*)pfile

open(unit=14,file=pfile,iostat=iovel) if(iovel/=0) then
  write(*,*)"file error, iostat =",iovel
end if

read(14,*)junk read(14,*)freq,junk,samppercycle,junk,nu,rho
read(14,150)sensorline 150 format(A100)

omega=freq*2*3.14159

!how many pressure sensors?  I've only had 8 or 11
if(trim(sensorline)=="Shot #, P1,P2,P3,P4,P5,P6,P7,P8,P9,P1&
&0,P11,") then
   nsensors=11
else
   nsensors=8
end if

count=0

do
    read(14,*,iostat=iovel)junk
    if(iovel/=0)then
        exit
    end if
```

```
    count=count+1
end do rewind(14)

write(*,*)count," samples were read." write(*,*)freq," was the
frequency." npshots=count allocate(pressure(npshots,nsensors+1))

read(14,*)junk read(14,*)junk read(14,*)junk

do i=1,npshots
  read(14,*)(pressure(i,j),j=1,nsensors+1)
end do

!Convert shot number (column 1) to time   (shot*(cycle/shot
!s)*(seconds/cycle)) pressure(:,1)=pressure(:,1)/samppercycle/freq
ncycles=int(npshots/samppercycle)

write(*,*)"============================================="
write(*,*)"Computing fourier transform..."

!convert all pressure to Pa pressure=pressure*6892.7
pressure(:,1)=pressure(:,1)/6892.7

!fffffffffffffffffffffffffffffffffffffffffffffffffffffffffffff
!discrete fourier transform stuff !pressure
allocate(pcosines(npshots,nsensors),psines(npshots,nsensors))
allocate(a(nsensors),b(nsensors))
allocate(acycle(nsensors,ncycles),bcycle(nsensors,ncycles))
allocate(cycleamp(nsensors,ncycles),cyclephase(nsensors,ncycles))
```

```
allocate(pamp(nsensors),pphase(nsensors))

do i=1,nsensors
    pcosines(:,i)=pressure(:,i+1)*cos(2*3.14159*pressure(:,1)*freq)
    psines(:,i)=pressure(:,i+1)*sin(2*3.14159*pressure(:,1)*freq)
end do

!whole set do i=1,nsensors
    a(i)=2.*sum(pcosines(1:npshots,i))/npshots
    b(i)=2.*sum(psines(1:npshots,i))/npshots
end do

do i=1,nsensors
    pamp(i)=sqrt(a(i)**2+b(i)**2)
    pphase(i)=atan2(a(i),b(i))
end do

!individual cycles do i=1,nsensors
  do j=1,ncycles
    acycle(i,j)=2.*sum(pcosines((j-1)*samppercycle+1:(j-1)&
    &*samppercycle+samppercycle,i))/samppercycle
    bcycle(i,j)=2.*sum(psines((j-1)*samppercycle+1:(j-1)*sa&
    &mppercycle+samppercycle,i))/samppercycle
  end do
end do

do i=1,nsensors
  cycleamp(i,:)=sqrt(acycle(i,:)**2+bcycle(i,:)**2)
```

```
  cyclephase(i,:)=atan2(acycle(i,:),bcycle(i,:))
end do


!convert cycle amp and phase to percent error do i=1,nsensors
  cycleamp(i,:)=(cycleamp(i,:)-pamp(i))/pamp(i)*100
  cyclephase(i,:)=(cyclephase(i,:)-pphase(i))/pphase(i)*100
end do

write(*,*)" " write(*,*)"Pressure info" write(*,*)" "
write(*,*)"     Sensor   Amp(Pa)      error(%)       Phase  &
&        error(%)"
do i=1,nsensors
  write(*,*)i, pamp(i), maxval(cycleamp(i,:)),pphase(i),maxval&
  &(cyclephase(i,:))
end do

!VVVVVVVVVVVVVVVVVVVVVVVVVVVVVVVVVVVVVVV !Velocity stuff
vshotspercycle=samppercycle/2     !THIS IS ASSUMING DOUBLE-PULSED
PIV nvcycles=nshots/vshotspercycle

allocate(vcosines(nshots,NHARMONICS),vsines(nshots,NHARMONICS))
ALLOCATE(AVEL(NHARMONICS),BVEL(NHARMONICS),VAMPS(NHARMONICS))
allocate(VPHASES(NHARMONICS))
allocate(avcycle(nvcycles),bvcycle(nvcycles))
allocate(vcycleamp(nvcycles),vcyclephase(nvcycles))

!convert shot # to time  (this assumes double-pulsed PIV)
```

```
averagev(:,1)=averagev(:,1)/freq/vshotspercycle

DO Q=1,NHARMONICS
vcosines(:,Q)=averagev(:,2)*cos(2*Q*3.14159*averagev(:,1)*freq)
vsines(:,Q)=averagev(:,2)*sin(2*Q*3.14159*averagev(:,1)*freq) END DO

!whole set DO Q=1,NHARMONICS
avel(Q)=2.*sum(vcosines(1:nshots,Q:Q))/nshots
bvel(Q)=2.*sum(vsines(1:nshots,Q:Q))/nshots END DO

vamp=sqrt(avel(1)**2+bvel(1)**2) vphase=atan2(avel(1),bvel(1))

VAMPS=SQRT(AVEL**2+BVEL**2) VPHASES=ATAN2(aVEL,bVEL)

!individual cycles do j=1,nvcycles
    avcycle(j)=2.*sum(vcosines((j-1)*vshotspercycle+1:(j-1)*&
    &vshotspercycle+vshotspercycle,1))/vshotspercycle
    bvcycle(j)=2.*sum(vsines((j-1)*vshotspercycle+1:(j-1)*vsh&
    &otspercycle+vshotspercycle,1))/vshotspercycle
end do

vcycleamp(:)=sqrt(avcycle(:)**2+bvcycle(:)**2)
vcyclephase(:)=atan2(avcycle(:),bvcycle(:))

!convert to percent error vcycleamp(:)=(vcycleamp(:)-vamp)/vamp*100.
vcyclephase(:)=(vcyclephase(:)-vphase)/vphase*100.

!convert vphase (radians) back to time (tr) and shot number
```

```
!(trshot) tr=vphase*(1 cycle/2Pi radians)*(1 s/1cycle)
tr=vphase/omega if(tr<0)tr=tr+1/freq trshot=tr*freq*vshotspercycle

write(*,*)" " write(*,*)"Velocity info" write(*,*)" "
write(*,*)"   Amp(m/s)     error(%)      Phase           error"
write(*,*)vamp, maxval(vcycleamp), vphase, maxval(vcyclephase)
!write(*,*)" Upper channel amp, equiv. lower channel amp, phase"
!write(*,*)topvamp, topvamp*48./10.,topvphase write(*,*)"  " DO
Q=2,NHARMONICS WRITE(*,*)VAMPS(Q), MAXVAL(VCYCLEAMP),VPHASES(Q) END
DO write(*,*)" " write(*,*)"Pressure leads velocity by ",
(pphase(1)-vphase)*1& &80./3.14159 ," degrees"
write(*,*)"================================================"
write(*,*)" " write(*,*)"Reynolds number \delta =
",vamp*sqrt(2*nu/(2*3.1415& &9*freq))/nu write(*,*)"Stroke length =
",vamp/freq/3.14159/(.655*.0254)
WRITE(*,*)"======================================="
WRITE(*,*)"Steady flow velocity was (m/s):",sum(averagev(1:nshots&
&,2:2))/real(nshots) WRITE(*,*)"u0/umax =
",sum(averagev(1:nshots,2:2))/real(nshots)/vamp
write(*,*)"============================================================"
vavg=sum(averagev(1:nshots,2:2))/real(nshots)



!=================================================================
!Time averaged pressure and minor losses allocate(tap(nsensors))

do i=1,nsensors
   tap(i)=sum(pressure(1:npshots,i+1))/npshots
```

```
end do

alphab=0. alphas=0. velocityrecordrate=freq*vshotspercycle

!do i=1,vshotspercycle/2 !
alphab=alphab+freq/vamp**2*averagev(i,2)**2/velocityrecordrate !end
do

!do i=vshotspercycle/2+1,vshotspercycle !
alphas=alphas+freq/vamp**2*averagev(i,2)**2/velocityrecordrate !end
do

!This is being changed to change the limits of integration for
!steady flow. !Instead of finding the zero crossing, I'm just having
it !contribute to alphab if the velocity !is positive and alphas if
the velocity is negative

do i=1,vshotspercycle
   if(averagev(i,2)>0.)alphab=alphab+freq/vamp**2*averagev(i,2)&
   &**2/velocityrecordrate
   if(averagev(i,2)<=0.)alphas=alphas+freq/vamp**2*averagev(i,2)&
   &**2/velocityrecordrate
end do

!Stroke length taking into account the change in the limits of
!integration do i=1,vshotspercycle
   if(averagev(i,2)>0.)strokeb=strokeb+averagev(i,2)/VELOCITY&
   &RECORDRATE/.655/.0254
```

```
   if(averagev(i,2)<=0)strokes=strokes+averagev(i,2)/VELOCITY&
   &RECORDRATE/.655/.0254
end do


!========================================================== !Phase
average stuff
allocate(pap(samppercycle,nsensors),pav(vshotspercycle))
allocate(abspav(vshotspercycle))
allocate(acceleration(samppercycle/2,2))
allocate(paphalf(samppercycle/2,nsensors)) sums=0. count=0

do k=1,nsensors
  do i=1,samppercycle
    do j=i,npshots,samppercycle
      sums=sums+pressure(j,k+1)
      count=count+1
    end do
  pap(i,k)=sums/real(count)
  sums=0.
  count=0
  end do
end do


do i=1,vshotspercycle
  do j=i,nshots,vshotspercycle
    sums=sums+averagev(j,2)
```

```
    count=count+1
  end do
  pav(i)=sums/real(count)
  sums=0.
  count=0
end do

!Take half the pressure data (for double pulsed PIV) do
i=1,samppercycle,2
  paphalf((i+1)/2,:)=pap(i,:)
end do

write(*,*)"  " write(*,*)"Outputting phase-averaged velocity and
pressure to:"
write(*,*)"c:\data\phaseaverage\12zin\1000shots\"//trim(casename)&
&//"phaseaveragePV.txt" write(*,*)"  "

open(unit=16,file="c:\data\phaseaverage\redo30\"//trim(casename)&
&//"phaseaveragePV.txt")

if(nsensors==8) then write(16,*)"t/T,P1,P2,P3,P4,P5,P6,P7,P8,V,dP
measured, dP calc,& &dPcalc5x" do j=1,samppercycle/2

abspav=abs(pav) minlocation=minloc(abspav,1) !MINLOCATION=1
correction=(paphalf(minlocation,2)-paphalf(minlocation,8))-.5*(-&
&.469*pav(minlocation)**2+.2298*omega*vamp*cos(omega*2.*real(min&
&location)/real(samppercycle)*2.*3.14159/omega+vphase))
!correction=1.
```

```
write(16,130)2.*real(j)/real(samppercycle),",",paphalf(j,1),",",&
&paphalf(j,2),",",paphalf(j,3),",",paphalf(j,4),",",paphalf(j,5)&
    &,",",paphalf(j,6),",",paphalf(j,7),",",paphalf(j,8),",",pav&
    &(j),",",paphalf(j,2)-paphalf(j,8)&
    &,",",.5*(-.469*pav(j)**2+.2298*omega*vamp*cos(omega*2.*real&
    &(j)/real(samppercycle)*2.*3.14159/omega+vphase)),",",&
    &.5*(-.469*pav(j)**2+.2298*(omega*vamp*cos(omega*2.*real(j)&
    &/real(samppercycle)*2.*3.14159/omega+vphase)+OMEGA*vampS(2)&
    &*cos(omega*4.*real(j)/real(samppercycle)&
    &*2.*3.14159/omega+vphaseS(2))+OMEGA*vampS(3)*cos(omega*6.*&
    &real(j)/real(samppercycle)*2.*3.14159/omega+vphaseS(3))+&
    &OMEGA*vampS(4)*cos(omega*8.*real(j)/real(samppercycle)*&
    &2.*3.14159/omega+vphaseS(4))+OMEGA*vampS(5)*cos(omega*10.&
    &*real(j)/real(samppercycle)*2.*3.14159/omega+vphaseS(5))))&
    &+correction
    130 format(F6.2,A1,20(F10.4,A1))

end do end if

!Find both zero crossings for velocity do j=1,samppercycle/2-1
  if(pav(j)>0. .and. pav(j+1)<0.) then
    vzeroshotdown=pav(j)/(pav(j)-pav(j+1))+j
  end if
end do

DO j=1,samppercycle/2-1
  if(pav(j)<0. .and. pav(j+1)>0.) then
```

```
    vzeroshotup=pav(j)/(pav(j+1)-pav(j))+j+1
  end if
end do


if(filenumber==1)then
  open(unit=43,file="c:\data\zeros\zeros.txt")
  write(43,*)"casename,vzeroshotup,vphase"
end if write(43,*)trim(casename),vzeroshotup,vphase/3.14159*50.


tr=vzeroshotdown/50./freq trshot=vzeroshotdown
phinew=vphase+vzeroshotup/50.*2.*3.14159
if(phinew<-3.14159)phinew=phinew+2*3.14159
if(phinew>3.14159)phinew=phinew-2*3.14159



!topaverage=(tap(9)+tap(10)+tap(11))/3.
!bottomaverage=(tap(5)+tap(6)+tap(8))/3.

!topaverage=tap(9) topaverage=tap(8) bottomaverage=tap(6)
xdifference=.381  !15 inches T=1/freq alphab=alphab*T/tr
alphas=alphas*T/(T-tr)

write(*,*)"alphab = ", alphab,"        alphas =", alphas write(*,*)"
" write(*,*)"average p's:  p8(Pa)=",topaverage, " p10(Pa)=",&
&bottomaverage, " diff=",bottomaverage-topaverage write(*,*)"Kb-Ks
```

```
for alphab=alphas=.25, using sensors 9 and 6 & &(100000 data)"
write(*,*)8*(bottomaverage-topaverage)/rho/vamp**2+2-2*eta**2-corr
write(*,*)"  " write(*,*)"Kb-Ks for calculated alphas and new
correction using & &sensors 9 and 6 (10000 data)"
write(*,*)4*(bottomaverage-topaverage)/rho/(alphab+alphas)/vamp**&
&2+2-2*eta**2+16*3.14159*omega/(alphab+alphas)/vamp*sin(omega*tr)&
&*xdifference-corr write(*,*)"  " write(*,*)"strokeb = ",strokeb,"
strokes =",-strokes write(*,*)"  " write(*,*)"Kb for Ks=0.1 and new
calc alphas is:",2*(bottomavera&
&ge-topaverage)/rho/alphab/vamp**2-alphas/alphab*(eta**2-1.1)+1-&
&eta**2+integral

write(*,*)"============================="
write(*,*)16*3.14159*omega/(alphab+alphas)/vamp*sin(omega*tr)*&
&xdifference,tr,trshot,phinew,vphase,vzeroshotup,vzeroshotdown
write(*,*)4/3.14159*omega/(alphab+alphas)/vamp*sin(omega*tr)*x&
&difference,tr,trshot,vzeroshotup,vzeroshotdown


!Losses output if(filenumber==1)write(98,*)"Casename, Re, Lo/h,
u0/vamp, omega& &, phinew,u0, u(t=0),
dp,Kb_a=.25,Kb4calc_a,Kb4ks01,newintegralterm"
write(98,158)trim(casename),",",vamp*sqrt(2*nu/(2*3.14159*freq))&
&/nu,",",vamp/freq/3.14159/(.655*.0254),",",sum(averagev(1:nshots&
&,2:2))/real(nshots)/vamp,",",omega,",",phinew,",",sum(averagev(1&
&:nshots,2:2))/real(nshots),",",vamp*sin(phinew)+sum(averagev(1:&
&nshots,2:2))/real(nshots),",",bottomaverage-topaverage,",",8*(bot&
&tomaverage-topaverage)/rho/vamp**2+2-2*eta**2-corr,",",4*(bottoma&
```

```
&verage-topaverage)/rho/(alphab+alphas)/vamp**2+2-2*eta**2-corr,","&
&,2*(bottomaverage-topaverage)/rho/alphab/vamp**2-alphas/alphab*(eta&
&**2-1.1)+1-eta**2+integral,",",integral 158
format(A14,A1,F10.5,A1,F10.5,A1,F10.5,A1,F10.5,A1,F10.5,A1,F10&
&.5,A1,F10.5,A1,F10.5,A1,F10.5,A1,F10.5,A1,F10.5,A1,F10.5)



write(*,*)bottomaverage-topaverage write(*,*)rho write(*,*)vamp
write(*,*)eta write(*,*)omega write(*,*)1/freq write(*,*)xdifference
write(*,*)tr write(*,*)alphab write(*,*)alphas write(*,*)phinew
write(*,*)"=================="

!Bernoulli stuff to compare measured pressure to theroetical !from
velocity data

if(nsensors==11) then
write(16,*)"t/T,P1,P2,P3,P4,P5,P6,P7,P8,P9,P10,P11,V,dP measured,& &
dP calc CORR, DP NOT CORR" do j=1,samppercycle/2
   write(16,131)2.*real(j)/real(samppercycle),",",paphalf(j,1),",&
   &",paphalf(j,2),",",paphalf(j,3),",",paphalf(j,4),",",paphalf(j,5)&
   &,",",paphalf(j,6),",",paphalf(j,7),",",paphalf(j,8),",",paphalf&
   &(j,9),",",paphalf(j,10),",",paphalf(j,11),",",pav(j),",",paphalf&
   &(j,4)-paphalf(j,9)&
   &,",",.5*(-.469*pav(j)**2+.2298*omega*vamp*cos(omega*2.*real(j)/&
   &real(samppercycle)*2.*3.14159/omega+vphase))+correction,",",&
   &.5*(-.469*pav(j)**2+.2298*(omega*vamp*cos(omega*2.*real(j)/real&
   &(samppercycle)*2.*3.14159/omega+vphase)+OMEGA*vampS(2)*cos(omega&
```

```
   &*4.*real(j)/real(samppercycle)&
   &*2.*3.14159/omega+vphaseS(2))+OMEGA*vampS(3)*cos(omega*6.*real(j)&
   &/real(samppercycle)*2.*3.14159/omega+vphaseS(3))+OMEGA*vampS(4)*&
   &cos(omega*8.*real(j)/real(samppercycle)*&
   &2.*3.14159/omega+vphaseS(4))+OMEGA*vampS(5)*cos(omega*10.*real(j)&
   &/real(samppercycle)*2.*3.14159/omega+vphaseS(10))))
   131 format(F6.2,25(A1,F10.3))
end do end if

!================================================================
!acoustic power stuff allocate(edot(nsensors))

bottomarea=.004455 toparea=.655/eta*6*.0254*.0254
averagearea=.5*bottomarea+.5*toparea area=averagearea

edot=0. do k=1,nsensors
  do i=1,samppercycle/2
    edot(k)=edot(k)+((paphalf(i,k)*pav(i)-tap(k)*vavg)*bottomarea/&
    &velocityrecordrate)
  end do
end do

!convert to watts edot=edot*freq

write(*,*)"Acoustic power (W)" write(*,*)"    sensor,    edot(W),
edot/rho a u^3" do i=1,nsensors
write(*,*)i,edot(i),edot(i)/rho/area/vamp**3,tap(i) end do
!write(*,*)"new#9",topedot
```

```
if(filenumber==1)open(unit=156,file="c:\data\acousticpower\12zin_&
&steady_edot.txt")

!20deg, phase1&9,edot3&9    12deg, phase 1&8, edot 2&8
if(filenumber==1)write(156,*)"casename, edot watts,
edot/rhoau^3,edot& &_fft,nondimedot_fft,u0,umax,dphibot,dphitop"
write(156,564)trim(casename),",",edot(2)-edot(8),",",(edot(2)-edot(8&
&))/rho/area/vamp**3,",",((vamp*bottomarea*pamp(2)*(cos(pphase(1)-vp&
&hase)))-(vamp*bottomarea*pamp(8)*(cos(pphase(8)-vphase)))),",",((vam&
&p*bottomarea*pamp(2)*(cos(pphase(1)-vphase)))-(vamp*bottomarea*pamp&
&(8)*(cos(pphase(8)-vphase))))/rho/area/(vamp+vavg)**3,",",vavg,",",&
&vamp,",",(pphase(1)-vphase),",",(pphase(8)-vphase) 564
format(A11,A1,10(F10.4,A1))
write(*,*)edot(2),edot(8),vamp*bottomarea*pamp(3)*cos(pphase(1)-&
&vphase),vamp*bottomarea*pamp(8)*cos(pphase(8)-vphase) !pause

!================================================================
!Impedance stuff area=.004455

!12 deg, 2&9    20deg, 3&9     30degold , 2&8 uppersensor=3
lowersensor=7

X=(pamp(uppersensor)*sin(pphase(uppersensor))-pamp(lowersensor)*sin&
&(pphase(lowersensor)))/(pamp(uppersensor)*cos(pphase(uppersensor))&
&-pamp(lowersensor)*cos(pphase(lowersensor))) phideltap=atan(X)
deltap=(pamp(uppersensor)*cos(pphase(uppersensor))-pamp(lowersensor)&
&*cos(pphase(lowersensor)))*sqrt(1+X**2)
```

```
rnu=deltap/vamp/area*cos(phideltap-vphase)
l=deltap/vamp/area/omega*sin(phideltap-vphase) rnu=abs(rnu)

write(*,*)"rnu,l,wl" write(*,*)rnu,l,l*omega

write(*,*)"x,phideltap,deltap" write(*,*)x,phideltap,deltap

write(*,*)"puppersensoramp,puppersensorphase,plowersensoramp,plower&
&sensorphase,vamp,vphase"
write(*,*)pamp(uppersensor),pphase(uppersensor),pamp(lowersensor),p&
&phase(lowersensor),vamp,vphase

!================================================= !fluctuation
stuff and whole-field phase average (only if B00___.txt ! files read
in) !if(fileflag==1) then

!allocate(input(nrows,4)) !allocate(velsums(nrows,4))
!allocate(fluctuation(nrows,4)) !velsums=0. !count=0

!write(*,*)"  " !write(*,*)"Computing fluctuation and phase average
velocity fields." !write(*,*)"Enter the output location (include
last \)" !read(*,*)directoryout

!do phase=1,vshotspercycle

!phase average loop !do j=phase,nshots,vshotspercycle
```

```
!call flucname(j,phase,veldirectory,velfile,velfileout,flufile,dir&
!&ectoryout)

!write(*,*)"filein,fileout,flufile" !write(*,*)trim(velfile)
!write(*,*)trim(velfileout) !write(*,*)trim(flufile)

!open(unit=18,file=velfile,action="read") !read(18,*)junk !do
row=1,nrows !  read(18,*)(input(row,i),i=1,4) !end do

!velsums=velsums+input !count=count+1 !close(unit=18) !end do

!Find average !velsums=velsums/real(count)

!Fluctuation velocity field stuff !do j=phase,nshots,vshotspercycle
!   call flucname(j,phase,veldirectory,velfile,velfileout,flufile,&
!&directoryout) !   open(unit=18,file=flufile,action="read") !
read(18,*)junk !   do row=1,nrows !
read(18,*)(input(row,i),i=1,4) !   end do

!   input(:,3)=input(:,3)-velsums(:,3) !
input(:,4)=input(:,4)-velsums(:,4)

!   open(unit=20,file=flufile,status="replace") !
write(20,191)'#DaVis 7.1.1 2D-vector 8 128 128 "position" "mm"& !&
"position" "mm" "velocity" "m/s"' !   191 format(A81) !   do
row=1,nrows !      write(20,*)(input(row,i),i=1,4) !   end do !
close(unit=20) !   close(unit=18) !end do !end do !end if
!deallocate(input,velsums,fluctuation)
```

```
!deallocate everything
deallocate(velocity,pcosines,psines,pressure,acycle,bcycle,cycleamp)
deallocate(acceleration,cyclephase,averagev,topaveragev,pap,paphalf)
deallocate(vcosines,vsines,a,b,pamp,pphase,avcycle,bvcycle,vcycleamp)
deallocate(vcyclephase,tap,pav,edot,abspav)
deallocate(VAMPS,VPHASES,AVEL,BVEL,xv,xvaverage,dudt)

write(*,*)"======================" end do

end program

![[[[[[[[[[[[[[[[[[[[[[[[[[[[[[[[[[[[[[[[[[[[[[[[[[[[[[[[[[[[[[[[[[[[
subroutine name(i,filein,directory) implicit none

integer::thousands,hundreds,tens,ones,i character(len=300)::filein
character(len=300)::directory

thousands=int(i/1000.) hundreds=int((i-1000.*thousands)/100.)
tens=int((i-1000.*thousands-100.*hundreds)/10.)
ones=int((i-1000.*thousands-100.*hundreds-10.*tens))
filein=trim(directory)//"B0"//char(thousands+48)//char(hundreds&
&+48)//char(tens+48)//char(ones+48)//".txt"

end subroutine
!]]]]]]]]]]]]]]]]]]]]]]]]]]]]]]]]]]]]]]]]]]]]]]]]]]]]]]]]]]]]]]]]]]]]
```

```
!=================================================================
subroutine flucname(i,phase,directory,filein,fileout,&
&flufile,directoryout) implicit none

integer::thousands,hundreds,tens,ones,i,phase,phasetens,phaseones
character(len=300)::directoryout,filein,fileout,flufile,directory



thousands=int(i/1000.) hundreds=int((i-1000.*thousands)/100.)
tens=int((i-1000.*thousands-100.*hundreds)/10.)
ones=int((i-1000.*thousands-100.*hundreds-10.*tens))
phasetens=int(phase/10.) phaseones=int(phase-(10*phasetens))

filein=trim(directory)//"B0"//char(thousands+48)//char(hundreds+&
&48)//char(tens+48)//char(ones+48)//".txt"
fileout=trim(directoryout)//"P"//char(phasetens+48)//char(phaseon&
&es+48)//".txt"
flufile=trim(directoryout)//"flucB0"//char(thousands+48)//char(hun&
&dreds+48)//char(tens+48)//char(ones+48)//".txt"

end subroutine
!=================================================================
```